THEORY AND EXPERIENCE ON CORROSION OF WATERWALL AND SUPERHEATER TUBES OF WASTE-TO-ENERGY FACILITIES

by Dionel O. Albina

Advisor: Prof. Nickolas J. Themelis

Submitted in partial fulfillment of the requirement for the degree of
Professional Engineer in Metallurgical Engineering

Department of Earth and Environmental Engineering
Fu Foundation School of Engineering and Applied Science
Columbia University

Research Sponsored by:
The Henry Krumb School of Mines (Department of Earth and Environmental Engineering)
The Waste-to-Energy Research and Technology Council (WTERT)

August 2005

Waste-To-Energy Research and Technology Council

THEORY AND EXPERIENCE ON CORROSION OF WATERWALL AND SUPERHEATER TUBES OF WASTE-TO-ENERGY FACILITIES

EXECUTIVE SUMMARY

Corrosion of boiler tubes remains an operational and economic constraint in waste-to-energy (WTE) facilities. Despite the long experience of the WTE industry in reducing corrosion, current methods of protection against corrosion remain costly. Understanding the theoretical mechanism and analyzing empirical data and related factors may help reduce corrosion. The research objective of this study was to analyze the theoretical data and empirical experience of the US WTE industry with corrosion, in the hope that this information may assist operators in reducing corrosion in waste-to-energy facilities.

The mechanism involving high temperature corrosion is discussed in detail in Chapter 2. The effects of municipal solid waste fuel (MSW) to corrosion and the corrosion sensitive areas in WTE facilities are presented. These are the waterwall and the superheater tubes. Corrosion in superheater tubes is due to either gaseous chloride or sulfate attack or to chloride or sulfate salt deposits. The mechanism of gaseous chloride/sulfate attack, also known as active oxidation, is discussed in detail. Each step in the mechanism of active oxidation of boiler tubes is described, with accompanying thermodynamic calculations. In general, the mechanism of active oxidation involves the formation and transport of chlorine in the gas into the metal/scale interface, chemical reaction with the metal surface and outward transport of gaseous metal chlorides.

The mechanism of corrosion of waterwall and superheater tubes by chloride or sulfate deposits is also discussed in detail. In general, corrosion by chloride or sulfates salts occurs at much lower temperatures and is mostly experienced at the waterwall tubes. Corrosion is due to the formation of low melting temperature salts of chloride-chloride, chloride-sulfate or sulfate-sulfate mixtures. The salt melts react with and dissolve the protective oxide films on the metal surface (fluxing). After fluxing, the oxide scale is porous and barely protective.

Current methods of protection are: refractory lining or coating of waterwall tubes with highly alloyed, corrosion-resistant materials; and use of surface coatings, such as weld overlay of nickel-chromium based alloys of superheater tubes. The methods of protection against corrosion in the lower and upper furnace, i.e. the waterwall tubes, and the heat exchanger sections, where the primary, secondary or final superheater tubes are located, are discussed in detail. The most popular method of protection is the use of nickel-chromium alloys applied as weld overlay on alloyed steel or as solid tubes, in particular the use of Alloy 625 (Inconel 625). A list of corrosion resistant alloys is presented in Chapter 3.

In order to understand the role of alloying elements and determine the best possible combination of alloying elements that fit a specific corrosion environment, a summary of

important findings from leading researchers on high temperature corrosion are presented and discussed.

The characteristics of base metals and alloys, i.e. iron, chromium, nickel, chromium-rich steels and nickel-based alloys are discussed in detail. Also, the responses of common alloys when subjected to different corrosive atmosphere are described. Results of laboratory studies of the corrosion of alloys when subjected to gaseous chloride-containing atmospheres, sulfur-containing atmospheres, and combinations of gaseous chloride and sulfur are discussed. The results of studies conducted on corrosion of alloys coated by chloride and sulfate salts are also presented. The results of field corrosion tests on novel alloys are also described and possible combinations of alloys that are best suited for a given corrosive atmosphere are suggested.

In Chapter 4, the kinetics on the transport of chlorides into the metal/scale interface are discussed. Various kinetic models are discussed for estimating the weight gain or loss over time. In an attempt to understand the effects of HCl and SO_2 in the furnace gas on tube corrosion, the percentage coverage of Inconel (Alloy 625) was correlated with the furnace HCl concentrations, SO_2 concentrations and HCl/SO_2 concentration ratio. Inconel coverage is assumed to be an indicator of the extent of corrosion in a facility, i.e. the larger area covered by cladding and solid tubes signifies higher corrosion. Based on the available data analyzed, the results suggest that: a) there is a correlation between an increase inconel coverage to an increase or decrease of HCl concentration in the furnace, b) an increase of SO_2 concentration somewhat increases inconel coverage, and c) the general trend demonstrated by the facilities analyzed show an increase in percentage inconel coverage with increased HCl/SO_2 concentration ratio.

Chapter 4 also presents the WTE emissions of sulfur dioxide, nitrogen oxides, hydrogen chloride, heavy metals and dioxins are presented both in terms of concentrations (in milligrams per dry standard cubic meter of gas) and energy emission factors (thermal energy input and electrical energy output). The current emissions demonstrate the beneficial impact of Maximum Achievable Control Technology (MACT) regulations to WTE emissions. The WTE emissions were also compared to coal-fired power plants. Coal is the major fuel used in the U.S. for generating electricity. MACT indeed has had a tremendous impact in lowering WTE of emissions, particularly heavy metals and dioxins.

Note by Prof. N.J. Themelis: *Because of serious illness in the family, Mr. Dionel Albina had to return to the Philippines in January 2005. He undertook to finish his analytical research on the kinetics of WTE corrosion but family, work, and other pressures (including the devastation of the tsunami) have not allowed it. The Earth Engineering Center decided that this report as presented contains much useful information and should be published without further delay. Research work on WTE corrosion continues at Columbia University by Mr. Shang Hsiu Lee, Department of Earth and Environmental Engineering.*

ACKNOWLEDGEMENTS

First and foremost, I would like to express my gratitude to Prof. Nickolas J. Themelis for giving me the wonderful opportunity of studying in Columbia.

I also gratefully acknowledge the financial support of Columbia University's Department of Earth and Environmental Engineering (Henry Krumb School of Mines) and the Waste-to-Energy Research and Technology Council-Earth Engineering Center (WTERT-EEC).

I would also like to thank Mark White, Zenon Semanyshyn, Joe Aldina and Gary Thein, all of Covanta Energy Corporation for their support throughout the length of my research. Thanks and appreciation also to Greg Epelbaum and Hanwei Zhang and American-Ref-fuel Corporation; to Leo Lakowski and Montenay Power Corporation; and, Artie Cole of Wheelabrator for all their support of my research.

I would also like to recognize Masato Nakamura, Liliana Themelis, Joe Di Dio, Dr Aylen Badilla, Dr Karsten Millrath, Frank Yeboah, Barbara Algin, Jaime Bradstreet, Kimberly Labor, Prof. Castaldi, Prof Duby, Prof Lall, Prof Lackner, Jennifer Wade, Monica de Angelo, and Karena Ostrem for their support.

Finally, I would like to thank my parents and family especially to my mother for their support and inspiration.

Dionel O. Albina

New York City, January 2004

TABLE OF CONTENTS

Executive Summary 3
Acknowledgement 6
Table of Contents 7
Lists of Figures 10
Lists of Tables 12

1. Introduction **13**
1.1 General background 13
1.2 Environmental concern and WTE emission 15
1.3 Corrosion in WTE 16
1.4 Objectives and scope of work 17
1.5 Methodology 18
2. High Temperature Corrosion Mechanism **19**
2.1 Introduction 19
2.2 Effects of feed composition 19
2.3 Corrosion sensitive areas 21
2.4 Corrosion mechanism 22
2.4.1 Oxidation 22
2.4.1.1 Principles of oxidation reaction 23
2.4.1.2 Active oxidation in WTE facilities 27
2.4.1.3 Active oxidation of high alloy steels 31
2.4.2 Corrosion in deposits by sulfation and molten salts 34
2.4.2.1 Corrosion by sulfation of chloride salts 34
2.4.2.2 Corrosion by chlorides at metal/oxide interface 35
2.4.2.3 Reaction involving molten salt mixtures 35
2.4.2.4 Molten sulfate corrosion 37
2.5 Summary 41
2.6 Thermodynamic Calculations 43
3. Current Method of Protection **54**
3.1 Introduction 54
3.2 Wastage rates 55
3.3 Corrosion in the lower furnace 55
3.3.1 Waterwall protection by refractory materials 55
3.3.2 Waterwall protection by corrosion-resistant alloys 56
3.4 Corrosion in the upper furnace and passes 57
3.4.1 Superheater tubes 57

3.4.2 Screen tubes and generating Banks 58
3.5 Development of Corrosion Resistant Alloys 59
3.5.1 Comparison on the corrosion behavior of Fe, Cr and Ni 59
3.5.2 Corrosion of low alloy steels and effect of HCl and SO_2 62
3.5.3 Corrosion in high alloy steels and nickel-containing alloys 64
3.5.4 Influence of gas composition and deposits on corrosion of steels and nickel-based alloys 68
3.5.4.1 Beneath deposits of sulfate mixtures 68
3.5.4.2 Beneath deposits of chloride mixtures 71
3.5.5 Development of new alloys based on Cr+Ni+Mo content 75
3.6 Summary 78
3.7 Thermodynamic Calculations 81
4. Corrosion Kinetics, WTE Emissions and Effects HCl and SO_2 to Corrosion 82
4.1 Introduction 83
4.2 Corrosion Kinetics 83
4.2.1 Basic Kinetics Principle 83
4.2.2 Reaction Kinetics 83
4.2.3
4.3 WTE Emissions and Effects to Corrosion 85
4.3.1 HCl and SO_2 emissions in WTE facilities 85
4.4 WTE and Coal-fired Power Plants Emissions 87
4.4.1 WTE emissions in comparison with Coal-fired power plants emissions on the basis of thermal energy input and electrical energy output 88
4.4.1.1 Emissions estimate methodology 88
4.4.1.2 Sulfur Oxides emissions 88
4.4.1.3 Nitrogen Oxides emissions 89
4.4.1.4 Particulate Matter 90
4.4.1.5 Heavy Metals (Cadmium, Lead and Mercury) 91
4.4.1.6 Dioxin and Furans 93
4.4.1.7 Emissions summary 95
4.4.2 WTE and coal-fired power plants emissions in terms of concentrations 95
4.4.2.1 Emissions estimate methodology 95
4.4.2.2 Discussion 95
4.5 Summary 97
References 98
Appendix A: Corrosion Questionnaire 103

Appendix B: Common Names and UNS Alloy Number of Alloys Used in High Temperature Application 107
Appendix C: Chemical Composition of Engineering Alloys 108

LIST OF FIGURES

Figure 1. Schematic of a typical waste-to-energy facility 14
Figure 2. Schematic view of the different configurations of boiler designs used in WTE. 15
Figure 3. Schematic of a) typical waste-to-energy facility and b) corrosion sensitive areas 22
Figure 4. The Ellingham diagram for metallurgically important oxides 25
Figure 5. Phase stability diagram of Fe-O-Cl system at 500°C 30
Figure 6. Schematic of the reaction mechanism for active oxidation 31
Figure 7. Equilibrium vapor pressure of solid chlorides at 400-700°C 33
Figure 8. Equilibrium partial pressures of the reaction from gaseous chlorides to solid oxides at 400-700°C 33
Figure 9. Binary phase diagram of KCl-$FeCl_2$ 37
Figure 10. Curve for the temperature dependence of corrosion on superheater tubes in coal-fired boilers 39
Figure 11. Schematic diagram for the sulfidation mechanism based on the increase in the sulfur potential caused by the transport of oxidizing species through the molten layer of alkali-metal sulfate 40
Figure 12. Schematic diagram of the influence of temperature on different corrosion mechanisms on boiler tubes 42
Figure 13. Schematic diagram of refractory installation a) top, b) side and c) front views of the SiC refractory tiles 56
Figure 14. Superimposed stability diagram of (Fe-Cr-Ni)-O-Cl system at 550°C 60
Figure 15. Thermogravimetric results for the corrosion of iron at 400-700°C, He-5% vol., and 500 ppmV HCl 61
Figure 16. Thermogravimetric results for the corrosion of chromium at 400-700°C, He-5% vol. O_2 and 500 ppmV HCl 60
Figure 17. Thermogravimetric results for the corrosion of nickel at 400-700°C, He-5% vol. O_2, and 500 ppmV HCl 62
Figure 18. Effects of SO_2 on the mass gain at 500°C in the presence of fly ash deposit 63
Figure 19. Effect of HCl on the mass change at 500°C in the presence of fly ash deposit 63
Figure 20. Effects of SO_2 and HCl in gas on mass gain at 500°C in the presence

of fly ash deposit 64
Figure 21. Mass gain of high alloy steels in He-O_2 at 700°C of 12 CrMoV-steel and 25Cr-20Ni-steel 65
Figure 22 Mass changes of the alloys investigated after 168 hr exposure in N_2-5% vol. O_2, 500 ppmV HCl at 400-700°C presented in logarithmic plot 66
Figure 23 Mass changes of the alloys investigated after 168 hr exposure in N_2-5% vol. O_2, 1500 ppmV HCl at 400-700°C presented in logarithmic plot. 66
Figure 24 Mass loss in steels and Ni-based alloys at different gas atmospheres beneath molten mixture of $CaSO_4$-K_2SO_4-Na_2SO_4-$PbSO_4$-$ZnSO_4$ at 600°C after 36h exposure 69
Figure 25 Mass loss of alloys exposed in a $ZnCl_2$-KCl melt in air for 340h at 400°C. 72
Figure 26 Phase stability diagram for Al-Zn-O_2-Cl systems at 450°C 74
Figure 27 Relationship between maximum thickness loss and combined Cr-Ni-Mo concentration of alloys after 3000-hour test 77
Figure 28 Relation between maximum corrosion thickness loss and Mo concentration 77
Figure 29 Proposed alloy combination based on prevailing corrosion atmosphere for water wall and superheater tubes. 80

LIST OF TABLES

Table 1. Ultimate analysis of MSW fuel based on U.S. MSW composition 20
Table 2. Chlorine concentration in U.S. MSW fuel 20
Table 3. Boiler parts and temperature levels 21
Table 4. Properties of metal oxides 27
Table 5. Melting temperatures of different eutectics for pure species and binary mixtures 29
Table 6. Melting points of common eutectics in waste-to-energy facilities 36
Table 7 Melting points of common eutectics in WTE facilities 36
Table 8 Chemical compositions of common alloys used in waterwall tubes. 57
Table 9 Chemical compositions of some common alloys used in superheater tubes of waste-to-energy boilers. 58
Table 10 Chemical compositions of alloys used in the laboratory experiments in % weight 65
Table 11 Chemical composition (% weight) used in the exposure tests. 68
Table 12 Nominal Chemical compositions of alloys tested (in % weight) 72
Table 13 Chemical Composition (Ni+Cr+ Mo Content) 75
Table 14 Chemical composition of alloys used in the field corrosion tests 76
Table 15 Actual furnace Hydrogen Chloride concentration in WTE facilities 86

Table 16	Furnace Sulfur Dioxide concentrations	87
Table 17	Sulfur Dioxide emissions in coal-fired plants and WTE facilities	89
Table 18	Nitrogen Oxide emissions in coal-fired plants and WTE facilities	90
Table 19	Particulate Matter emissions from-coal-fired and WTE facilities	91
Table 20	Typical Cadmium emission factors for coal combustion	91
Table 21	Measured Mercury emission factors for coal combustion	92
Table 22	Estimated nationwide emission factors of Cd, Pb and Hg	93
Table 23	Sources of Dioxin emissions in the U.S.	95
Table 24	Summary of emission factors of coal fired and WTE plants	95
Table 25	MACT rules for existing large Municipal Waste Combustion Units	96
Table 26	WTE and coal-fired power plants in terms of concentrations	96

CHAPTER 1

Introduction

1.1 General Background

The conversion of Municipal Solid Waste (MSW) to energy in Waste-to-Energy (WTE) facilities has been recognized globally as one of the means of effective Waste Management. The conversion of MSW to energy conserves fossil fuels, thus mitigates the emission of anthropogenic greenhouse gases, which result to global warming and climate change. The conversion of MSW to energy also reduces the environmental impact of MSW by lessening the amount of waste to be landfilled. In modern WTE facilities, MSW is combusted and converted to thermal heat and electricity. Over 130 million tons of wastes are combusted annually in over 600 WTE facilities worldwide and the recovered energy is converted to electricity and steam [1]. In the US alone, about 28 million tons of MSW are combusted annually in WTE facilities to produce about 2.8 GW (10^9 watts) of electricity and some steam for district heating [2].

WTE technology can be categorized into two broad categories based on fuel characteristics: 1) as Mass-burn and 2) as Refuse Derived Fuel (RDF). For mass burn, the fuel is fed directly into the furnace and burn on the moving grate "as-received", without pre-treatment, such as shredding or material separation. For RDF, the fuel is shredded to reduce size and sorted to recover and remove metal, glass and other products. The process concentrates the combustible components of MSW, and results in a fuel with higher heating value. Mass burn is the dominant WTE technology due to its simplicity and low capital cost to construct. Common grate technologies are the reverse acting roller grate and the co-current reciprocating grate.

Figure 1 shows a schematic of a conventional modern waste-to-energy facility. The main sections of the facility are: entrance zone with weighing facility and refuse receiving area, refuse holding pit and feeding section, the grate and the combustion chamber, combustion chamber integrated thermal equipment for heat recovery (boiler with water steam system and steam turbine), flue gas treatment system, residue treatment equipment, electrical installation and control system, and auxiliary equipment and buildings.

A variety of Air Pollution Control Equipment (APC) is installed in WTE facilities to clean the flue gases after the heat from the hot combustion gases has been recovered in the furnace waterwalls and superheater tubes. Some facilities use electrostatic precipitators to remove fly ash prior to scrubbing the gas while most utilize dry or semi-dry scrubbing systems that involve injection of an alkaline powder as slurry, and fabric bag filters after the scrubber (as in Figure 1). Additional pollution control measures include the use of activated

carbon particles for absorbing mercury and reduction of organic pollutants such as dioxin and furans.

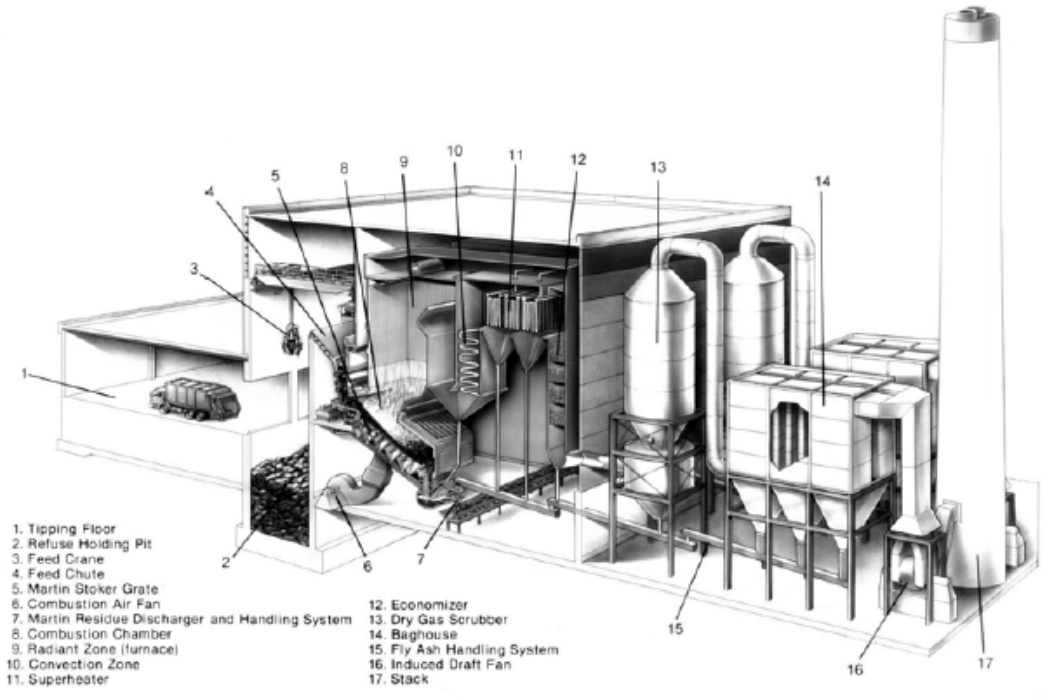

Figure 1 Schematic diagram of a typical waste-to-energy facility.

Figure 2 shows a schematic view of some typical designs of boilers. Each design has different characteristics relative to the following: temperature profile, gas mixing, ash separation, and heat transfer surfaces. Important considerations in the design of the facilities are: the design heating value of the MSW fuel, vertical vs. horizontal heat exchanger tubes, number of passes and turn-overs, position of the secondary air nozzles, tubes and the desired temperature profile in the flue gas path. The main heat transfer surfaces are: the boiler walls consisting of membrane waterwall tubes, superheater tube bundles, evaporator tubes and economizer tubes.

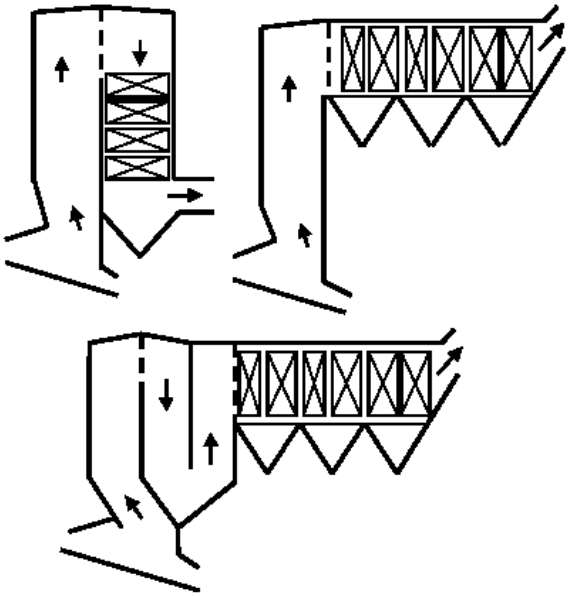

Figure 2. Schematic view of different configurations of boiler designs used in WTE units

1.2 Environmental Concerns regarding WTE Emissions

One of the issues of concern regarding WTE are the emissions to the atmosphere. The emissions of concern are trace organic compounds, particularly polychlorinated dioxin and furans; volatile trace metals such as mercury, lead and cadmium; total particulate matter, sulfur dioxide, nitrogen oxides and acidic gases such as hydrogen chloride, hydrogen fluoride. During the last decade, the WTE industry has implemented tremendous improvements to reduce these emissions. These improvements involve retrofitting and installation of modern pollution control system and effective process controls to existing WTE facilities. At present, WTE facilities in the US have to follow stringent air pollution control standards as mandated by the Maximum Achievable Control Technology (MACT). The enforcement of MACT has brought a significant drop of the emissions of concern in particular heavy metals, dioxin and furans [3,4]. Despite the significant reductions of emissions from WTE facilities during the last decade, negative perceptions still persist on the use of WTE particularly in the US. The negative perception could be attributed to the heavy emissions of MSW incinerators in the past, and to being unaware of the fact that other alternatives for MSW disposal, such as landfilling, for disposal of waste have much more adverse environmental impacts.

1.3 Corrosion in WTE Facilities

Apart from environmental concerns and their related environmental costs, e.g. retrofit/maintenance costs and control of Air Pollution Control equipment to comply safety emissions standards, another issue that burdens the operations of WTE facilities from an

economic standpoint is the cost related to corrosion of boilers tubes. Corrosion is a major cause of downtimes and shutdown in the operations of WTE facilities and represents a large percentage of the total maintenance cost of the facility. Corrosion in these areas is generally categorized as high-temperature corrosion. The lower section of the furnace is subjected to corrosion by high temperature impingement, corrosion by low-melting deposits of molten chloride and sulfide salts and corrosion/erosion due to high flue gas velocity. Corrosion occurs on the waterwall tubes in the radiant zone (furnace), the passes, the screen and evaporator tubes, and the superheater tubes. The superheater regions are subjected to high-temperature gaseous oxidation and molten sulfate corrosion.

Accumulated operating experience has resulted in reducing corrosion in the boiler tubes. Over the years, the industry has adopted general approaches to reduce corrosion, classified as primary and secondary measures. Primary measures seek to eliminate corrosion by influencing the process conditions in the boiler. Primary methods are directed to the following goals: a) improvement of combustion process, b) improvement of process control in particular the control of temperature of the gas, and c) design modifications, such as process gas recirculation to alter flow dynamics and encourage mixing of gases, and arrangement of the steam system. Secondary methods of protection are applied to extend the lifespan of the boiler tubes. One widely used option is application of protective layers of alloys designed to shield the steel tubes from corrosive deposits and flue gases. The use of alternative corrosion-resistant alloy combined with application of new engineering practice such as the use of overlay welding with nickel-based alloys is commonly used [5]. Other secondary measures include the injection of chemicals to remove deposits and use of refractory lining and ceramic tiles in particular the lower part of the combustion chamber.

Despite the long experience of industries in reducing corrosion, current methods of protection against corrosion remain costly. Understanding of the theoretical mechanism, empirical data and related factors should help address corrosion. This research study attempts to understand both theoretical and empirical data in the hope that this combination will result in information that may result in reducing WTE corrosion and its related costs.

1.4 Objectives and Scope of Work

This research was carried out to address corrosion issues in the boilers of WTE facilities. The research is divided according to the following objectives:

- ✓ Task 1: *To understand the mechanism of corrosion in WTE boilers.*

From a theoretical perspective, understanding of the thermodynamics that governs corrosion in boiler tubes operating at high temperatures and highly corrosive atmosphere is one of the most important steps in reducing corrosion. In the section on high temperature corrosion mechanisms, factors that contribute to corrosion in WTE are discussed and areas sensitive to corrosion are identified. In Chapter 2, detailed principles of oxidation reaction

and the different types of corrosion mechanisms are discussed both for high temperature gaseous oxidation, and low temperature corrosion brought about by deposits and molten chloride and sulfates.

- ✓ *Task 2: Identify the prevailing method of protection used to reduce corrosion in WTE facilities and examine why such methods are effective.*

From a practical perspective, the next logical continuation, once the mechanism is understood is to know what has been done in the WTE facilities to protect and reduce corrosion. Chapter 3 is dedicated to discuss the current methods of protection to combat corrosion as it occurs in the furnaces and boilers of WTE facilities. This chapter presents possible explanations why such methods of protection have been adopted, prevailed and why they are effective as means for reducing corrosion.

Task 3: Compile and analyze corrosion data from different WTE facilities in the US.

Compilation and analysis of corrosion data from operating facilities provides actual information on the extent and present status of corrosion with current methods of protection. The corrosion questionnaire shown in Appendix 4 will be used to obtain corrosion data from several WTE facilities, operated by the four major WTE companies in the US (Covanta, ARF, Montenay and Wheelabrator). The questionnaire was distributed in November 2004. Therefore, the results of this survey were not available at the time of writing this report.

Task 4: Identify areas of further research to reduce corrosion based on a) theoretical understanding and b) the analysis of operating data.

The research work up to this date identifies and suggests possible research areas that may result in reducing corrosion. The subsequent analysis of the responses to the corrosion questionnaire may provide additional useful information for reducing the maintenance cost of waste-to-energy facilities.

1.5 Research Methodology

An analysis of the literature on high temperature corrosion was carried out, i.e. the mechanism of corrosion in particular the role of chlorine, molten chlorides and sulfates. The approach consisted of an assessment of the process conditions and critical boiler parts, identification of principal corrosion mechanisms and the behavior of different types of alloys as identified from different papers in the literature. Most of the chemical reactions were verified using HSC Chemistry, a thermodynamic calculation software [ref].

CHAPTER 2

High Temperature Corrosion Mechanisms

2.1 Introduction

A major problem of concern in the operation of waste-to-energy plants is the issue of high temperature corrosion in boilers. High temperature boiler corrosion is a frequent cause of shutdown in waste to energy plants, along with problems such boiler slagging and/or fouling, and excessive refractory and metal wear. It is estimated that high-temperature corrosion related shutdowns account to 70% of waste to energy plant shutdowns [6]. It is also estimated that corrosion-related maintenance cost accounts to a third of the annual maintenance budget and can be as high as 10% of the annual turnover [6]. This section identifies the corrosion sensitive areas and describes the different corrosion mechanisms to set the stage for the development of strategies for limiting corrosion.

2.2 Effects of Feed Composition [6]

The rate of corrosion in WTE boilers is reported to be much higher in comparison with conventional coal fired plants that operate at higher temperatures. It is generally assumed that this high rate of corrosion is inherent to the heterogeneous nature of the fuel and its variable chlorine content. The heterogeneous nature of the fuel makes it difficult for operators to maintain uniform combustion conditions that are desired in steam boilers. The poor characteristics of the feed also result in product of incomplete combustion, i.e. high CO levels, occasional heat flux on the wall caused by flame impingement, and formation of aggressive deposits. MSW contains alkali metals such as sodium and potassium, heavy metals such as lead, tin and zinc and various chlorine containing compounds, all of which can form potential corrosive agents. Tables 1 and 2 show the compositions of MSW fuels and the estimated chlorine content respectively.

The composition of the fuel coupled with operating parameters influence the gas composition and deposit characteristics in the boiler tubes. Other factors such as high surface temperatures of the waterwall and gas also influence high temperature corrosion in WTE boilers. High temperatures of metal surfaces, either due to high radiation fluxes to the wall or inadequate transfer of heat to the water/steam result in the melting of deposits and acceleration of the rate of corrosion. The temperature gradient between gas temperature and the metal surface determines the condensation of vapor species, rate of deposition and the composition of the deposit. The presence of lead and zinc in the deposit lower its melting temperature. It is generally accepted that the high level of chlorides in waste contributes to the problem of high-temperature corrosion in boilers, either in the form of HCl, Cl_2 or combined with sodium, potassium, zinc, lead, tin, and other elements.

Table 1. Ultimate analysis of MSW fuel based on U.S. MSW composition [7]

Components of Waste Stream	% in MSW	Percent by Weight (dry basis)[a]						
		Carbon	Hydrogen	Oxygen	Nitrogen	Sulfur	Ash	Chlorine[b]
Paper and paperboard	35.7	43.5	6	44	0.3	0.2	6	0.071
Plastics	11.1	60	7.2	22.8	-	-	10	0.278
Textiles	4.3	55	6.6	31.2	4.6	0.2	2.5	0.054
Rubber and Leather	4.6	69	9	5.8	6	0.2	10	0.058
Wood	5.7	49.5	6	42.7	0.2	0.1	1.5	} 0.224
Yard waste	12.2	47.8	6	38	3.4	0.3	4.5	
Glass and Metals	13.4	2.5	0.35	2.9	<0.1		94	0.008
Food waste	11.4	48	6.4	37.6	2.6	0.4	5	0.034
Others (dirt, ash, etc.)	1.6	26.3	3	2	0.5	0.2	68	-
Ultimate Analysis of composite MSW		42.3	5.5	31	1.3	0.18	18.6	0.72

Reference: [a]based on [8], [b] [b]P. Redmakers, W. Hesseling and J. van de Wetering (2003). Review on corrosion in waste incinerators, *TNO report*

Table 2. Chlorine concentration in U.S. MSW fuel [7]

Component of Waste Stream	Mass in MSW (%)[a]	Chlorine Content (g/kg of componet.)[b]	Chlorine in MSW (g/kg)
Paper/cardboard	35.7	2	0.71
Plastics	11.1	25	2.78
Food Wastes	11.4	3	0.34
Textiles	4.3	12.5	0.54
Wood and yardwaste	17.9	12.5	2.24
Miss.Combustible	4.6	12.5	0.58
Glass and Metals	13.4	0.6	0.08
Total	**98.4**		**7.26**

Reference: [a] USEPA Report (2003), Municipal Solid Waste in the United States: Facts and Figures, Office of Solid Waste and Emergency Response, EPA530-R-03011

[b]P. Redmakers, W. Hesseling and J. van de Wetering (2003). Review on corrosion in waste incinerators, *TNO report*

An analysis of the three types of MSW (U.S., NYC and UK) showed that the chlorine content ranged from 0.4 to 0.7%. In contrast, chlorine in US coal is in the order of 0.05 to 0.1%.

2.3 Corrosion Sensitive Areas

Due to the composition of the MSW fuel, the flue gas environment in waste-to-energy facilities is very aggressive because of gas components such as Cl_2, HCl, S, alkali metals, and heavy metals such as Zn and Sn. These gases when cooled down form deposits on tube walls by condensation or sublimation; soft and sticky particles can also attach to the heat transfer surfaces. These deposits contain salt of chlorides and sulfates, oxides, silicates and unburned particles. Most sensitive areas attacked by corrosion are the heat transfer surfaces like waterwalls, screen tubes between the passes and the superheater tube bundles. Screen tubes are installed in some boilers in front of the superheater tubes bundles to reduce the temperature and velocities of the flue gas entering into the superheater tubes. Most modern waste-to-energy facilities are operated at 40 bars steam pressures and steam temperature of 400°C, while some other designs, for reasons of thermal efficiency make use of even higher steam pressures and temperature. Figure 3 shows a schematic of a typical waste-to-energy boiler and the corresponding corrosion sensitive areas in the facility. Table 3 shows the process conditions relevant to this part respectively [9].

Table 3. Boiler parts and temperature and pressure levels

Boiler Part	Steam system	T_{metal} (°C)	T_{gas} (°C)
Waterwall	Evaporator, (~265 °C)	~200-300 °C	~1000-800 °C
Screen Tubes	Evaporator, (~265 °C)	~200-300 °C	~800-700 °C
Superheater	Steam, (~400 °C)	~400-530 °C	~700-600 °C

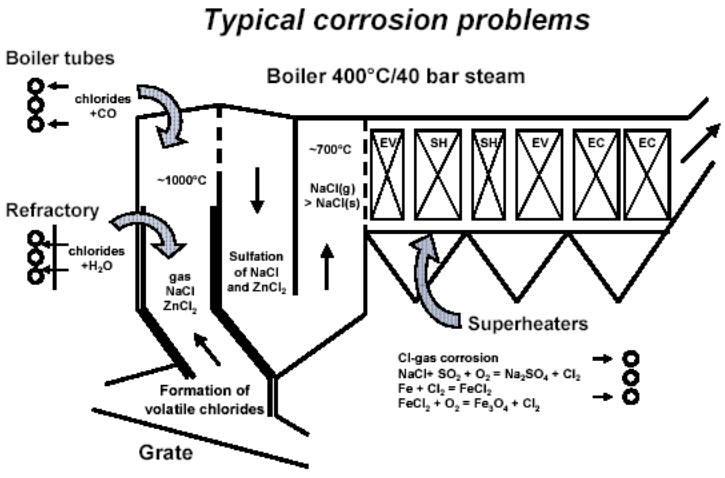

Figure 3. Corrosion sensitive areas in a WTE unit

2.4 Corrosion Mechanisms

High temperature corrosion is a form of corrosion that does not require the presence of a liquid electrolyte. Alloys often rely upon oxidation reaction to develop a protective oxide to resist corrosion attacks such as sulfidation, carburization, and other forms of high temperature attacks. In general, the names of the corrosion mechanism are determined by the most abundant dominant corrosion products, i.e. oxidation for oxides, sulfidation implies sulfides, sulfidation/oxidation implies sulfides plus oxides, and carburization implies carbides. Oxidizing or reducing environments refer to the amount of oxygen present: oxidizing environment refers to oxygen rich environment, while reducing environment refers to very low oxygen concentration in the flue gas. The properties of high-temperature oxide films such as their thermodynamic stability, ionic defect structure and detailed morphology, play a crucial role in determining the oxidation resistance of a metal or alloy in a specific environment [10].

2.4.1 Oxidation

Oxidation is the most commonly encountered form of high temperature corrosion. Oxidation is not always detrimental, e.g. as stated above most heat resistant alloys form an oxide film coating that provides corrosion resistance. The operating temperature plays a critical role in determining the oxidation rate for a given material; as temperature increases the rate of oxidation increases. Chromium oxide or chromia (Cr_2O_3) is one of the most common of those protective oxide films, thus increased chromium content in alloys is one of the most common ways of improving corrosion resistance. Other than chromium, alloying metals used to enhance oxidation resistance include aluminum, silicon, nickel and some of the rare earth metals. Alloys that rely on protective Al_2O_3 (alumina) scale formation are to be preferred over those forming chromia for oxidation resistance above 1200 °C [11]. Austenitic steels are steels that have enough chromium and nickel to maintain austenite (ferric carbide/carbon in iron) at atmospheric temperature. Increasing the nickel content of the austenitic steels up to 30% can have strong beneficial synergistic effect with chromium.

There are metallurgical considerations that impose limits on the amount of alloying additions that can be made in the design of engineering alloys, such as mechanical properties and the processing and manufacturing characteristics. Severe embrittlement tends to form in highly alloyed materials during high temperature exposure. It is therefore imperative to consider other properties besides the corrosion resistance when considering specific alloys for high-temperature applications, i.e. strength requirements. Few commercial alloys contain more than 30% chromium; silicon is usually limited to 2% and aluminum to less than 4% in wrought alloys. Yttrium, cerium and other rare elements are usually added only as a fraction of one percent [12]. A common approach to evade the problem of bulk alloying is the use of surface alloying. In this approach, a highly alloyed and oxidation resistant surface layer is deposited on a substrate layer that has the conventional composition and metallurgical

properties. *Appendix B* lists the alloys used in high-temperature applications with their Unified Numbering System (UNS) alloy number. The composition of these alloys can be found on *Appendix C*.

2.4.1.1 Principles of oxidation reaction

The principle of high-temperature oxidation of pure metals is described as follows [13]. A metal, M, reacts with oxygen or other gases at high temperature by initial absorption of oxygen, and chemical reaction to form the surface oxide, by oxide nucleation and lateral growth into a continuous film that may protect the underlying metal. The film may also be thickening into a non-protective scale with various defects including cavities, microcracks and porosities [13]. Oxidation in air by oxygen proceeds according to the reaction such as:

$$M + O_2 \rightarrow MO_2 \qquad (1)$$

or generally:

$$xM + 1/2(yO_2) \rightarrow M_xO_y \qquad (2)$$

A metal, M, can also be oxidized similarly by either water vapor or carbon dioxide according to the reactions,

$$xM + yH_2O \rightarrow M_xO_y + yH_2 \qquad (3)$$

$$xM + yCO_2 \rightarrow M_xO_y + yCO \qquad (4)$$

$$\Delta G^\circ = RT \ln p_{O2/MO} \qquad (5)$$

The M_xO_y formed on the metal surface becomes a barrier between the substrate metal and oxidizing environment. Chemical thermodynamics predicts whether any reaction is possible under given conditions, however the rate of oxidation cannot be predicted from thermodynamics. Each reactions (2), (3), and (4), for any metal is characterized thermodynamically by a standard free-energy change ($\Delta G°$) which must be negative in order for the reaction to proceed spontaneously from left to right as written. Since $\Delta G° = \Delta H° - T\Delta S°$, a plot of $\Delta G°$ versus T approximates a straight line, which changes in slope where new phases form, i.e. at melting point or boiling point. These plots of standard free energy of reaction ($\Delta G°$) as a function of temperature are known as the Ellingham diagram. Such a diagram can help visualize the relative stability of metals and their oxidized products. Figure 4 shows an Ellingham diagram for many simple oxides [14]. The values of $\Delta G°$on in Ellingham diagram are expressed as kilojoules per mole of O_2 to normalize the scale and allow comparison of the stability of these oxides directly. The lower on the diagram a metal is found, the more negative the standard free energy of formation, and the more stable its oxide will be. For a given reaction (1), and assuming that the activities of M and MO_2 are taken as unity since activities of pure solids in the stable form are defined as unity at all

temperatures and pressures, equation (5) may be used to express the oxygen partial pressure at which the metal and the oxide coexist (i.e. the dissociation pressure of the oxide).

The non-standard state oxygen dissociation pressures leading to oxide formation or reduction on pure metals can be found in the scales shown on the sides of the Ellingham diagram, i.e. for copper at 900°C, the oxygen dissociation pressure is about 10^{-8} atmosphere. Any oxygen pressure above this value will oxidize pure copper; any value below it will reduce copper oxide to pure copper at 900°C. Oxygen dissociation pressure ($P_{O2/MO}$) can be obtained directly from the Ellingham diagram by drawing a straight line from the origin marked O through the free-energy line of the temperature of interest and reading the oxygen pressure from its intersection with the scale at the right side labeled (p_{O2}).

The oxidation rate of an alloy will be minimized if the oxide film has a combination of favorable properties that include: a) The film should have good adherence, to prevent flaking and spalling, b) the melting point of the oxide should be high, c) the oxide should have low vapor pressure to resist evaporation, d) the oxide film and the metal should have close to the same thermal expansion coefficients, e) the film should have high temperature plasticity to accommodate temperature differences in specific volumes of oxide and parent metal and differences in thermal expansion, and f) the film should have low electrical conductivity and low diffusion coefficients for metal ion and oxygen. Oxide scales are much stronger in compression than in tension. If the oxide has a greater specific volume than the parent metal, as the oxide grows at the oxide metal interface, will be in compression and will be more likely protective.

Pilling and Bedworth [10] proposed that the ratio of the oxide metal volume is a predictor of oxide protectiveness. The Pilling-Bedworth ratio expressed as follows:

$$PB\ ratio = \frac{volume\ oxide\ produced}{volume\ metal\ consumed} = \frac{Wd}{nDw} \qquad (6)$$

where W= molecular weight of the oxide

D= density of the oxide

n= number of metal atoms in the oxide molecule

d= density of the metal

w= atomic weight of the metal

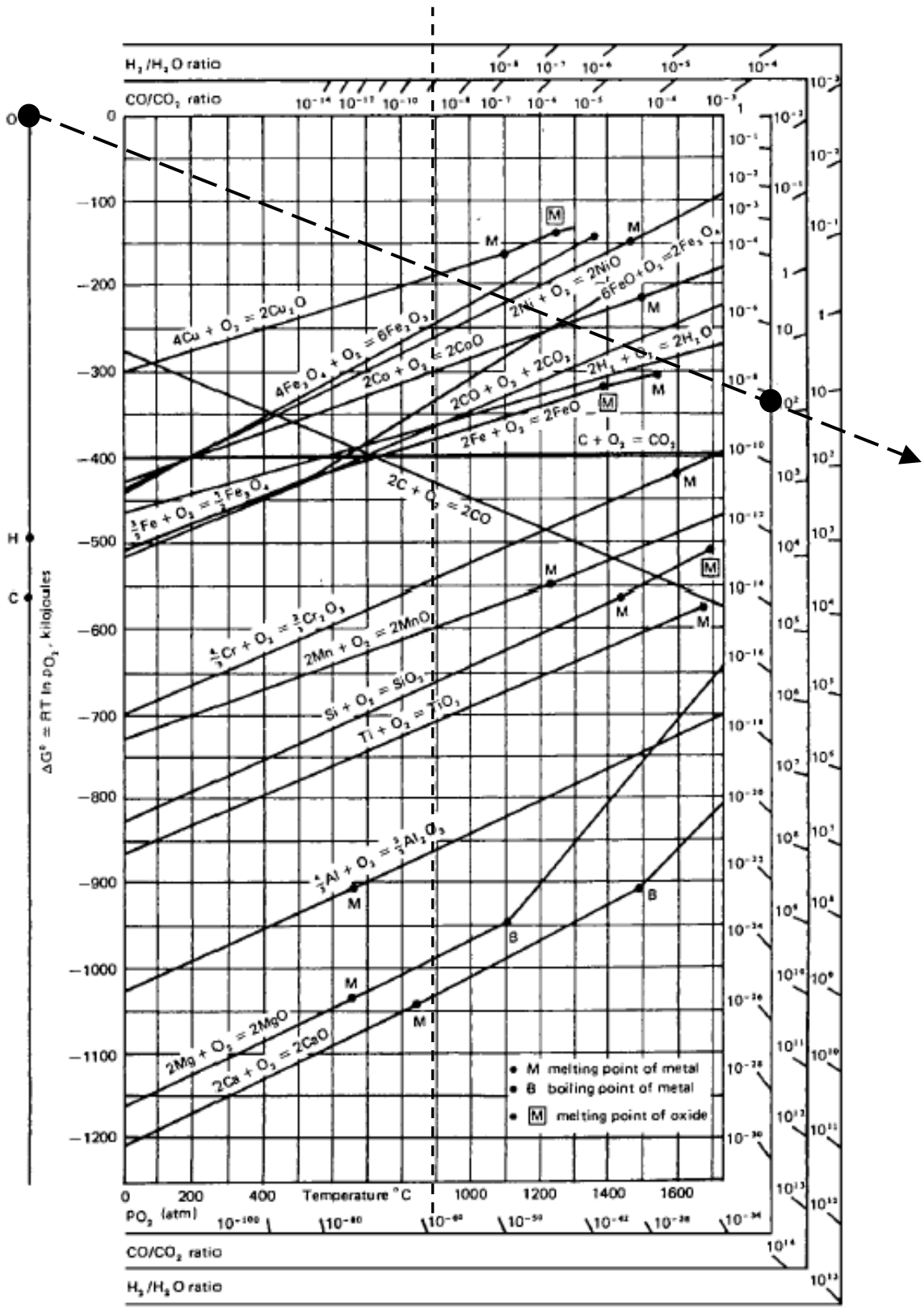

Figure 4. The Ellingham diagram for metallurgically important oxides

In general, the PB ratio should be slightly better than 1 to be protective, to foster moderate compressive stresses in the oxide and adherence to substrate metal. Very high PB ratios may result in excessive compressive stresses which buckle the film and destroy adherence. Table 4 lists the PB ratio of few metal/oxide systems. In practice, it has been found that PB ratios are generally poor indicators of the actual protective properties of the scale. Some reasons for this deviation from the PB rule include [13]:

- Some oxides actually grow at the oxide-air interface, as opposed to the metal-oxide interface.
- Specimen and component geometries can affect the stress distribution in the oxide films
- Continuous oxide films are observed even if PB<1.
- Cracks and fissures in oxide layer can be self-healing as oxidation progresses.
- Oxide porosity is not actually predicted by the PB parameter.
- Oxides may be highly volatile at high temperatures, leading to non-protective properties, even if predicted otherwise by the PB parameter.

2.4.1.2 Active oxidation in WTE facilities

As mentioned previously, the composition of the fuel has enormous effect on the corrosion of boilers tubes in WTE facilities. MSW typically contain plastics, leather textiles, batteries, food waste and alkalis. When combusted, MSW materials form highly corrosive gases such as CO, Cl_2, HCl, S, alkali metals, and heavy metals such as Zn and Sn. These form deposits on the tubes and interact with the metal oxide coating. In the literature [15, 16, 17], it is known that the presence of chlorine in most cases prevents the formation of the protective oxide layer and causes accelerated attack in oxidizing environment. Chlorine can either be in the form of HCl, Cl_2, or combined with Na, K, Zn, Pb, Sn and other elements. Several studies in chlorine containing oxidizing atmospheres, on a number of different metals and alloys, have shown that even small changes in temperature or of the oxygen/chlorine ratio influence the corrosion behavior. The mechanism of active oxidation is described, and is generally accepted for metal temperatures above 450°C. *For clarification purposes, the term deposits as used here means chlorides and sulfates due to deposition of condensed chlorides, fly ash, and others, while the term scale is used to describe the protective oxides.*

Table 4. Properties of Metal Oxides [13]

Metal	**Oxide**	**PB Ratio**	**Protectiveness**[a]
Aluminum	Al_2O_3	1.28	P
Calcium	CaO	0.64	NP
Cadmium	CdO	1.42	NP
Cobalt	Co_2O_3	2.40	P
Copper	Cu_2O	1.67	P
Chromium	Cr_2O_3	2.02	P
Iron	FeO	1.78	P
Magnesium	MgO	0.81	P
Manganese	MnO_2	2.37	P
Molybdenum	MoO_3	3.27	NP
Nickel	NiO	1.70	P
Lead	PbO	1.28	NP
Silicon	SiO_2	2.15	P
Tantalum	Ta_2O_5	2.47	NP
Titanium	Ti_2O_3	1.76	NP
Uranium	UO_2	1.97	NP
Zinc	ZnO	1.58	NP
Zirconium	ZnO_2	1.57	P

[a]P: Protective; NP: Not Protective

The mechanism of active oxidation comprises several steps: a) the formation of chlorine at the scale surface, b) penetration of chlorine into the scale to the oxide/metal interface, c) formation of chlorides on the metal surface components, d) diffusion of chlorides outwards and, e) reaction of chloride with available oxygen in the atmosphere to give metal oxide and chlorine [18]. The mechanism of the active oxidation for iron is described in reactions below (7-10) and can be understood on the basis of some thermodynamic fundamentals and some experimental observations.

a) Formation of Chlorine: Chlorine can be formed from the oxidation of HCl and catalyzed by the oxides of the scale, or from the reaction of chlorides such as NaCl with the oxides of the scale [18], as shown in equations (7-8). Studies by Abels et al. [19] showed that Cl_2 is the main aggressive species at least for a short exposure time The equilibrium of reaction (7) is established in the gas phase, but metal oxides act as catalysts for the reaction, therefore, it may be assumed that the equilibrium of reaction (7) is approached on and in the oxide layer. (Thermodynamic calculations for all the chemical reactions presented are listed at the end of the chapter using HSC software.)

$$2HCl + 0.5O_2 \rightarrow Cl_2 + H_2O \qquad (7)$$

$$2NaCl(g) + Fe_2O_3 + 0.5O_2 \rightarrow Na_2Fe_2O_4 + Cl_2 \qquad (8)$$

b) Penetration of chlorine and formation of metal chlorides [9,18,20]:

Thermodynamic calculations [25] of the dissociation constant of HCl as function of temperature shows that chlorine is present as Cl_2 up to a temperature of 600°C, while above 600°C and in the presence of water vapor the formation of HCl is enhanced. Metals can also react directly with HCl to produce metal chlorides according to reaction (10), as shown by thermodynamic calculations.

Chlorine/HCl diffuses through the oxide layer presumably through the pores and any cracks of the oxide scale, thus allowing metal chlorides to be formed at the metal/oxide interface. The reasons are: a) thermodynamics are favorable, i.e. Gibb's free energy for metal chloride formation is strongly negative and b) at the low oxygen partial pressure that exists, the metal chlorides are more stable than the oxide scale. Grabke et al. [18] reported that the partial pressure of Cl_2 below chloride containing deposits is in the range of 10^{-10}-10^{-13} bar. With thermodynamics allowing the reaction and partial pressure of chlorine sufficiently high to react with the metal, metal chloride can be formed as shown below.

$$Fe + Cl_2 \rightarrow FeCl_2(s) \qquad (9)$$

$$Fe + 2HCl = FCl_2(s) + H_2(g) \qquad (10)$$

The vapor pressure of $FeCl_2$ at the interface, even at low temperatures is relatively high; some values are given in Table 5. Vapor pressures depend primarily on the temperature and the HCl content of the gas [9].

Table 5. Vapor pressure of metal chlorides at 450°C in equilibrium with mixed oxides

		Vapor pressure in bar	
Metal Oxide	Metal Chloride	At 1000 ppm HCl	At 2200 ppm HCl
Fe_3O_4	$FeCl_2$	6.2×10^{-3}	2.9×10^{-2}
$FeCr_2O_4$	$FeCl_2$	2.2×10^{-6}	1.0×10^{-5}
$FeCr_2O_4$	$CrCl_2$	1.0×10^{-13}	1×10^{-13}
$FeAl_3O_4$	$AlCl_3$	1.3×10^{-15}	1.4×10^{-14}

c. Diffusion of metal chlorides outward: Due to the volatility of the iron chloride, continuous evaporation takes place (reaction 11) and the volatile metal chloride diffuses outward through the crack and pores of the scale. On its way outward, the chloride is oxidized to Fe_3O_4 and/or Fe_2O_3 (reactions 12-13), as the oxygen partial pressure increases near the oxide/gas interface. These oxides do not form as a perfect layer; they are porous and non-protective. By means of reactions (12) and (13), chlorine is released and diffuses to the bulk gas; however, a fraction of the liberated chlorine migrates back through the oxide-deposit interface to react with the metal at the oxide/metal interface and form metal chlorides again. Thus, a cycle is formed that provides a continuous transport of metal away from the metal surface towards higher oxygen partial pressure; the rate of this phenomena depends on the rate of diffusion of chlorine between the gas phase and the metal. Gas diffusion through the scale is believed to be the rate-controlling step in the corrosion process [18]. Figure 5 shows the phase stability diagram of the system Fe-O-Cl at 500°C showing stability of $FeCl_2$ corresponding to the Fe/Fe_3O_4 phase boundary.

$$FeCl_2(s) \rightarrow FeCl_2(g) \qquad (11)$$

$$3FeCl_2 + 2O_2 \rightarrow Fe_3O_4 + 3Cl_2 \qquad (12)$$

$$2FeCl_2 + 1.5O_2 \rightarrow Fe_2O_3 + 2Cl_2 \qquad (13)$$

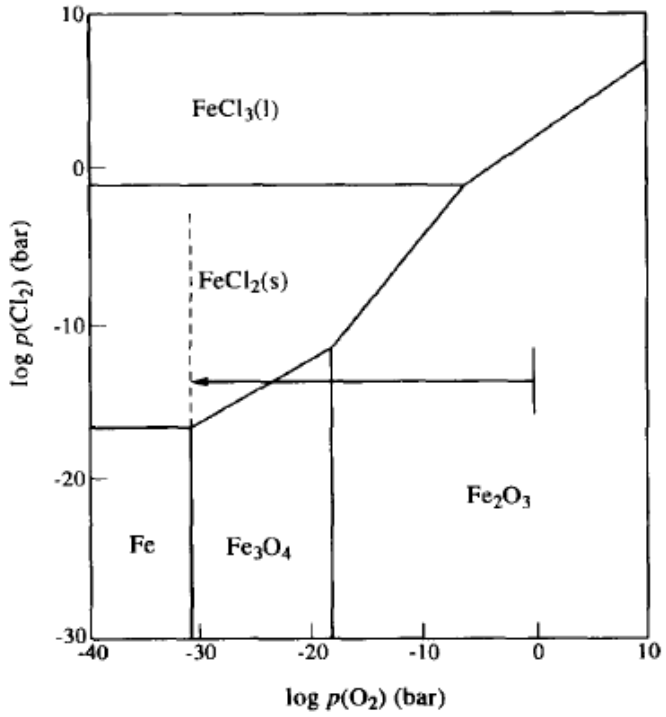

Figure 5.Phase stability diagram of the Fe-O-Cl system at 500°C

The fact that reactions (7), (9), and (11-14) comprise the main reaction path in the active corrosion of iron and low alloy steels has also been proven by observations: a) ferrates formed by the interaction of solid alkali chlorides on scales on steels, b) the formation of solid metal chlorides, mainly $FeCl_2$ (g) at the metal/oxide interface and c) the appearance of scales after some time of active oxidation, (Fe_2O_3) is mainly observed in the crystalline structure. A schematic of the reaction circuit of active oxidation of iron is presented in Figure 6.

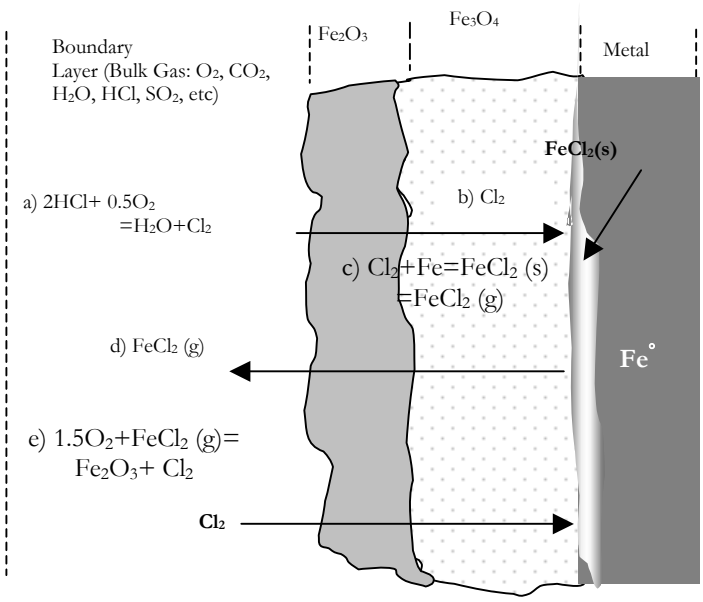

Figure 6. Schematic of the reaction mechanism for active oxidation for active oxidation

2.4.1.3 Active oxidation of high alloy steels [15,18]

The reaction path for active oxidation of high alloy steel (chromium and nickel alloys) is similar to that of iron. The chlorine is produced by catalytic oxidation of hydrochloric acid or the reaction of chlorides in the deposits with the oxide scale, i.e. Cr_2O_3 , according to the following reaction:

$$4NaCl(g) + Cr_2O_3(s) + 2.5O_2 \rightarrow 2Na_2CrO_4(s) + 2Cl_2(g) \quad (14a)$$

$$4KCl(g) + Cr_2O_3(s) + 2.5O_2 \rightarrow 2K_2CrO_4(s) + 2Cl_2(g) \quad (14b)$$

$$4NaCl(s,l) + Cr_2O_3(s) + 2.5O_2 \rightarrow 2Na_2CrO_4(s) + 2Cl_2(g) \quad (14c,d)$$

$$4KCl(s,l) + Cr_2O_3(s) + 2.5O_2 \rightarrow 2K_2CrO_4(s) + 2Cl_2(g) \quad (14e,f)$$

It is noted that thermodynamic calculations using HSC chemistry [25] reveal that the reaction can only proceeds with gaseous chloride ($-\Delta G°$); with condensed chlorides the free energy is positive (14c-14f).

As chlorine penetrates the deposit/scale (oxide) interface and reaches the metal/scale (oxide) interface, under sufficient chlorine partial pressure and low oxygen partial pressure, the formed chlorides are stable. Depending on the alloying elements, several volatile solids and gaseous chlorides can form at the interface (reactions 15-17). The Gibbs

free energies of formation of the different metal chlorides at 600°C indicate that $CrCl_2$ has the highest negative value at –286 kJ/mole (-68.6 kcal/mol) followed by $FeCl_2$ at –232 kJ/mol (-554kcal/mole), and $NiCl_2$ at –174.2 kJ/mole (-41.6 kcal/mole). This indicates that it is expected that nickel is less reactive than iron and chromium. The solid chlorides formed have considerable equilibrium vapor pressures and evaporate continuously (reactions 18-20). The equilibrium vapor pressures as a function of temperatures, for iron, chromium and nickel are shown in Figure 7.

$$Cr + Cl_2 \rightarrow CrCl_2(s) \quad (15)$$

$$Fe + Cl_2 \rightarrow FeCl_2(s) \quad (16)$$

$$Ni + Cl_2 \rightarrow NiCl_2(s) \quad (17)$$

$$FeCl_2(s) \rightarrow FeCl_2(g) \quad (18)$$

$$NiCl_2(s) \rightarrow NiCl_2(g) \quad (19)$$

$$CrCl_2(s) \rightarrow CrCl_2(g) \quad (20)$$

The gaseous metal chlorides evaporate and diffuse outwards toward the gas/oxide interface. As regions of increasing oxygen partial pressure are reached, the gaseous metal chlorides react with oxygen to form solid oxides and releasing gaseous chlorine as shown in reactions (21-25).

$$2CrCl_2(g) + 0.5O_2 \rightarrow Cr_2O_3 + 2Cl_2 \quad (21)$$

$$2CrCl_3(g) + 1.5O_2 \rightarrow Cr_2O_3 + 3Cl_2 \quad (22)$$

$$3FeCl_2(g) + 2O_2 \rightarrow Fe_3O_4 + 3Cl_2 \quad (23)$$

$$2FeCl_2(g) + 1.5O_2 \rightarrow Fe_2O_3 + 2Cl_2 \quad (24)$$

$$NiCl_2(g) + O_2 \rightarrow NiO + Cl_2 \quad (25)$$

The volatile chromium chlorides are oxidized closer to the metal surface than iron and nickel chlorides, since chromium chloride is converted into oxide at lower oxygen partial pressure than iron oxides and nickel oxides. Iron chloride needs significantly higher oxygen pressure and even higher oxygen partial pressure is needed to convert nickel chloride to NiO. Figure 8 shows the equilibrium partial pressures for the different metal chloride/oxide equilibria, calculated for the chlorine activity of the gas atmosphere with 500 ppm volume of HCl and for the equilibrium vapor pressure of the metal chlorides.

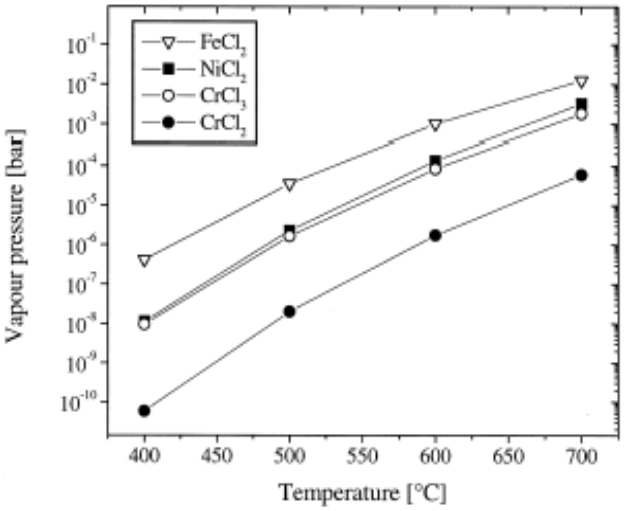

Figure 7. Equilibrium vapor pressure of solid chlorides at 400-700°C [15]

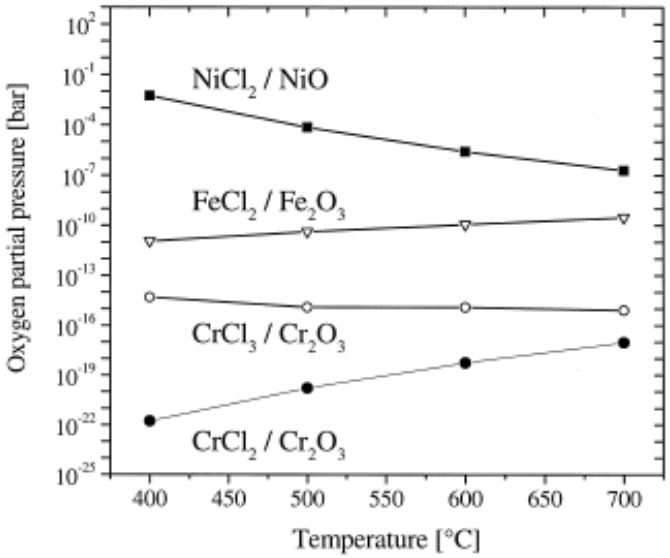

Figure 8. Equilibrium partial pressures of reaction between gaseous chlorides and solid oxides [15]

2.4.2 Corrosion due to Deposits by Sulfation and by Molten Salts [4,12]

Gases containing Cl_2, HCl and gaseous alkali chlorides, e.g. NaCl and KCl, can cause direct corrosion by accelerating the oxidation of the metal alloys as discussed in the section on active oxidation (Section2.4.1.2). Such gases also influence the corrosion of boiler tubes

as parts of the volatilized salt chlorides are deposited on the boiler tubes during cooling. The presence of chlorides in deposits affect corrosion in two ways:

1) Generation of chlorinated species in the deposit in the metal/oxide interface, causing a reaction similar to gas phase/active oxidation (gaseous chlorine may be generated from the sulfation of alkali chlorides or reaction between the chlorides in the deposit and the metal,

2) The chloride in the deposits may form low-temperature melting eutectics (mixture characterized by the lowest possible melting point), which may flux (dissolve) the oxide layer.

2.4.2.1 Corrosion by sulfation of chloride salts

The effects of chloride salts on corrosion have been observed and there is an overwhelming consensus in the literature [9,16-18] that chlorides are a major factor of corrosion either in gas phase active oxidation or at low temperature oxidation. The deposition of sulfates and chlorides occurs by condensation and/or from attachment of particles (fly ash), which may contain sulfates and alkali chlorides. Analysis of deposits has shown that the outer layers of the protective oxide scales contain sulfates such as $CaSO_4$, Na_2SO_4, K_2SO_4, $PbSO_4$, and $ZnSO_4$ while the inner scales contain metal chlorides like $CaCl_2$, KCl, $PbCl_2$ and $ZnCl_2$. The formation of sulfates in the deposit is believed to be due to the sulfation of the alkali chlorides in the deposit and is believed to occur at the outer surface of the deposit [18]. Deposited metal chlorides react with gaseous SO_2 and or SO_3 forming condensed alkali sulfates, as shown by equations (26a,b) and (27a,b).

$$2NaCl(s,l) + SO_2 + O_2 \rightarrow Na_2SO_4 + Cl_2 \qquad (26a,b)$$

$$2KCl(s,l) + SO_2 + O_2 \rightarrow K_2SO_4 + Cl_2 \qquad (27a,b)$$

These reactions release gaseous chlorine that diffuses towards the metal/oxide interface creating a net reaction that leads to a continuous transport of metal from the metal/oxide interface towards a higher oxygen partial pressure. Therefore, after sulfation, the reaction mechanism is similar to that of active oxidation.

2.4.2.2 Corrosion by chlorides at metal/oxide interface

In this case, gaseous chlorine is liberated by the reaction of condensed alkali chlorides in particular, KCl, with the metal scale (28a,b) [21]:

$$4KCl(s,l) + 2Fe_2O_3(s) + 0.5O_2 \rightarrow 2K_2O \bullet Fe_2O_3 + Cl_2 \qquad (28a,b)$$

These reactions result in high partial pressures of Cl_2 and the corrosion mechanism can proceed similar to that of active oxidation. Thermodynamics do not favor the reaction of condensed sodium chloride with oxides of iron (reaction 29a,b) since the Gibbs free energy of formation is positive.

$$4NaCl(s,l) + 2Fe_2O_3 + 0.5O_2 \rightarrow 2Na_2O \bullet Fe_2O_3 + Cl_2 \quad (29a,b)$$

2.4.2.3 Reaction involving molten salts mixtures

Formation of salt mixtures is generally believed to be the main reason for low temperature metal corrosion, in the temperature range of 250°C to 400 °C. Salt mixtures either chloride-chloride or chlorine-sulfate, can have relatively low melting temperatures (eutectic solutions), for example, KCl has a melting point of 774°C but can form low-temperature eutectics in solution with several other substances. Figure 9 shows the binary phase diagram of KCl and $FeCl_2$ showing a eutectic temperature of 350°C. Once the melting point temperature is reached, the presence of a liquid phase on the surface of the metal increases the corrosion rate due to the following reasons [16]: a) chemical reaction is faster in the liquid phase than a solid-solid reaction and b) a liquid phase provides an electrolyte, i.e. a pathway for ionic charge transfer, for the electrochemical attack. The melting points of some binary systems and common eutectics in waste-to-energy facilities are listed in Tables 6 and 7 respectively.

Table 6. Melting temperatures of different eutectics for pure species and *binary mixtures* [16]

System	Melting/eutectic temperature (°C)	Composition of eutectic point (mol% alkali)
NaCl	801	
KCl	772	
$FeCl_2$	677	
$FeCl_3$	300	
$NaCl$-$FeCl_2$	*370-374*	*~50*
$NaCl$-$FeCl_3$	*151*	*45.3*
KCl-$FeCl_2$	*340-393*	*45.8-91.8*
KCl-$FeCl_3$	*202-202*	*24-47*
$CrCl_2$	845	
$CrCl_3$	947	
$NaCl$-$CrCl_2$	*437*	*53.7*
$NaCl$-$CrCl_3$	*544-593*	*68-95*
KCl-$CrCl_2$	*462-475*	*36-70*
KCl-$CrCl_3$	*700-795*	*54-8*
Na_2CrO_4	792	
K_2CrO_4	980	

$NaCl\text{-}Na_2CrO_4$	557	
$KCl\text{-}K_2CrO_4$	*650*	*68.4*
$Na_2Cr_2O_7$	356.7	
$NaCl\text{-}Na_2Cr_2O_7$ (l)	*592*	*30*
$KCl\text{-}K_2Cr_2O_7$	*366-368*	*25-27.5*

Table 7. Melting points of common eutectics in WTE facilities

System	**Melting/eutectic temperature (°C)**	**Composition in percent weight**
$ZnCl_2$-KCl	250	48:52
$ZnCl_2$-KCl	262	82:18
$ZnCl_2$-KCl	262	84:16
$ZnCl_2$-$PbCl_2$	300	73:27
NaCl-$PbCl_2$	410	31:69
KCl-$PbCl_2$	411	21:79
NaCl-$PbCl_2$	415	17:83
$ZnCl_2$-KCl-$PbCl_2$	275	39:50:11
$ZnCl_2$-NaCl-$PbCl_2$	350	35:48:17
NaCl-KCl-$PbCl_2$	400	16:40:44
K_2SO_4-Na_2SO_4	384	-
KCl-$ZnCl_2$-K_2SO_4-$ZnSO_4$	292	-

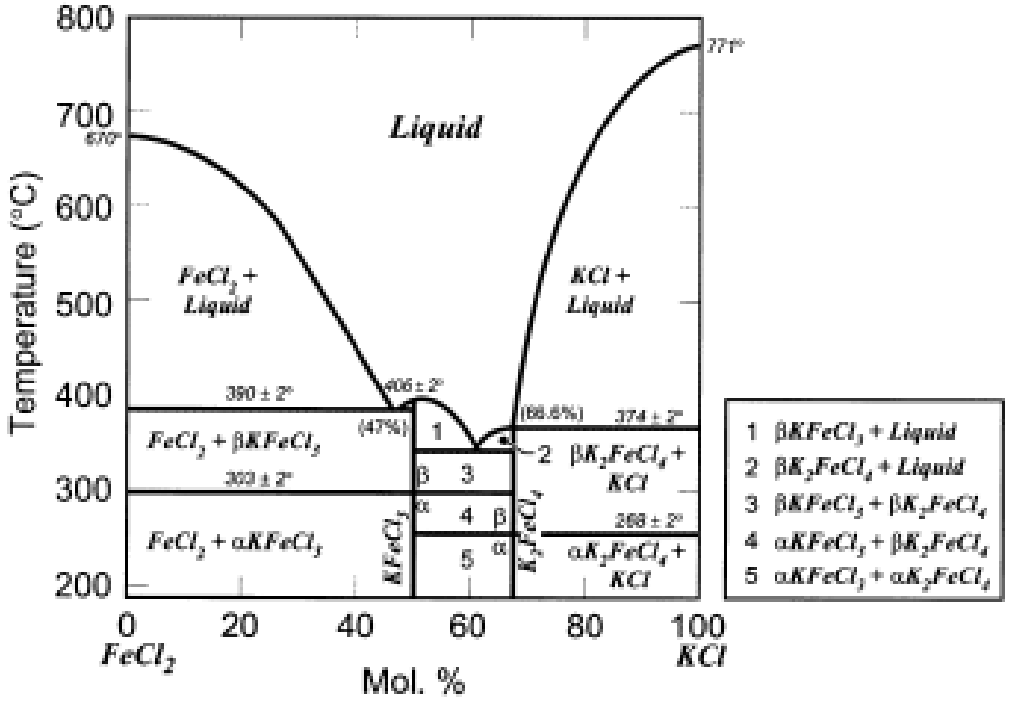

Figure 9. Binary phase diagram of KCl-$FeCl_2$ [16]

2.4.2.4 Corrosion by molten sulfates

There are two types of sulfate reactions generally accepted: 1) the formation of pyrosulfates and 2) the formation of alkali metal trisulfate, from the reaction of iron oxides in contact with alkali sulfates in an oxidizing atmosphere and in the presence of sulfur dioxide. Alkali iron trisulfate is known to have serious corrosive effects but only in the liquid state. The melting points of sodium iron trisulfate and potassium iron trisulfate are at 624°C and 618°C respectively, above which catastrophic corrosion may occur. A mixture of these two compounds however, has a melting point as low as 550°C.

a) Formation of pyrosulfates [9,22,23]: The general reaction for the formation of a liquid phase containing pyrosulfates can start with the reaction of alkali chloride deposits on metal-oxide interface according to reaction (30) [22]:

$$2NaCl(s) + 2SO_2(g) + 1.5O_2 = Na_2S_2O_7(s) + Cl_2(g) \qquad (30)$$

$$(\Delta G^{\circ}(T) = -137 + 0.308T(K)\ kJmol^{-1}\ pyrosulfate)$$

The Gibbs free energy of the reaction is negative below 723K (450°C), and thus the reaction will only proceed below this temperature. The following mechanism has been proposed for reaction (30):

- Formation of SO_3: Given sufficient amount of SO_2 in the flue gas, SO_3 can be formed, as the oxides (iron oxide) can catalyze the oxidation of SO_2.

$$SO_2 + 0.5O_2 \rightarrow SO_3 \quad (catalyzed\ by\ Fe_2O_3) \quad (31)$$

- Formation of pyrosulfates: If the deposit contains iron oxides that catalyze the oxidation of SO_2 to SO_3 then pyrosulfates can form [9,23]:

$$Na_2SO_4 + SO_3 = Na_2S_2O_7 \quad (32)$$

b) Formation of alkali-metal-trisulfates:

The most common form of accelerated corrosion of the superheater tubes on conventional coal-fired boilers is caused by the presence of liquid phase alkali-metal trisulfates. The deposit alkali sulfates react with SO_2 and iron oxide to form liquid alkali-iron sulfates according to reactions (33)-(34).

$$3Na_2SO_4(s) + 3SO_2 + Fe_2O_3 \rightarrow 2Na_3Fe(SO_4)_3(s,l) \quad (33)$$

$$3K_2SO_4(s) + 3SO_2 + Fe_2O_3 \rightarrow 2K_3Fe(SO_4)_3(s,l) \quad (34)$$

The following mechanisms describe the formation of alkali-metal trisulfates (reactions 33-34) and the subsequent corrosion of the metal:

- Formation of alkali metal trisulfate: With pyrosulfates formed (reaction 32), and at about 500°C and above, the trisulfate can attack the protective metal oxide according to reaction (35):

$$Na_2S_2O_7 + Fe_2O_3 \rightarrow 2Na_2Fe(SO_4)_3(s,l) \quad (35)$$

- Sulfidation of the metal: At 550°C and higher metal temperatures, the alkali-metal tri-sulfate can attack the metal according to reaction (36). The SO_3 liberated is available again to react with Na_2SO_4 resulting in cyclic corrosion reaction.

$$2Na_3Fe(SO_4)_3 + 19Fe = 6Fe_3O_4 + 3FeS + 3Na_2S \quad (36a)$$

also:

$$Na_2S + 2O_2 = Na_2SO_4 \quad (36b)$$

$$3FeS + 5O_2 = Fe_3O_4 + 3SO_2 \quad (36c)$$

$$2SO_2 + O_2 = 2SO_3 \quad (36d)$$

This type of corrosion is generally described by what is called the basic fluxing model involving corrosive attack by forming a basic solute of the protective scale. The rate of corrosion is observed to be a function of the metal temperature as illustrated in Figure 10 [24].

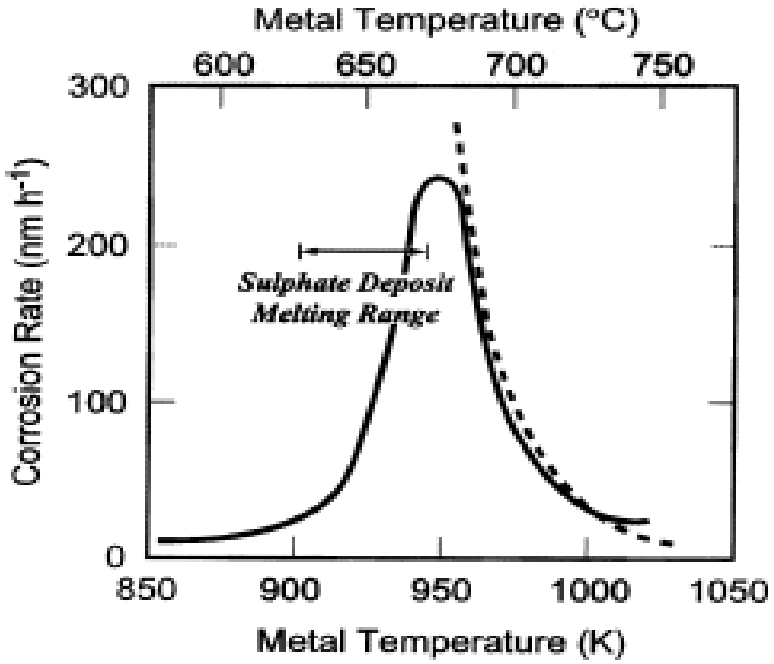

Figure 10. Temperature dependence of corrosion on superheater tubes in coal fired boilers. The dotted line is a theoretical prediction [Adapted from Cutler and Raask [24]]

Figure 10 shows the corrosion rate of the superheater tubes of coal-fired plants at metal temperature above 550°C. The profile of the curve has something to do with the behavior of the ash deposit (which contains sulfates and chlorides [18]). At the metal temperatures at the lower end of the range for the superheater tubes, the ash deposit forms a porous layer and the normal oxidation of the metal proceeds, controlled by the growth of the protective oxide layer on the metal surface. As the metal temperatures increase (650°C), the alkali metal sulfate combustion residues form a molten layer next to the protective oxide on the surface of the metal and the corrosion rates increase rapidly over the temperature range in which the melting occurs. The reduction of corrosion rate after the peak (right side of the bell-shape curve) may be explained by the decreasing stability of the iron or chromium sulfates at higher temperatures.

The molten sulfate influences the corrosion mechanism in two ways: 1) it modifies the oxidizing potential at the outer surface of the oxide layer that is formed on the metal,

and 2) it allows the dissolution of this protective oxide by the metal sulfate. The oxidation of the metal requires the transport of the oxidizing species through the molten sulfate layer. SO_3 is much more soluble than oxygen in the molten sulfate because of the chemical interaction involving the formation of the pyrosulfate ion, thus SO_3 acts as the oxidizing species under these conditions. Oxidation of the metal decreases the oxygen potential at the interface between the protective oxide and the molten sulfate layer; the chemical equilibrium between the oxy-sulfur species that are established at this interface then cause an increase in the sulfur potential to a value that is much greater that in the bulk of the flue gas. This increase in the sulfur potential then allows sulfidation of the metal to take place and leads to the formation of a scale that is less protective than that from simple oxidation. Figure 11 shows a schematic diagram for the sulfur mechanism based on the increase in sulfur potential caused by transport of oxidizing species through the molten layer of the alkali-metal sulfate.

Molten sulfate corrosion *per se* should not be a problem in waste-to-energy boilers. One of the reasons is that metal temperatures in waste-to-energy boilers, in particular the superheater tubes do not exceed 530°C. Also, the amount of sulfur in the feed is not as high as in conventional coal-fired power plants. However, the presence of chlorides can affect molten sulfate corrosion in a number of ways: Chlorides may cause the breakdown of the normally protective layer, by the same mechanism as the molten chloride salts fluxing the oxide scale. When there is a protective scale, normally SO_2/SO_3 cannot diffuse through the scale. In case the oxide break or ruptures, SO_2/SO_3 can penetrate the oxide layer, and result in increased sulfate corrosion of the superheater tube. Also, the presence of chlorides in the alkali sulfate decreases the melting temperature of the salt mixture, thus increasing the temperature range of corrosion up to a point where the superheaters of the waste-to-energy facilities are vulnerable (extending the lower end of the bell-shape curve of Figure 10).

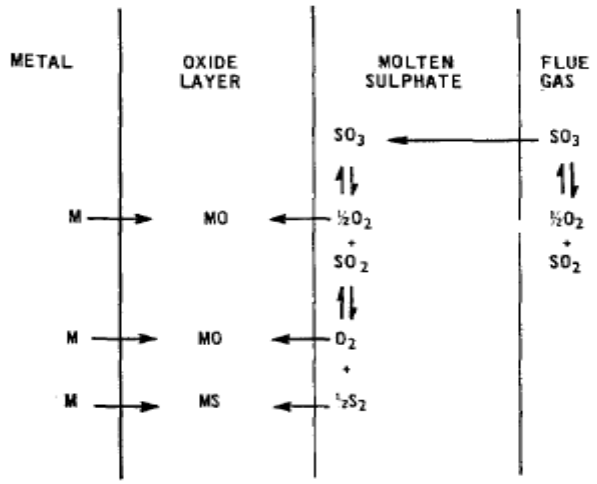

Figure 11. Schematic diagram for the sulfidation mechanism and transport of oxidizing species.

2.5 Summary

The general principles involving high-temperature corrosion on boiler tubes in waste-to-energy facilities were presented in this section. Corrosion in waste to energy facilities is thought to be inherent due to the nature of the municipal solid waste fuel. The corrosion sensitive areas are: the waterwalls and the superheater tube bundles. Waterwall metal temperatures are operated in the range of 200-300°C while superheater tube metal temperatures are estimated to be in the range of 400-530°C. A schematic of the influence of metal temperature on different corrosion mechanism is illustrated in Figure 12.

The superheater tube corrosion is either due to gaseous chloride attack and deposits containing chloride salts (active oxidation) or a combination of molten chlorides and molten sulfates. The mechanism of active oxidation is discussed and consists of several steps: 1) the formation of chlorine on the scale surface, 2) the penetration of chlorine into the scale to the oxide/metal interface, 3) the formation of metal chlorides of the alloy components, 4) the diffusion of metal chlorides from the metal/scale interface to the oxide/deposit interface, to the deposit/gas interface, and 5) the liberation of chlorine due to the oxidation of metal chlorides to metal oxides. Gas diffusion through the scale is believed to be the rate-controlling step in the corrosion process of active oxidation.

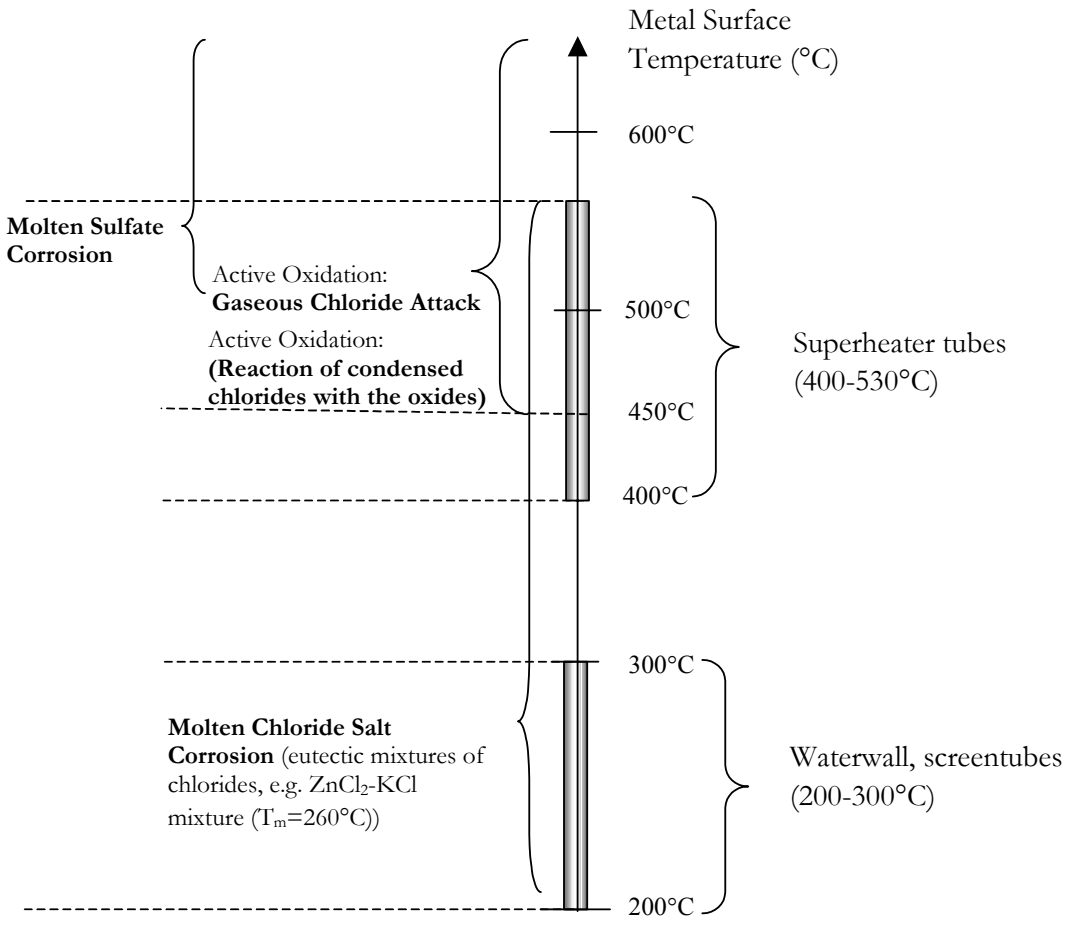

Figure 12. Schematic on the influence of temperature on different corrosion mechanisms on boiler tubes.

Waterwall tubes are generally attacked by molten chloride salts. Formation of low-melting salt mixtures is believed to be the main driving factor for low temperature corrosion. Once the melting point of the eutectic mixture is reached, the presence of liquid phase on the surface of the metal increases the corrosion rate due to faster chemical reaction and the possibility for ionic charge transfer or electrochemical attacks.

2.6 Thermodynamic Calculations

Tabulations of heats of reaction formation and equilibrium constants presented in this chapter are listed. The calculations were done using the HSC Chemistry software [25].

$4HCl(g) + O_2(g) = 2H_2O(g) + 2Cl_2(g)$ (7)

T °C	ΔH kcal	ΔS Cal/K	ΔG kcal	K	Log(K)
0	-27.3	-30.6	-18.9	1.39E+15	15.1
100	-27.5	-31.3	-15.8	1.86E+09	9.3
200	-27.7	-31.7	-12.7	7.15E+05	5.9
300	-27.8	-32.0	-9.5	4.15E+03	3.6
400	-27.9	-32.1	-6.3	1.10E+02	2.0
500	-28.0	-32.3	-3.1	7.34E+00	0.9
600	-28.1	-32.4	0.2	9.05E-01	0.0
700	-28.2	-32.5	3.4	1.71E-01	-0.8
800	-28.3	-32.6	6.7	4.38E-02	-1.4
900	-28.4	-32.7	9.9	1.41E-02	-1.9
1000	-28.5	-32.7	13.2	5.41E-03	-2.3

$4NaCl\ (g) + 2Fe_2O_3 + O_2 = 2Na_2O{*}Fe_2O_3 + 2Cl_2\ (g)$ (8)

T °C	ΔH kcal	ΔS cal/K	ΔG kcal	K	Log(K)
0	-101.3	-121.7	-68.0	2.73E+54	54.4
100	-99.1	-114.8	-56.2	8.84E+32	32.9
200	-97.5	-111.0	-44.9	5.96E+20	20.8
300	-96.3	-108.6	-34.0	9.25E+12	13.0
400	-95.3	-107.0	-23.2	3.47E+07	7.5
500	-94.6	-106.1	-12.6	3.58E+03	3.6
600	-94.3	-105.7	-2.0	3.15E+00	0.5
700	-94.4	-105.8	8.6	1.18E-02	-1.9
800	-93.1	-104.6	19.1	1.28E-04	-3.9
900	-91.6	-103.2	29.5	3.19E-06	-5.5

1000	-89.9	-101.8	39.7	1.50E-07	-6.8

$Fe + Cl_2$ (g) = $FeCl_2$ **(9,16)**

T °C	ΔH kcal	ΔS cal/K	ΔG kcal	K	Log(K)
0	-81.7	-32.0	-72.9	2.32E+58	58.4
100	-81.3	-30.7	-69.8	7.78E+40	40.9
200	-80.8	-29.7	-66.8	7.19E+30	30.9
300	-80.4	-28.9	-63.9	2.27E+24	24.4
400	-80.1	-28.4	-61.0	6.43E+19	19.8
500	-79.8	-28.0	-58.2	2.81E+16	16.4
600	-79.7	-27.8	-55.4	7.37E+13	13.9
700	-69.3	-16.9	-52.9	7.51E+11	11.9
800	-69.0	-16.6	-51.2	2.68E+10	10.4
900	-68.5	-16.2	-49.6	1.71E+09	9.2
1000	-68.1	-15.8	-48.0	1.71E+08	8.2

Fe + 2HCl (g) = $FeCl_2$ (s) + H_2 (g) **(10)**

T °C	ΔH kcal	ΔS cal/K	ΔG Kcal	K	Log(K)
0	-37.6	-36.9	-27.5	1.03E+22	22.0
100	-37.0	-35.2	-23.9	1.01E+14	14.0
200	-36.5	-33.8	-20.5	2.83E+09	9.5
300	-35.9	-32.8	-17.1	3.41E+06	6.5
400	-35.5	-32.0	-13.9	3.24E+04	4.5
500	-35.0	-31.5	-10.7	1.07E+03	3.0
600	-34.7	-31.1	-7.6	7.96E+01	1.9
700	-24.2	-20.0	-4.7	1.17E+01	1.1
800	-23.9	-19.7	-2.8	3.66E+00	0.6
900	-23.3	-19.1	-0.8	1.43E+00	0.2
1000	-22.8	-18.7	1.1	6.54E-01	-0.2

$3FeCl_2$ (s)+ $2O_2$(g) = Fe_3O_4 (s)+ $3Cl_2$(g) (12,23)

T °C	ΔH kcal	ΔS cal/K	ΔG kcal	K	Log(K)
0	-22.3	13.1	-25.9	5.26E+20	20.7
100	-23.0	10.8	-27.1	7.09E+15	15.9
200	-23.4	9.9	-28.1	9.45E+12	13.0
300	-23.6	9.6	-29.1	1.21E+11	11.1
400	-23.4	9.8	-30.0	5.61E+09	9.7
500	-22.7	10.9	-31.1	6.00E+08	8.8
600	-21.4	12.4	-32.2	1.16E+08	8.1
700	-52.4	-20.2	-32.7	2.23E+07	7.3
800	-53.7	-21.5	-30.6	1.73E+06	6.2
900	-55.3	-22.9	-28.4	1.96E+05	5.3
1000	-56.9	-24.2	-26.0	2.96E+04	4.5

$2FeCl_2$ + $1.5O_2$ = Fe_2O_3 + $2Cl_2$ (13,24)

T °C	ΔH kcal	ΔS cal/K	ΔG kcal	K	Log (K)
0	-33.4	-1.9	-32.9	2.03E+26	26.3
100	-33.9	-3.6	-32.6	1.23E+19	19.1
200	-34.2	-4.3	-32.2	7.45E+14	14.9
300	-34.4	-4.6	-31.8	1.28E+12	12.1
400	-34.4	-4.6	-31.3	1.44E+10	10.2
500	-34.3	-4.5	-30.8	5.21E+08	8.7
600	-34.0	-4.1	-30.4	4.08E+07	7.6
700	-54.2	-25.3	-29.5	4.26E+06	6.6
800	-55.1	-26.2	-26.9	3.07E+05	5.5
900	-56.0	-27.1	-24.3	3.33E+04	4.5
1000	-57.0	-27.9	-21.5	4.96E+03	3.7

$4NaCl(g) + Cr_2O_3 + 2.5O_2\ (g) = 2Na_2CrO_4 + 2Cl_2(g)$ (14a)

T °C	ΔH kcal	ΔS cal/K	ΔG kcal	K	Log(K)
0	-197.0	-171.1	-150.2	1.6E+120	120.2
100	-196.3	-169.2	-133.2	1.1E+78	78.0
200	-195.1	-166.2	-116.4	6.1E+53	53.8
300	-193.3	-162.8	-100.0	1.3E+38	38.1
400	-191.0	-159.1	-83.9	1.7E+27	27.2
500	-182.1	-146.4	-68.9	2.9E+19	19.5
600	-179.7	-143.6	-54.4	4.1E+13	13.6
700	-177.2	-140.8	-40.2	1.0E+09	9.0
800	-162.7	-127.1	-26.3	2.2E+05	5.4
900	-159.9	-124.6	-13.7	3.6E+02	2.6
1000	-157.2	-122.4	-1.3	1.7E+00	0.2

$4KCl(g) + Cr_2O_3(s) + 2.5O_2\ (g) = 2K_2CrO_4 + 2Cl_2$ (14b)

T °C	ΔH kcal	ΔS cal/K	ΔG kcal	K	Log(K)
0	-194.8	-168.8	-148.7	9.6E+118	119.0
100	-194.1	-166.6	-131.9	1.9E+77	77.3
200	-192.8	-163.6	-115.4	2.0E+53	53.3
300	-191.3	-160.7	-99.2	6.7E+37	37.8
400	-189.5	-157.8	-83.3	1.1E+27	27.0
500	-187.2	-154.7	-67.6	1.3E+19	19.1
600	-184.5	-151.4	-52.3	1.3E+13	13.1
700	-176.9	-143.2	-37.6	2.7E+08	8.4
800	-174.2	-140.6	-23.4	5.7E+04	4.8
900	-170.9	-137.6	-9.5	5.8E+01	1.8
1000	-151.4	-122.0	3.8	2.2E-01	-0.7

$4NaCl + Cr_2O_3 + 2.5O_2\ (g) = 2Na_2CrO_4 + 2Cl_2\ (g)$ (14c)

T °C	ΔH kcal	ΔS cal/K	ΔG kcal	K	Log(K)
0	22.9	-19.1	28.1	3.3E-23	-22.5
100	22.0	-21.7	30.2	2.2E-18	-17.7
200	21.8	-22.3	32.4	1.1E-15	-15.0
300	21.9	-22.1	34.6	6.4E-14	-13.2
400	22.5	-21.2	36.8	1.2E-12	-11.9
500	29.5	-11.2	38.1	1.7E-11	-10.8
600	29.7	-10.9	39.2	1.5E-10	-9.8
700	29.9	-10.7	40.3	8.9E-10	-9.1
800	41.8	0.5	41.3	3.9E-09	-8.4
900	14.6	-24.8	43.7	7.1E-09	-8.1
1000	14.4	-25.0	46.2	1.2E-08	-7.9

$4NaCl(l) + Cr_2O_3 + 2.5O_2\ (g) = 2Na_2CrO_4 + 2Cl_2\ (g)$ (14d)

T °C	ΔH kcal	ΔS cal/K	ΔG kcal	K	Log(K)
0	60.2	90.6	35.4	4.65E-29	-28.3
100	27.1	-14.4	32.5	9.50E-20	-19.0
200	10.0	-55.5	36.3	1.80E-17	-16.7
300	0.4	-74.1	42.8	4.59E-17	-16.3
400	-5.1	-82.9	50.8	3.32E-17	-16.5
500	-1.8	-78.1	58.6	2.78E-17	-16.6
600	-3.9	-80.7	66.5	2.24E-17	-16.7
700	-5.1	-82.0	74.7	1.71E-17	-16.8
800	6.1	-71.5	82.8	1.36E-17	-16.9
900	5.9	-71.7	90.0	1.72E-17	-16.8
1000	5.7	-71.8	97.2	2.10E-17	-16.7

$4KCl + Cr_2O_3 + 2.5O_2\ (g) = 2K_2CrO_4 + 2Cl_2\ (g)$ (14e)

T °C	ΔH kcal	ΔS cal/K	ΔG kcal	K	Log(K)
0	17.9	-18.1	22.8	5.42E-19	-18.3
100	17.2	-20.4	24.8	3.11E-15	-14.5
200	16.9	-21.1	26.8	3.97E-13	-12.4
300	16.7	-21.4	29.0	8.95E-12	-11.0
400	16.7	-21.3	31.1	7.91E-11	-10.1
500	17.0	-21.0	33.2	4.03E-10	-9.4
600	17.6	-20.3	35.3	1.46E-09	-8.8
700	22.7	-14.8	37.1	4.62E-09	-8.3
800	-2.8	-39.2	39.3	9.86E-09	-8.0
900	-2.8	-39.2	43.2	8.80E-09	-8.1
1000	13.3	-26.3	46.8	9.20E-09	-8.0

$4KCl\ (l) + Cr_2O_3 + 2.5O_2\ (g) = 2K_2CrO_4 + 2Cl_2\ (g)$ (14e)

T °C	ΔH kcal	ΔS cal/K	ΔG kcal	K	Log(K)
0	-6.7	-99.2	20.4	4.90E-17	-16.3
100	-9.5	-108.0	30.8	9.32E-19	-18.0
200	-11.7	-113.3	41.9	4.58E-20	-19.3
300	-13.7	-117.0	53.4	4.37E-21	-20.4
400	-15.3	-119.6	65.2	6.63E-22	-21.2
500	-16.5	-121.2	77.3	1.43E-22	-21.8
600	-17.1	-122.1	89.4	4.07E-23	-22.4
700	-12.9	-117.6	101.5	1.61E-23	-22.8
800	-13.7	-118.3	113.3	8.46E-24	-23.1
900	-13.7	-118.3	125.1	4.88E-24	-23.3
1000	2.4	-105.4	136.6	3.53E-24	-23.5

$Cr+Cl_2=CrCl_2$ **(15)**

T °C	ΔH kcal	ΔS cal/K	ΔG kcal	K	Log(K)
0	-94.6	-31.7	-85.9	5.78E+68	68.8
100	-94.2	-30.6	-82.8	3.25E+48	48.5
200	-93.8	-29.6	-79.8	7.39E+36	36.9
300	-93.4	-28.8	-76.9	2.10E+29	29.3
400	-92.9	-28.0	-74.1	1.11E+24	24.0
500	-92.4	-27.3	-71.3	1.43E+20	20.2
600	-91.9	-26.7	-68.6	1.48E+17	17.2
700	-91.3	-26.1	-66.0	6.52E+14	14.8
800	-90.8	-25.5	-63.4	8.10E+12	12.9
900	-79.4	-15.1	-61.6	3.00E+11	11.5
1000	-78.7	-14.6	-60.1	2.09E+10	10.3

$Ni + Cl_2 = NiCl_2$ **(17)**

T °C	ΔH kcal	ΔS cal/K	ΔG kcal	K	Log(K)
0	-73.1	-37.4	-62.8	1.94E+50	50.3
100	-72.8	-36.4	-59.2	4.48E+34	34.7
200	-72.5	-35.7	-55.6	4.58E+25	25.7
300	-72.2	-35.3	-52.0	6.77E+19	19.8
400	-72.0	-35.0	-48.5	5.55E+15	15.7
500	-71.7	-34.6	-45.0	5.30E+12	12.7
600	-71.4	-34.2	-41.6	2.55E+10	10.4
700	-71.1	-33.8	-38.2	3.74E+08	8.6
800	-70.7	-33.5	-34.8	1.23E+07	7.1
900	-70.4	-33.1	-31.5	7.31E+05	5.9
1000	-70.0	-32.8	-28.2	6.88E+04	4.8

$FeCl_2$ (s) = $FeCl_2$ (g) **(18)**

T °C	ΔH kcal	ΔS cal/K	ΔG kcal	K	Log(K)
0	46.8	42.4	35.3	6.21E-29	-28.2
100	46.5	41.2	31.1	6.29E-19	-18.2
200	46.1	40.3	27.0	3.38E-13	-12.5
300	45.6	39.5	23.0	1.68E-09	-8.8
400	45.2	38.7	19.1	6.29E-07	-6.2
500	44.7	38.1	15.3	4.85E-05	-4.3
600	44.2	37.4	11.5	1.33E-03	-2.9
700	33.3	26.0	8.0	1.58E-02	-1.8
800	32.4	25.1	5.5	7.68E-02	-1.1
900	31.5	24.3	3.0	2.75E-01	-0.6
1000	30.6	23.5	0.6	7.83E-01	-0.1

$NiCl_2$(s) = $NiCl_2$ (g) **(19)**

T °C	ΔH kcal	ΔS cal/K	ΔG kcal	K	Log(K)
0	55.377	47.315	42.453	1.07E-34	-33.97
100	55.031	46.238	37.778	7.45E-23	-22.128
200	54.658	45.353	33.2	4.61E-16	-15.336
300	54.278	44.623	28.702	1.13E-11	-10.945
400	53.894	44.006	24.271	1.32E-08	-7.881
500	53.504	43.465	19.898	2.37E-06	-5.625
600	53.1	42.975	15.577	1.26E-04	-3.899
700	52.676	42.515	11.302	2.89E-03	-2.539
800	52.221	42.071	7.073	3.63E-02	-1.441
900	51.728	41.631	2.888	2.90E-01	-0.538
1000	51.185	41.188	-1.253	1.64E+00	0.215

$CrCl_2(s) = CrCl_2\ (g)$ **(20)**

T °C	ΔH kcal	ΔS cal/K	ΔG kcal	K	Log(K)
0	62.5	42.0	51.0	1.57E-41	-40.8
100	62.1	41.0	46.8	3.64E-28	-27.4
200	61.7	39.9	42.8	1.69E-20	-19.8
300	61.2	39.0	38.9	1.52E-15	-14.8
400	60.7	38.1	35.0	4.32E-12	-11.4
500	60.1	37.3	31.2	1.48E-09	-8.8
600	59.4	36.5	27.5	1.28E-07	-6.9
700	58.7	35.8	23.9	4.23E-06	-5.4
800	58.0	35.1	20.4	7.05E-05	-4.2
900	46.4	24.5	17.7	5.13E-04	-3.3
1000	45.5	23.8	15.2	2.41E-03	-2.6

$2CrCl_2(g) + 1.5O_2\ (g) = Cr_2O_3 + 2Cl_2\ (g)$ **(21)**

T °C	ΔH kcal	ΔS cal/K	ΔG kcal	K	Log(K)
0	-207.1	-86.6	-183.5	6E+146	146.8
100	-206.5	-84.7	-174.9	3E+102	102.4
200	-206.1	-83.6	-166.5	8E+76	76.9
300	-205.5	-82.6	-158.2	2E+60	60.3
400	-204.9	-81.7	-150.0	5E+48	48.7
500	-204.4	-80.9	-141.8	1E+40	40.1
600	-203.8	-80.2	-133.8	3E+33	33.5
700	-203.2	-79.5	-125.8	2E+28	28.3
800	-202.6	-78.9	-117.9	1E+24	24.0
900	-202.0	-78.4	-110.0	3E+20	20.5
1000	-201.4	-77.9	-102.2	4E+17	17.5

$2CrCl_3$ (g) + 1.5O_2 (g) = Cr_2O_3 + 3Cl_2 (g) (22)

T °C	ΔH kcal	ΔS cal/K	ΔG kcal	K	Log(K)
0	-111.9	-60.4	-95.5	2.4E+76	76.4
100	-111.4	-58.8	-89.5	2.6E+52	52.4
200	-111.0	-57.9	-83.7	4.4E+38	38.6
300	-110.6	-57.0	-77.9	5.2E+29	29.7
400	-110.2	-56.3	-72.2	2.9E+23	23.5
500	-109.8	-55.8	-66.6	6.9E+18	18.8
600	-109.4	-55.3	-61.1	2.0E+15	15.3
700	-109.0	-54.9	-55.6	3.1E+12	12.5
800	-108.7	-54.6	-50.1	1.6E+10	10.2
900	-108.4	-54.3	-44.7	2.1E+08	8.3
1000	-108.1	-54.0	-39.3	5.5E+06	6.7

$2NiCl_2$ (g) + O_2(g) =2NiO +2Cl_2 (g) (25)

T °C	ΔH kcal	ΔS cal/K	ΔG kcal	K	Log(K)
0	-79.2	-64.9	-61.5	1.57E+49	49.2
100	-79.0	-64.4	-55.0	1.66E+32	32.2
200	-78.4	-63.0	-48.6	2.93E+22	22.5
300	-77.6	-61.4	-42.4	1.51E+16	16.2
400	-77.1	-60.6	-36.3	6.26E+11	11.8
500	-76.7	-60.0	-30.3	3.68E+08	8.6
600	-76.3	-59.5	-24.3	1.23E+06	6.1
700	-75.8	-59.0	-18.4	1.35E+04	4.1
800	-75.4	-58.6	-12.5	3.54E+02	2.5
900	-74.9	-58.2	-6.7	1.75E+01	1.2
1000	-74.4	-57.8	-0.9	1.42E+00	0.2

$2NaCl\ (s)+SO_2\ (g)+O_2(g) = Na_2SO_4 + Cl_2(g)$ (26a)

°T C	ΔH kcal	ΔS cal/K	ΔG kcal	K	Log(K)
0	-64.2	-53.6	-49.6	4.59E+39	39.7
100	-64.3	-54.0	-44.2	7.54E+25	25.9
200	-64.2	-53.7	-38.8	8.22E+17	17.9
300	-61.2	-47.9	-33.7	7.37E+12	12.9
400	-60.7	-47.1	-29.0	2.60E+09	9.4
500	-60.3	-46.5	-24.3	7.49E+06	6.9
600	-59.8	-45.9	-19.7	8.53E+04	4.9
700	-59.3	-45.3	-15.1	2.51E+03	3.4
800	-58.6	-44.7	-10.6	1.46E+02	2.2
900	-65.7	-51.7	-5.0	8.67E+00	0.9
1000	-65.4	-51.5	0.1	9.51E-01	0.0

$2NaCl\ (l)+SO_2\ (g)+O_2(g) = Na_2SO_4 + Cl_2(g)$ (26b)

T °C	ΔH kcal	ΔS cal/K	ΔG kcal	K	Log(K)
0	-45.6	1.3	-45.9	5.4E+36	36.7
100	-61.8	-50.4	-43.0	1.6E+25	25.2
200	-70.1	-70.3	-36.8	1.0E+17	17.0
300	-72.0	-73.9	-29.6	2.0E+11	11.3
400	-74.5	-78.0	-22.0	1.4E+07	7.1
500	-75.9	-80.0	-14.1	9.6E+03	4.0
600	-76.6	-80.8	-6.0	3.3E+01	1.5
700	-76.8	-81.0	2.0	3.5E-01	-0.5
800	-76.4	-80.6	10.1	8.6E-03	-2.1
900	-70.1	-75.2	18.1	4.3E-04	-3.4
1000	-69.8	-74.9	25.6	4.0E-05	-4.4

$2KCl\ (s)+SO_2\ (g)+O_2(g) = K_2SO_4 + Cl_2(g)$ (27a)

T °C	ΔH kcal	ΔS cal/K	ΔG kcal	K	Log(K)
0	-63.9	-52.4	-49.6	4.75E+39	39.7
100	-64.0	-52.6	-44.3	9.13E+25	26.0
200	-63.8	-52.3	-39.1	1.12E+18	18.1
300	-63.6	-52.0	-33.9	8.17E+12	12.9
400	-63.3	-51.5	-28.7	2.06E+09	9.3
500	-62.7	-50.6	-23.6	4.64E+06	6.7
600	-59.7	-47.0	-18.6	4.60E+04	4.7
700	-59.5	-46.8	-13.9	1.35E+03	3.1
800	-71.9	-58.7	-8.9	6.55E+01	1.8
900	-71.8	-58.6	-3.1	3.71E+00	0.6
1000	-71.5	-58.3	2.8	3.32E-01	-0.5

$2KCl\ (l)+SO_2\ (g)+O_2(g) = K_2SO_4 + Cl_2(g)$ (27b)

T °C	ΔH kcal	ΔS cal/K	ΔG kcal	K	Log(K)
0	-76.2	-92.9	-50.8	4.52E+40	40.7
100	-77.3	-96.5	-41.3	1.58E+24	24.2
200	-78.1	-98.4	-31.6	3.81E+14	14.6
300	-78.8	-99.8	-21.7	1.81E+08	8.3
400	-79.3	-100.6	-11.6	5.97E+03	3.8
500	-79.4	-100.7	-1.6	2.76E+00	0.4
600	-77.0	-97.9	8.4	7.68E-03	-2.1
700	-77.3	-98.1	18.3	7.96E-05	-4.1
800	-77.3	-98.2	28.1	1.92E-06	-5.7
900	-77.2	-98.1	37.9	8.73E-08	-7.1
1000	-76.9	-97.9	47.7	6.50E-09	-8.2

$4KCl(s) + 2Fe_2O_3 + O_2(g) = 2K_2O*Fe_2O_3 + 2Cl_2$ (28a)

T °C	ΔH kcal	ΔS cal/K	ΔG kcal	K	Log(K)
0	-373.1	20.7	-378.8	1.2E+303	3.0E+02
100	-373.1	20.7	-380.9	1.2E+223	2.2E+02
200	-373.3	20.3	-382.9	7.6E+176	1.8E+02
300	-373.6	19.8	-384.9	6.1E+146	1.5E+02
400	-374.0	19.1	-386.9	4.1E+125	1.3E+02
500	-374.8	18.0	-388.7	7.8E+109	1.1E+02
600	-375.9	16.6	-390.5	5.5E+97	9.8E+01
700	-377.7	14.7	-392.0	1.1E+88	8.8E+01
800	-403.6	-10.1	-392.8	9.8E+79	8.0E+01
900	-404.4	-10.8	-391.7	9.5E+72	7.3E+01
1000	-405.0	-11.3	-390.6	1.1E+67	6.7E+01

$4KCl(l) + 2Fe_2O_3 + O_2(g) = 2K_2O*Fe_2O_3 + 2Cl_2$ (28b)

T °C	ΔH kcal	ΔS cal/K	ΔG kcal	K	Log(K)
0	-397.7	-60.4	-381.2	1.1E+305	305.1
100	-399.8	-67.0	-374.8	3.6E+219	219.6
200	-401.9	-71.9	-367.9	8.8E+169	169.9
300	-404.0	-75.8	-360.5	3.0E+137	137.5
400	-406.0	-79.2	-352.7	3.4E+114	114.5
500	-408.2	-82.2	-344.7	2.7E+97	97.4
600	-410.6	-85.1	-336.3	1.5E+84	84.2
700	-413.3	-88.1	-327.6	3.9E+73	73.6
800	-414.5	-89.2	-318.8	8.4E+64	64.9
900	-415.3	-89.9	-309.8	5.3E+57	57.7
1000	-415.9	-90.4	-300.8	4.4E+51	51.6

$4NaCl + 2Fe_2O_3 + O_2(g) = 2Na_2O*Fe_2O_3 + 2Cl_2$ (g) **(29a)**

T °C	ΔH kcal	ΔS cal/K	ΔG kcal	K	Log(K)
0	118.6	30.2	110.3	5.59E-89	-88.3
100	119.3	32.7	107.1	1.82E-63	-62.7
200	119.4	32.9	103.8	1.09E-48	-48.0
300	119.0	32.1	100.6	4.45E-39	-38.4
400	118.2	30.9	97.4	2.34E-32	-31.6
500	117.0	29.2	94.4	2.04E-27	-26.7
600	115.2	27.0	91.6	1.18E-23	-22.9
700	112.7	24.3	89.0	1.01E-20	-20.0
800	111.3	23.0	86.7	2.23E-18	-17.7
900	83.0	-3.4	86.9	6.39E-17	-16.2
1000	81.8	-4.4	87.3	1.02E-15	-15.0

$4NaCl$ (l) $+ 2Fe_2O_3 + O_2(g) = 2Na_2O*Fe_2O_3 + 2Cl_2$ (g) **(29b)**

T °C	ΔH kcal	ΔS cal/K	ΔG kcal	K	Log(K)
0	155.8	140.0	117.6	7.85E-95	-94.1
100	124.4	40.1	109.4	7.95E-65	-64.1
200	107.6	-0.3	107.7	1.76E-50	-49.8
300	97.4	-19.9	108.8	3.17E-42	-41.5
400	90.6	-30.8	111.4	6.72E-37	-36.2
500	85.7	-37.8	114.9	3.38E-33	-32.5
600	81.5	-42.8	118.9	1.73E-30	-29.8
700	77.7	-47.0	123.4	1.93E-28	-27.7
800	75.7	-48.9	128.2	7.75E-27	-26.1
900	74.2	-50.2	133.2	1.55E-25	-24.8
1000	73.0	-51.2	138.2	1.85E-24	-23.7

SO_2 (g) +0.5O_2 = SO_3 (g) **(31)**

T °C	ΔH kcal	ΔS cal/K	ΔG kcal	K	Log(K)
0	-47.2	-44.8	-35.0	1.06E+28	28.0
100	-47.4	-45.2	-30.5	7.49E+17	17.9
200	-47.4	-45.3	-26.0	1.01E+12	12.0
300	-47.3	-45.2	-21.5	1.54E+08	8.2
400	-47.2	-44.9	-17.0	3.22E+05	5.5
500	-47.1	-44.7	-12.5	3.37E+03	3.5
600	-46.9	-44.5	-8.0	1.02E+02	2.0
700	-46.7	-44.3	-3.6	6.37E+00	0.8
800	-46.5	-44.1	0.8	6.76E-01	-0.2
900	-46.2	-43.9	5.2	1.06E-01	-1.0
1000	-46.0	-43.7	9.6	2.24E-02	-1.7

Na_2S + 2O_2 = Na_2SO_4 **(36b)**

T °C	ΔH kcal	ΔS cal/K	ΔG kcal	K	Log(K)
0	-244.1	-85.0	-220.9	5.8E+176	176.8
100	-244.4	-85.8	-212.4	2.4E+124	124.4
200	-244.3	-85.7	-203.8	1.4E+94	94.1
300	-241.2	-79.7	-195.5	3.7E+74	74.6
400	-240.6	-78.7	-187.6	8.3E+60	60.9
500	-239.9	-77.7	-179.8	6.8E+50	50.8
600	-239.1	-76.8	-172.1	1.2E+43	43.1
700	-238.2	-75.8	-164.5	8.6E+36	36.9
800	-237.2	-74.8	-156.9	9.1E+31	32.0
900	-230.9	-69.3	-149.6	7.3E+27	27.9
1000	-232.0	-70.2	-142.6	3.0E+24	24.5

$3FeS + 5O_2 = Fe_3O_4 + 3SO_2$ **(36c)**

T °C	ΔH kcal	ΔS cal/K	ΔG kcal	ΔK	Log(K)
0	-407.0	-74.9	-386.6	1.0E+308	308.0
100	-408.0	-77.8	-379.0	9.5E+221	222.0
200	-410.8	-84.7	-370.8	1.9E+171	171.3
300	-411.7	-86.4	-362.2	1.3E+138	138.1
400	-411.8	-86.6	-353.5	6.2E+114	114.8
500	-410.6	-84.9	-345.0	3.3E+97	97.5
600	-408.6	-82.5	-336.6	1.8E+84	84.3
700	-407.8	-81.6	-328.4	5.7E+73	73.8
800	-407.3	-81.2	-320.3	1.7E+65	65.2
900	-407.2	-81.0	-312.1	1.4E+58	58.2
1000	-407.3	-81.1	-304.0	1.6E+52	52.2

$2SO_2 + O_2 = 2SO_3$ **(36d)**

T °C	ΔH kcal	ΔS cal/K	ΔG kcal	K	Log(K)
0	-47.2	-44.8	-35.0	1.06E+28	28.0
100	-47.4	-45.2	-30.5	7.49E+17	17.9
200	-47.4	-45.3	-26.0	1.01E+12	12.0
300	-47.3	-45.2	-21.5	1.54E+08	8.2
400	-47.2	-44.9	-17.0	3.22E+05	5.5
500	-47.1	-44.7	-12.5	3.37E+03	3.5
600	-46.9	-44.5	-8.0	1.02E+02	2.0
700	-46.7	-44.3	-3.6	6.37E+00	0.8
800	-46.5	-44.1	0.8	6.76E-01	-0.2
900	-46.2	-43.9	5.2	1.06E-01	-1.0
1000	-46.0	-43.7	9.6	2.24E-02	-1.7

CHAPTER 3

Current Method of Protection

3.1 Introduction

There are two methods to reduce corrosion in boiler tubes: One is to influence the operating conditions of the heat exchanger tubes and the other is to use better corrosion resistant material. Some of the suggested ways to influence the combustion conditions are: a) improvement of the combustion process to get less corrosive environment, b) improved process control, i.e. particular control of the flue gas and temperature, and c) modification of the design, in particular flow dynamics and mixing, and the overall design of the system. With respect to application of corrosion resistant materials, there are a number of options: a) application of composite tubing consisting of two layers, with the inner layer from a boiler steel and the outer layer made from a highly corrosion-resistant material, b) application of surface welding (cladding), c) application of resistant coatings from resistant materials, e.g. high velocity oxygen flame (HVOF) to produce high quality coatings and d) application of refractory lining or ceramic tiles in particular on the wall of the first pass.

Causes of corrosion in WTE boiler tubes can be categorized into the following: a) corrosion due to high temperature flame impingement, b) chlorine and chloride salt corrosion, and c) corrosion/erosion due to high velocity streams. The problem of corrosion of the waterwall due to flame impingement is presently minimized by using refractory materials above the grate and extend to near the top of the combustion chamber. Chlorine and chloride salts corrosion in waterwalls and superheaters are minimized by the use of corrosion-resistant alloying materials, e.g. inconel 625. Attempts by operators to minimize corrosion/erosion in boiler tubes are also made such as the use of screen tubes installed in some boilers in front of the superheater bundles. Innovative measures are also used in the combustion chamber to minimize the causes of corrosion; innovative designs have included changing the configuration of the combustion chamber to streamline flow of the flue gas to promote good mixing and also flue gas recirculation. This chapter discusses the current method of protection against corrosion in lower furnace (waterwall) and the upper furnace and subsequent passes (screen tubes, superheater and the generating banks). In order to find the best combination of alloys to provide protections, significant findings in laboratory and field corrosion tests are also presented and discussed.

3.2 Wastage Rates [26,27,29,30]

Wastage rates in WTE boilers ranges from 1-3 mm/year (40-120 mills, i.e. thousandth of an inch per year) on carbon steel boilers and on some occasion even higher. It was estimated that corrosion rates range from 1-2 mm/year (40-80 mpy) for carbon steel waterwalls and are 2.5 mm/year (100 mpy) or higher for carbon steels superheater tubes. These high corrosion rates cause shutdown of the boilers frequently. Because of this

experience, it has been accepted that some type of protection is required for boiler tubes in WTE boilers. The corrosion problems in WTE boilers vary with unit design, geographical region, time of year and several other factors. Recently, a clear trend that has been observed is that the increased amounts of plastics in MSW have resulted in an increase in the chloride content of MSW fuel and correspondingly an increase in the corrosive nature of the boiler environment. A number of solutions have been tried to improve the life of the boiler tubes over the years. Different corrosion-resistant alloys have been evaluated and the most successful of which were the application of nickel-based alloys.

3.3 Corrosion in the Lower Furnace

3.3.1 Protection by refractory materials

The current method of protection for waterwall tubes from flame impingement, particulate erosion and abrasion is by the use of refractory materials. In WTEs, refractory usage varies from cast-aluminum oxide-based cements having low heat transfer capability to highly engineered silicon carbide-based cements and special shapes with heat transfer characteristics [28]. State-of-the-art refractory systems employ silicon carbide gunned, cast or rammed cement tiles with metal anchors for attachment of tiles to the tube walls (see Figure 13). Silicon carbide refractory tiles are pressed or cast during manufacturing and fired at high temperatures sufficient to achieve a bonded shape with good mechanical and thermal properties.

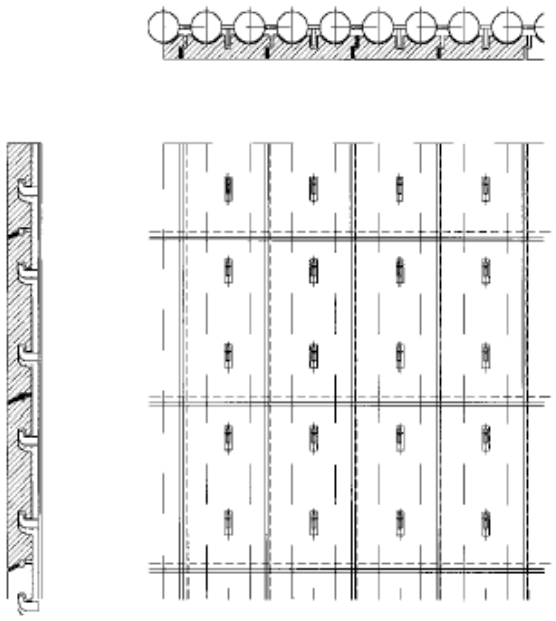

Figure 13. Schematic diagram of refractory installation a) top, b) side and c) front views of the SiC refractory tiles

3.3.2 Protection by Corrosion-Resistant Alloys

At present, the most popular method of protection for furnace waterwall from corrosion due to molten chloride salts and active oxidation is by welding sheets of protective cladding on carbon steel waterwalls. The most popular alloy is Inconel 625; this can be in the form of field-applied overlay or by replacement with spiral weld overlay panels during maintenance shutdown. If applied in the furnace, a number of welding machines are used simultaneously for overlay welding. If the waterwalls are damaged beyond repair on site, the tubes are removed and replaced by shop-fabricated overlay panels. The construction of overlay panels consist of fabricating panels of steel tubes and membranes, which is then followed by overlay welding of the panel using the same techniques of the field overlay [26].

Other methods of applying corrosion resistant materials are by application of resistant coating such as spray coating and diffusion coating. It is reported that spray coating has historically had mixed success in WTE boilers. Flame spray coatings have some degree of porosity. This allows corrosive gases to permeate beneath the protective coating and corrode the carbon steel subrates and cause disbanding of spray coatings. A diffusion coating has also been tried; in general all of these coatings have some degree of porosity or inherent defects in the coating system that may lead to unacceptable localized corrosion [27].

Other than Inconel 625, other materials that have been applied as weld-overlay into carbon steel waterwall tubes in WTE facilities are Alloys 50 and 59. The compositions of these alloys are shown in Table 8.

Table 8. Chemical compositions of common alloys used in waterwall tubes.

Alloy	UNS No.	Ni (%)	Cr (%)	Mo (%)	Fe (%)	Other (%)
625	N06625	63	22	9	1.5	3.4 Nb, 0.2Si,0.2Mn
59	N06059	59	23	16	2	
50	N06650	53	19.5	11	14	0.25 Al, 0.25 Nb, 1.5 W

Note: Complete chemical composition of alloys is listed in Appendix C.

3.4 Corrosion in the Upper Furnace and Subsequent Passes

3.4.1 Superheater tubes

Corrosion protection in the superheater tubes varies from using stainless steel tubes, refractory to surface cladding, and use of solid tubing of highly corrosion-resistant alloy. The use of stainless steel tubes can provide protection from corrosion/erosion. Tube shields are generally exposed to the temperature of the flue gas that enters into the superheater bundles. The metal temperature of the tube shields is typically the same as that of the entering flue gas, thus the shield suffers severe chloride and sulfide attacks, and also deformation and distortion due to high temperature [27]. The use of refractory shields can also provide protection to the superheater tubes. Problems with using refractory shielding are that it reduces the heat transfer efficiency of the superheater and refractory cracking can also occur. At present, the use of surface cladding by weld overlay or the use of solid tubes of highly alloyed materials for superheater tubes are popular long-term solution in order to avoid the problems arising from frequent shutdown for repair or installation of refractory or metallic tube shields.

Causes of corrosion on the superheater tubes are more complex than those for the waterwall in the lower furnace. Superheater tubes can suffer from gaseous chlorides attack, molten sulfates, or molten chlorides attack; because of the mixed corrosion modes in the superheater, the selection of corrosion-resistant alloys is more complicated than for the waterwalls.

Solid alloy 825 and weld overlay alloy 625 are perhaps the most common materials now used in superheater tubes in WTE boilers. The decision whether to use solid tube or weld overlay depends on economics. It should be noted that corrosion rates in solid tubes will not change as a result of tube wall thinning while corrosion rates of weld overlay will accelerate as the cladding corrodes away. Therefore, solid tubes will last longer than weld

overlay tubes at the same corrosion rates. While Alloy 825 solid tubes and Alloy 625 weld overlay have a proven history in many boilers, there are also many boilers where corrosion continues to be a problem. Alloy 825 can be unsatisfactory in many superheater applications while Alloy 625 does not always give the desired superheater life [27]. Table 9 shows the chemical composition of some common alloys used in superheater tubes of WTE facilities.

Table 9. Chemical compositions of some common alloys used in superheater tubes of waste-to-energy boilers.

Alloy	UNS No.	Ni (%)	Cr (%)	Mo (%)	Fe (%)	Other (%)
625[27]	N06625	63	22	9	1.5	3.4 Nb, 0.2Si, 0.2Mn
825[28]	N08825	42	21.5	3	29.8	2.2 Cu, 0.9 Ti
45TM[27]	N06045	46	27	--	23	2.75 Si, 0.1 RE
SA213-T22[29]	K21590	---	2.25	1	95.5	0.32Si, 0.1C, 0.5Mn
TP347H[29]	S34709	12	18	--	66.4	0.9C, 0.4Si, 1.5 Mn, 0.8 Nb
SA213-TP310H[30]		20	25	--	51.8	0.75Si, 2Mn, 0.6C, 0.8Nb

Note: Alloy 825, 45TM, SA213-T22, TP347H and SA213-TP310 are solid tubes, Alloy 625 (applied as weld overlay), composition may not total 100% as some elements are omitted, for complete chemical composition, see Appendix C

3.4.2 Screen Tubes and Generating Banks

Screen tubes are installed in some boilers in front of the superheater tubes bundles to reduce the temperature and velocities of the flue gas entering into the superheater tubes. The reduction in temperature and flue gas velocity consequently protects the superheater from erosion-corrosion. The screen tubes are water-cooled and the metal temperature at the surface (outer diameter) is the same as for waterwall, thus the screen tubes are expected to experience the same corrosion rates as the waterwall. The common method of protection is by cladding with corrosion-resistant nickel-based alloy [31]. The generating bank, which is typically located behind the superheater tubes, is protected by stainless steel tubes and by cladding of corrosion-resistant alloy. The corrosion rate of the generating bank is much less than that of the screen tubes and superheater tubes due to its much lower metal temperature. It is reported that wastage rates for alloy 625 weld overlay are less than 0.125 mm/year (5mpy) [32]; the base metal is generally cladded with alloys with thickness in the range of 1.5-2 mm (60-80 mills).

3.5 Development of Corrosion-Resistant Alloys

This section discusses the resistance of different metals and alloys to corrosion and the results of laboratory and field corrosion tests.

3.5.1 Comparison of the Corrosion Behavior of Iron, Chromium and Nickel

The corrosion behavior of iron, chromium and nickel as base metals have been investigated and clearly showed characteristic differences. These differences were mainly caused by the different reactivities of the metals in the following phenomena: a) the formation of chlorides and the oxides, b) differences in vapor pressures and c) differences the thermodynamic equilibria between volatile chlorides and solid oxides. Figure 14 shows the stability diagram of Fe-Cr-Ni-O-Cl system. Figures 15-17 shows the result of experimental studies by Zahs [15] on the reaction of iron, chromium and nickel in HCl atmospheres at different temperatures. The changes in mass with time affect the formation of chlorides and their volatilization.

The most severe corrosion was expected for iron (Figure 15) as a consequence of the high negative Gibbs free energy of formation of the chloride. The accelerated mass loss at 700°C was due to the fact that $FeCl_2$-chlorides melts were already in liquid state (T_m=676°C). The investigation of the corroded specimen showed that the chlorides on the surface metal were covered with an oxide layer formed directly by the chloride melts. Chromium was also strongly attacked since the Gibbs free energy of the chloride formation is also very negative. The corrosion kinetics is characterized by continuous mass gain at all temperatures (Figure 16).

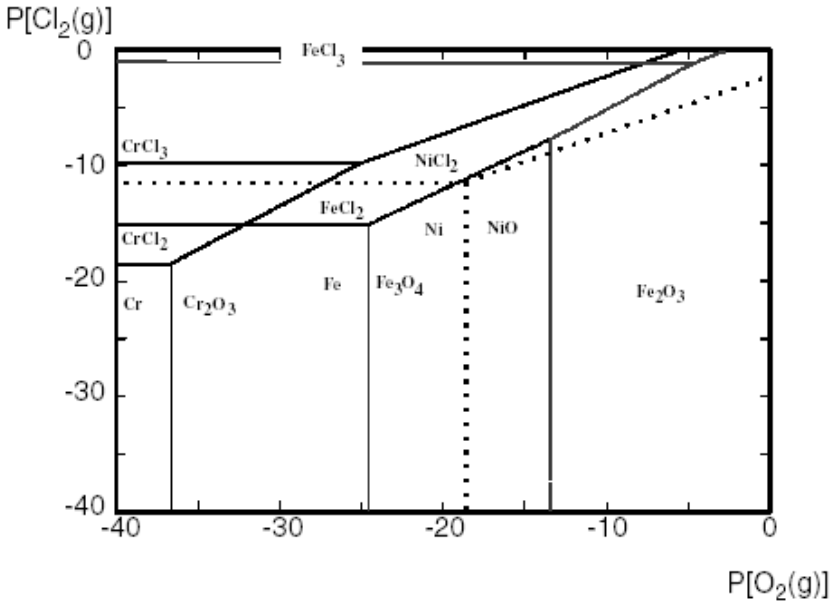

Figure 14. Superimposed stability diagram of (Fe-Cr-Ni)-O-Cl system at 550°C[20].

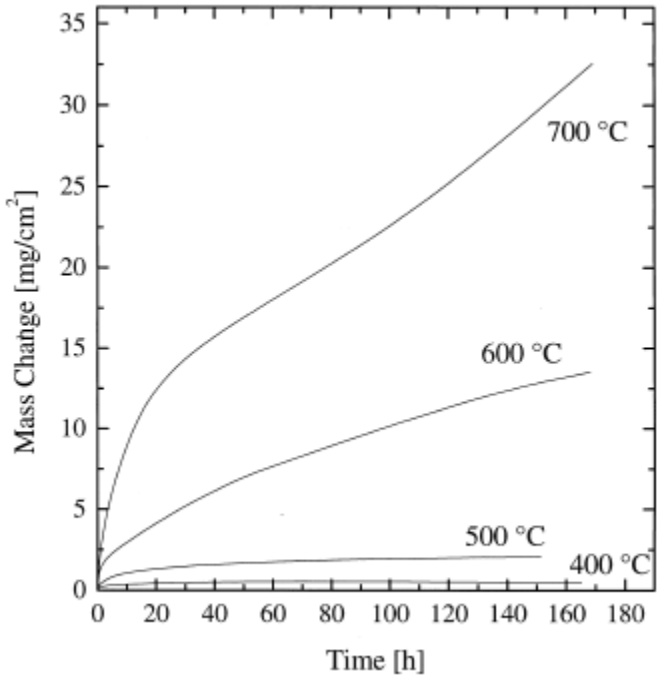

Figure 15. Thermogravimetric results for the corrosion of iron at 400-700°C, He-5% vol. and 500 ppmV HCl [15]

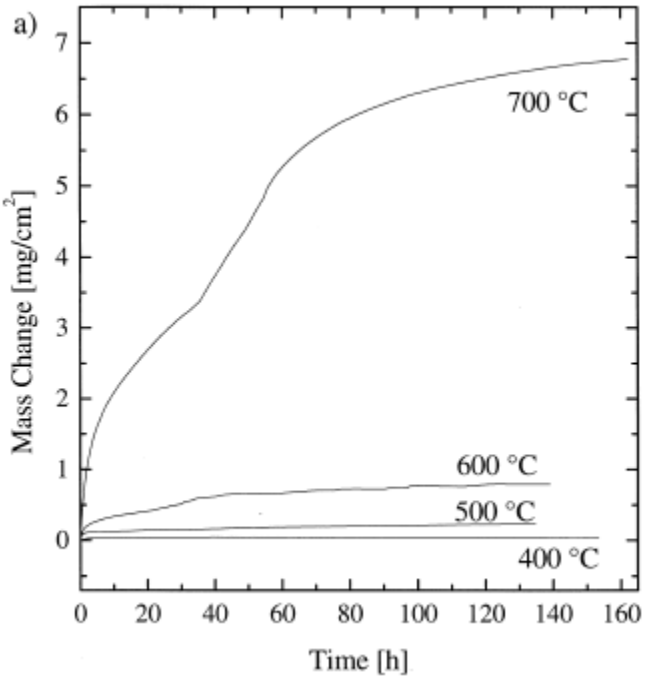

Figure 16. Thermogravimetric results for the corrosion of chromium at 400-700°C, He-5% vol. O_2 and 500 ppmV HCl [15]

The Zahs tests showed that nickel was more resistant due to its less negative free energy of $NiCl_2$ formation (Fig.17). The vapor pressure of $NiCl_2$ is higher than that of the iron and chromium chlorides. Thermogravimetric results for nickel showed little mass gain at 400°C, whereas at 500°C, the mass loss from evaporation of $NiCl_2$ exceeded the mass gain by formation of solid chlorides and oxides. At 600°C, a well adherent corrosion scale is formed which mainly consists of NiO at the start; subsequently gaseous $NiCl_2$ evaporates resulting to mass loss after an initial mass gain. The evaporation of $NiCl_2$ was enhanced at 700°C due to the increasing vapor pressure of $NiCl_2$. At this temperature, the thermodynamic stability of $NiCl_2$ relative NiO was so high that significant evaporation of gaseous $NiCl_2$ at high temperature led to significant mass loss with time

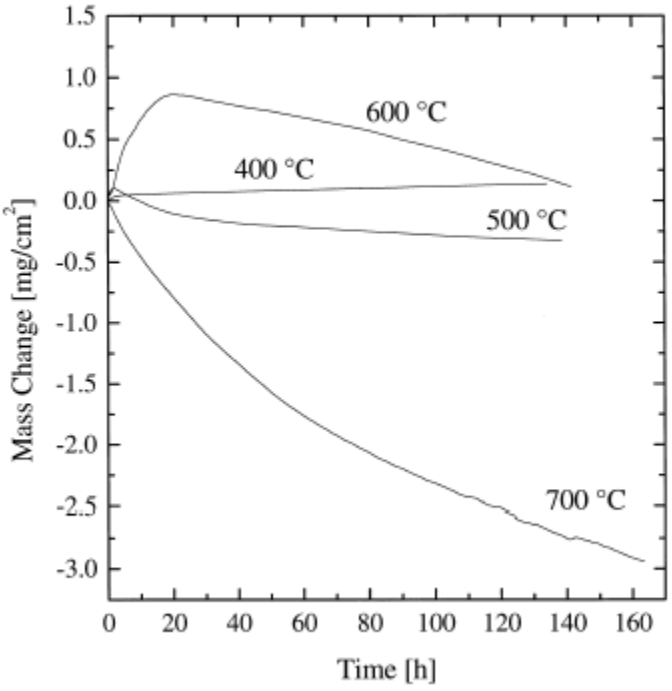

Figure 17. Thermogravimetric results for the corrosion of nickel at 400-700°C, He-5% vol.O_2, and 500 ppmV HCl [15]

3.5.2 Corrosion of Low Alloy Steels and Effect of HCl and SO_2

The corrosion of low alloy steels had been studied in laboratory scale in great detail by a number of authors [15, 18]. The following were the summaries of their findings: a) there was a strong effect of chlorine, in the form of HCl, to corrosion in low alloy steels, b) corrosion increased as temperature increased, and c) the combined effect of HCl and SO_2 in the gas may retard corrosion in low alloy steels.

Figures 18-20 [18] show the effects of SO_2 and HCl on the mass change at gas temperature of 500°C for 2.25Cr-1%Mo low alloy steel. In this laboratory experiment, the samples were pre-oxidized for several hours and a small amount of chloride-containing fly ash was placed on the oxide scale. The individual effects of HCl and sulfur were investigated. As expected, mass gain increased as the concentration of SO_2 in the gas increased (Figure 18). The effect of HCl on deposit/scale/steel sample showed considerable mass gain, and corrosion was strongly enhanced by the presence of HCl (Figure 19).

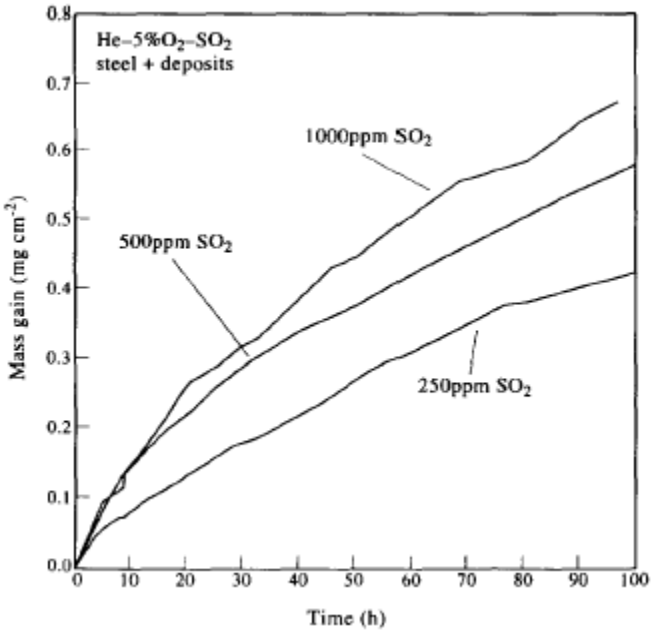

Figure 18. Effects of SO_2 on the mass gain at 500°C in presence of fly ash deposit [18].

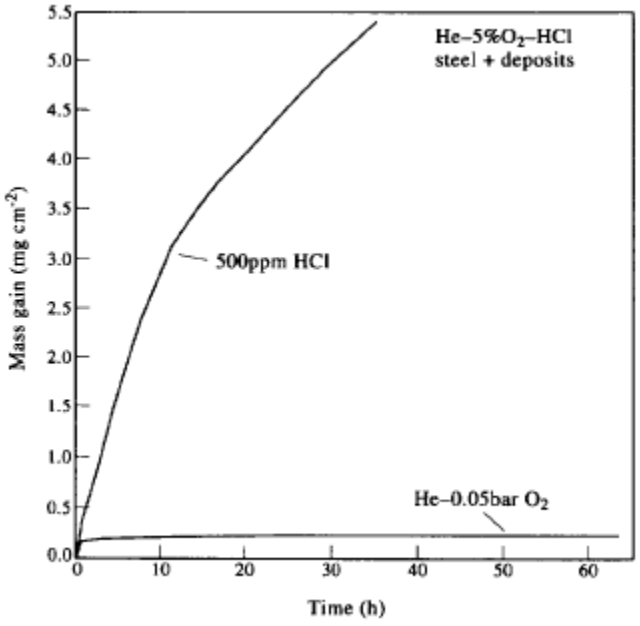

Figure 19. Effect of HCl in gas on mass gain of low alloy steels at 500°C in the presence of fly ash.

The combined effects of HCl and SO_2, in the presence of fly ash deposit, on the corrosion of the steel are shown in Figure 20. The mass gain caused by HCl was clearly decreased by the presence of SO_2 in the atmosphere. As discussed earlier, this may be

explained by assuming that the presence of SO_2 in the gas, the conversion of HCl to Cl_2 at the deposit/scale interface is reduced and thus less chlorine gas is available to diffuse through the scale to the scale/metal interface.

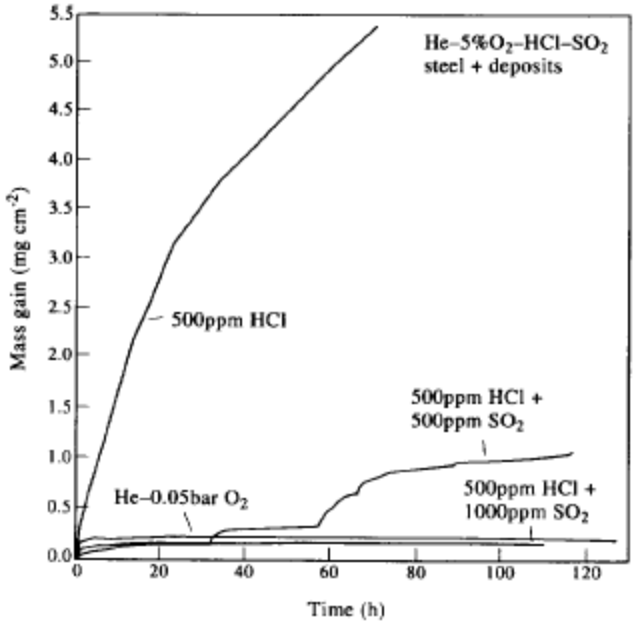

Figure 20. Effects of SO_2 and HCl in gas on the mass gain of low alloy steel at 500°C in the presence of fly ash deposit [18]

3.5.3 Corrosion in High Alloy Steels and Nickel-containing alloys

Grabke et al. [18] conducted thermogravimetric studies on the oxidation of high alloy steels, a 12%CrMoV-steel and a 25%Cr-20%Ni-steel, at 700°C by pre-oxidizing the steels and then depositing NaCl on the oxide [18]. The chemical compositions of these alloys are shown in Table 10. As in the case of low alloy steel, an immediate strong acceleration of the mass gain rate was observed (Figure 21). The oxide scale in this experiment was less adherent and porous and consisted mainly of Fe_2O_3. The phases $FeCr_2O_4$ and Cr_2O_3, which could be detected after pre-oxidation, were not found by X-ray diffraction after active oxidation. For the steels, the species that evaporated mainly was $FeCl_2$ (g), due to its higher vapor pressure than that of the chlorides of the other alloying metals. The partial oxidation of the evaporating $FeCl_2$(g) resulted in the formation of a porous non-protective scale of Fe_2O_3.

Table 10. Chemical compositions of alloys used in the laboratory experiments in % weight [18,20].

Alloys	Fe (%)	Ni (%)	Cr (%)	Others
12CrMoV	87.6	-	11.9	1.27Mo, 0.32V, 0.18C
25Cr-20Ni	51.5	20.5	25.6	1.85Si, 0.1Nb, 0.45C
Fe-15Cr	85	-	15	-
Fe-35Cr	65	-	35	-
Alloy 800	45.6	32.5	21	0.3Al,0.3 Ti
Alloy 825	30.7	40.8	22.4	Mo: 3.2, Cu: 1.9
Alloy 600	8.3	75.7	16	-

The 20Cr-12Ni steel showed comparatively very rapid active oxidation. This may be explained by the fact that after pre-oxidation, this steel has formed only a very thin oxide layer as compared with 25Cr-20Ni, which had an oxide layer about five times thicker. The thicker oxide layer has an advantage regarding susceptibility against the chlorine-induced active oxidation, since the rate controlling process, i.e. the evaporations and diffusion through the scale and evaporation of metal chloride is inversely proportional to the thickness of the scale.

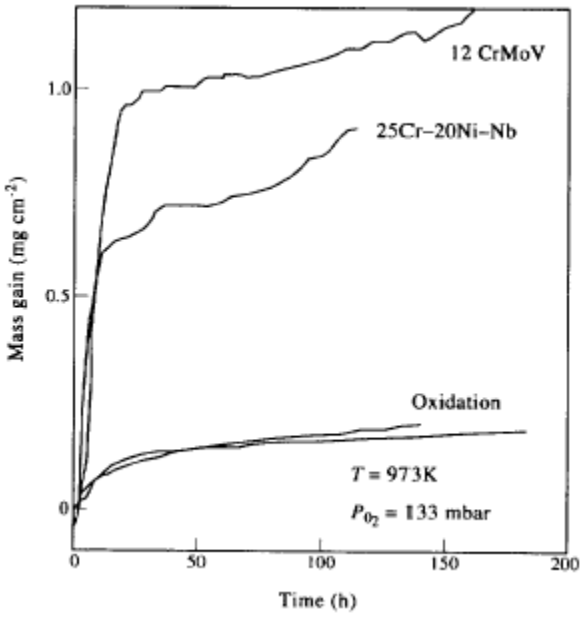

Figure 21. Mass gain of high alloy steels in He-O_2 at 700°C of 12 CrMoV-steel and 25Cr-20Ni-steel [18].

Figures 22 and 23 are logarithmic plots of the mass changes of different types of iron-chromium alloys and nickel-containing alloys with time of exposure in N_2-5% O_2 and 500 ppmV HCl gas in the temperature range of 400-700°C as reported by Zahns et al. [15]. The results showed that the corrosion of iron-chromium alloys, Fe-15Cr and Fe-35Cr, was strongly dependent on the temperature and little on the HCl content. At low temperatures, (400-500°C), very small mass gains were observed for 500 and 1500 ppmV HCl. Protective Cr_2O_3 layers were formed which were locally destroyed by the outgrowth of solid metal chlorides, i.e. $FeCl_2$ and $CrCl_2$.

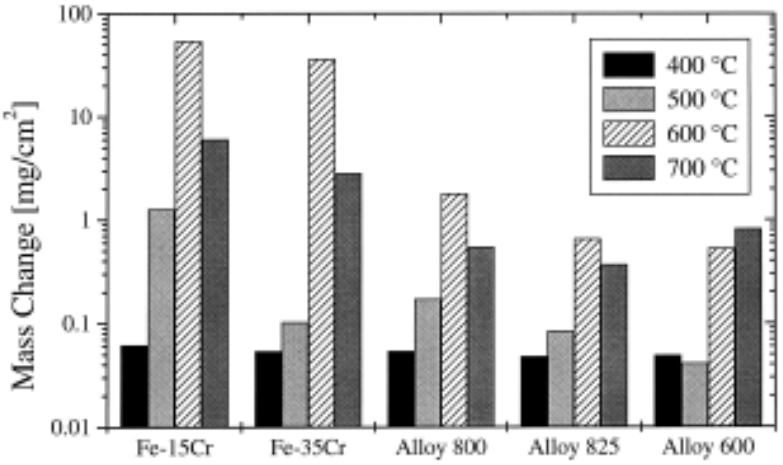

Figure 22. Mass changes of the alloys investigated after 168 hr exposure in N_2-5% vol. O_2 plus 500 ppmV HCl at 400-700°C, presented in logarithmic plot [15]

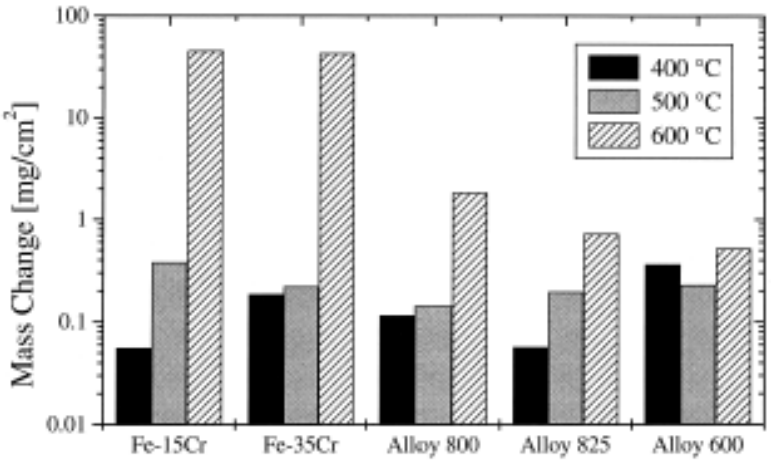

Figure 23. Mass changes of the alloys investigated after 168 hr exposure in N_2-5% vol. O_2 plus 1500 ppmV HCl at 400-700°C, presented in logarithmic plot [15]

At 600°C, Fe-15Cr and Fe-35Cr exhibited the highest corrosion attack due to severe active oxidation. The corrosion behavior was similar for 500 and 1500 ppmV HCl in the atmosphere. The higher chromium content did not improve the corrosion resistance. The observed corrosion mechanism was characterized by the adverse features of the corrosion behavior of both iron and chromium, formation of thick oxide scales and spalling of the scale. Frequent spalling was due to the fact that the scales consisted of multi-layered structure of oxide layers alternating either very porous or compact and was very poorly adherent at the metal/scale interface. The higher chromium content of alloy Fe-35Cr did not change the general corrosion behavior, but resulted in more compact layers that were thinner in comparison to Fe-15Cr due to decreasing iron content. At 700°C, this resulted in better corrosion resistance of the iron-chromium alloy, as shown by the lower mass gain in Figure 22. This was because the oxide scale formed were more adherent than at 600°C, with a significantly denser morphology and higher chromium content.

The corrosion of nickel containing alloys (Alloys 800, 825 and 600) demonstrated strong dependence on the nickel content. At 400°C, small mass gains were observed at 500 ppmV HCl and higher mass loss at 1500 ppmV HCl. At 500°C, evaporation of gaseous $NiCl_2$ was observed for the nickel containing alloys. On the iron rich Alloy 800, a multi-layered non-protective oxide scale formed by active oxidation; the similar case was observed in the corrosion of the Fe-15Cr where the scale consisted mainly of Fe_2O_3 or Cr_2O_3, but was much thinner. For the nickel-rich Alloy 600, mainly Ni-Cr chlorides were observed, while for increasing iron content in the alloy the formation of iron chlorides were enhanced. Overall, nickel-containing alloys have the advantage that the base metal, nickel, was relatively inert. For Ni-Fe-Cr alloy matrix, chromium and iron were reacting to chloride first. At low temperatures below 500°C, there was no formation of $NiCl_2$(s).

3.5.4 Influence of Gas Composition and of Deposits on Corrosion of Steels and Nickel-based Alloys

3.5.4.1 Beneath deposits of sulfate mixtures

The influence of gas phase composition, i.e. HCl and SO_2, on the corrosive effect of sulfate deposition on highly alloyed corrosion steels and nickel-based alloys was investigated by Spiegel [33]. In this laboratory study, exposure tests were carried out on the corrosion of several iron-based and nickel-based alloys beneath a molten mixture of $CaSO_4$-Na_2SO_4-K_2SO_4-$ZnSO_4$ in a N_2-5%O_2 atmosphere with varying additions of HCl, SO_2 and combination of HCl/SO_2. In this study, the exposure experiments were carried out at 600°C, using sulfate mixtures of 36 % (by weight) $CaSO_4$, 21%K_2SO_4, 15%Na_2SO_4, 21%$PbSO_4$, 7%$ZnSO_4$ and with different alloys as listed in Table 12. Samples were pre-oxidized in N_2-5%O_2 vol. for 5 hours at 600°C and embedded in 1.5 grams of salt mixtures. The extent of

corrosion was determined by measuring the mass loss after 360 hour of reaction after removal of the corrosion products.

The results showed that in every atmosphere, corrosion products were formed and different morphologies of the scales were detected. Figure 24 shows the summary of the results on mass loss of the samples at different atmospheres. The chemical compositions of the alloys used are listed in Table 11.

Table 11. Chemical composition (% weight) used in the exposure tests [33]

Alloys	Fe	Cr	Ni	Si	Others
2.25Cr-1Mo		2.21	-	-	0.91Mo
X 20 CrMoV 12 1		10-12	-	-	0.25-0.35V
X 5 CrNiCeNb 32 27		27.35	31.45	0.21	0.83Nb, 0.09Ce
Alloy 602 CA	9.65	25.3		-	2.13Al
Inconel 625	4.65	22.22		0.09	9.2Mo, 3.5Nb
Alloy 45 TM	22.65	27.40		2.26	0.36Mn

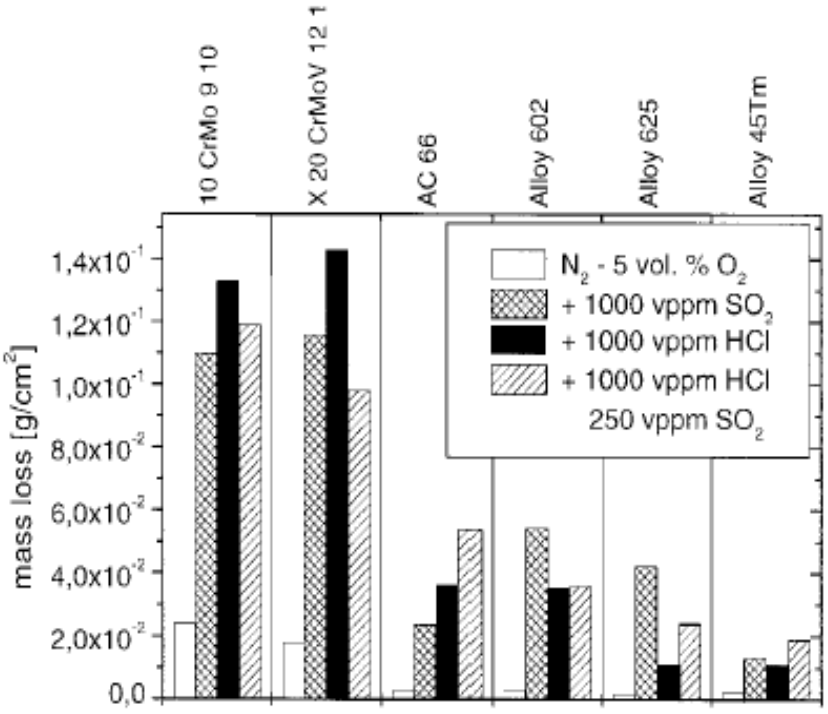

Figure 24. Mass loss in steels and nickel-based alloys in different gas atmospheres beneath molten mixture of $CaSO_4$-K_2SO_4-Na_2SO_4-$PbSO_4$-$ZnSO_4$ at 600°C after 36h exposure [33].

Effect of SO_2 addition: With the addition of 1000 ppmV (ppm by volume) SO_2, the corrosion of every alloy was enhanced as compared to the N_2-5%O_2 atmosphere (Figure 24). The following observations were made a) Separation of $CaSO_4$-K_2SO_4-Na_2SO_4-$PbSO_4$-$ZnSO_4$ melts occurred by formation of $K_2S_2O_7$ which spread underneath the Ca-rich melt, b) dissolved iron and nickel were detected in the $K_2S_2O_7$ melt; c) in the Ca-rich part, precipitates of NiO and iron oxides were formed; d) at the metal scale/interface, sulfides of iron, chromium and nickel were formed. The mechanism of formation of $K_2S_2O_7$ was discussed previously in Chapter 2. $K_2S_2O_7$ is most stable at 600°C compared to $Na_2S_2O_7$ [34]; no other known pyrosulfates are known to be stable. Nickel oxide and iron oxides were dissolved in the $K_2S_2O_7$-rich melt by acidic fluxing (reactions 37,38):

$$Fe_2O_3 + 3O_3(diss) = 2Fe^{3+} + 3SO_4^{2-} \qquad (37)$$

$$NiO + SO_3(diss) = Ni^{2+} + SO_4^{2-} \qquad (38)$$

The dissolved SO_3 was transported from the gas/melt interface to the metal scale interface via $S_2O_7^{2-}$ ions. For chromium-rich alloys, NiO and Fe_2O_3 exist in solid solution of chromium-rich spinels and may be dissolve selectively in the surface melts. The mechanism of dissolution of chromium-containing spinels in sulfates is not fully elucidated up to now [33]. The relatively poor behavior of nickel-based containing alloy under these conditions is due to the higher solubility of NiO rather than Fe_2O_3 in the form of sulfates.

Effect of HCl addition: The corrosion products on the iron-based alloys formed with the addition of HCl were similar to the corrosion products in the N_2-5%O_2 atmosphere but enhanced corrosion was observed. The enhanced corrosion attack was due to the formation of more precipitates in the melt; obviously, the solubility of the oxides was enhanced by the presence of HCl in the gas phase. For the nickel-based alloys, the mass loss is much less but was also enhanced by the HCl addition to the N_2-5%O_2 atmosphere. In comparison to the addition of 1000 ppmV SO_2, mass loss was less, and it seems that nickel-based alloys were more affected by corrosion in the SO_2 containing gas than in the HCl containing gas. In these experiments, the evaporation of volatile species was observed mainly $ZnCl_2$ and $PbCl_2$ from condensates of the furnace due to reactions (37) and (38). Because of reactions (37) and (38), the concentration of $ZnSO_4$ and $PbSO_4$ in the melt decreased:

$$ZnSO_4(l) + 2HCl = ZnCl_2(g) + H_2O + SO_2 + 0.5O_2 \qquad (39)$$

$$PbSO_4(l) + 2HCl = PbCl_2(g) + 2H_2O + SO_2 + 0.5O_2 \qquad (40)$$

The corrosion products formed with HCl addition were iron and nickel oxides in the solidified melt and inward growing, chromium rich and zinc free corrosion products. On the high alloy steel (A66) and also on the nickel-based alloys, the corrosion products contained more iron oxide, more alumina for Alloy 602A, more silica for Alloy 45TM and dissolved molybdenum for Alloy 625 as compared to absence of HCl in the gas. It was observed that

the dissolution of the metals was significantly enhanced by basic fluxing in the presence of HCl-containing gas. Due to evaporation of $ZnCl_2$, the formation of protective $ZnCr_2O_4$ was also retarded. Metal chlorides were formed at the metal/scale interface; the higher concentration of iron oxides, alumina, silica, and molybdenum oxide indicated enhanced evaporation of metal chlorides, i.e. $FeCl_2$, $AlCl_3$, $SiCl_4$, and $MoCl_3$. These metal chlorides have significant vapor pressures at 600°C [35].

Effects of both HCl and SO_2: In the presence of both HCl and SO_2 in the gas, the results showed that for low alloy steels, the mass loss was retarded in comparison to only HCl-containing gas. On the other hand, the mass loss of the AC60 and nickel-based alloys was enhanced. At the metal scale interface, more sulfides were detected than metal chlorides. Small amounts of $K_2S_2O_7$ were formed in the inner scale, containing dissolved amount of iron and nickel oxides. Thus, the nickel-containing alloys were relatively more attacked than the iron-based materials.

3.5.4.2 Alloys beneath deposits of chloride mixtures

The corrosion of alloys under chloride deposits was also investigated by different authors [34,36]. Li et al. investigated the effects of $ZnCl_2$-KCl on several iron-based alloys with different chromium content. As expected, the corrosion rates were heavy accelerated once the alloys were covered by the $ZnCl_2$-KCl deposits and a rapid formation of thick and porous oxide was observed. The enhanced corrosion was mainly induced by the presence of molten salts with fluxing of the oxide scale likely responsible for the fast degradation. Under the low oxygen partial pressure established at the salt/metal interface, the iron oxide may dissolve the salt forming soluble chlorides, e.i.,$FeCl_2$, according to reaction (41). The dissolved iron chloride and the oxide ions then diffuse outward through the molten salt to the salt/gas interface, where Fe_2O_3 precipitates and forms an oxide scale that is porous non-protective.

$$Fe_3O_4 + 6Cl^- = 3FeCl_2(diss) + 3O^- + 0.5O_2 \qquad (41)$$

It was found from this study that the higher chromium content of the iron-based alloy did not provide effective protection from the chlorine-containing deposits. Similar results have also been reported in the literature [35, 37,38]. In an examination of the hot corrosion behavior of NaCl-coated two phase stainless steels, Shinata et al [37] found that chromium content was always oxidized selectively and formed non-protective scales, and that corrosion increased with increasing chromium content. As discussed previously, studies by Zahs et al. found that increasing chromium content did not lead to better corrosion resistance and that 15%Cr and 35%Cr were covered with a thick and porous scale, which was very poorly adherent at the metal/scale interface and exhibited frequent spalling [35].

Li and Spiegel [34] investigated the effects of using iron-aluminum and nickel aluminum alloys to provide protection from both chlorine and sulfur containing

atmospheres. As discussed previously, nickel-based alloys suffer less corrosion by chlorine but are susceptible to accelerated corrosion in environments of high sulfur. High Cr alloys seem also less effective in chlorine-containing environment. Figure 25 shows the mass loss of the different alloys (Table12) covered by a molten $ZnCl_2$-KCl deposit at 400°C.

Table 12. Nominal Chemical composition of alloys tested (in % weight) [34]

	Fe	**Al**	**Ni**	**Others**
NiAl	-	50	50	
Fe-10Al	90	10	-	-
Fe-20Al	80	20	-	-
Fe-45Al	55	45	-	-
P91	89.8	-	0.26	8.6Cr, 0.93Mo, 0.41Mn

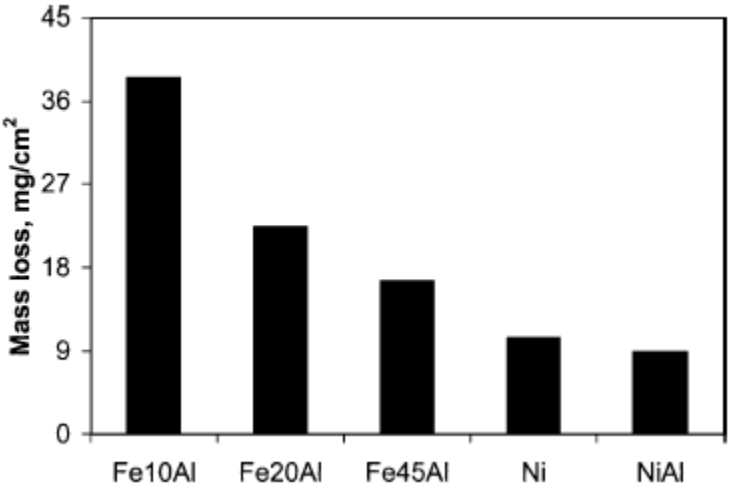

Figure 25. Mass loss of alloys exposed in a $ZnCl_2$-KCl melt in air for 340h at 400°C [34]

It can be seen that the NiAl suffered a small mass loss, while increasing the Al content in the Fe-Al alloy resulted in a smaller mass loss. The two lowest Al-content iron-aluminum alloys, Fe-10%Al and Fe-20%Al, form similar corrosion products, mainly a very thick and porous mixture of oxides, chlorides and pure metal. The external scale consisted of Fe_2O_3 and some KCl and metallic zinc. Fe-45%Al, more metallic zinc particles were produced at the gas/scale interface and a multi-layered scale of iron oxide was not formed in the innermost zone; instead, there was a thin interface layer, depleted in aluminum, was detected near the alloy/scale interface. The metal loss and the composition of the corrosion products of Ni and Ni-Al were different from the Fe-Al alloys under the same conditions. Pure Ni experienced rapid corrosion at 400 and 450°C and formed a porous NiO scale on

the surface. On Ni-Al, at 400°C, the composition of the outmost layer was not uniform and was mainly composed of metallic zinc particles, KCl and a complex mixture of aluminum oxide and KCl. Nickel oxide was not detected in the external corrosion products on the NiAl alloys.

Since the $ZnCl_2$-KCl_2 salt used in the study was in the molten state at the reaction temperatures, the metal was attacked by the chloride melt, due to fluxing of the protective oxide. The fluxing mechanism that describes the corrosion process for aluminum-free alloys is shown in reactions (42- 45).

$$2ZnCl_2(l) + 2Fe_2O_3 + O_2 = 2ZnFe_2O_4 + 2Cl_2(diss) \quad (42)$$

$$ZnCl_2(l) + 0.5O_2 = ZnO + Cl_2(diss) \quad (43)$$

$$Fe + 3Cl_2(diss) = 2FeCl_3(diss) \quad (44)$$

$$2FeCl_3(diss) + 1.5O_2 = Fe_2O_3 + 3Cl_2 \quad (45)$$

Reaction (42) is the reaction of zinc chloride with the oxide and reaction (43) is direct oxidation of zinc chloride and the gas phase. By these reactions, zinc chloride in the melt are consumed while free chlorine is released and dissolves into the salt, and then acts as an oxidant for iron, resulting into the soluble $FeCl_3$ (44). The dissolved $FeCl_3$ diffuses outwards through the molten salt to the salt/gas interface, where Fe_2O_3 is precipitated again. As previously discussed, the oxide scale formed in this case is porous and adheres poorly, thus providing no effective protection of the metal surface.

The presence of metallic zinc on the surface of the Al-bearing materials indicates different corrosion mechanism that is described by reactions (46-47):

$$2Al + 3ZnCl_2(l) = 3Zn(l) + 2AlCl_3(l,g) \quad (46)$$

$$2AlCl_3(l,g) + 1.5O_2 = Al_2O_3 + 3Cl_2 \quad (47a,b)$$

At the beginning of the corrosion process, the chloride is more stable than Zn (Figure 26), and a displacement reaction takes place between $ZnCl_2$ in the melt and the alloy (equation 46). From an electrochemical point of view, Zn^{+2}(from $ZnCl_2$) is the oxidant for metallic Al. This is in contrast to other metals such as Cr, Fe and Ni, where a dissolved gas (O_2 or Cl_2) is the oxidizing agent [34]; after reaction (46), the $AlCl_3$ can be oxidized to Al_2O_3 (reaction 47). However, most of the $AlCl_3$ escapes into the gas atmosphere due to its very high volatility (T_m=178°C). Some of the aluminum is retained beneath the oxide layer in the form of oxide and chloride.

The above study concluded that the corrosion resistance of the alloys can be improved by large addition of aluminum. For Ni-Al, the corrosion process in the very early stages was very similar to that of Fe-Al alloys, i.e. displacement of $ZnCl_2$ by $AlCl_3$ and

formation of metallic zinc. However, in comparison to iron and aluminum, nickel is more resistant to chlorine attack in this temperature and thus, it remains in metallic scale at the metal/scale interface. As chlorine penetrates the scale, aluminum was selectively removed from the alloy as aluminum chloride ($AlCl_3$). The chloride was transformed into aluminum oxide as it diffused outward. This oxidation reaction occurs at relatively low oxygen pressures, thus, alumina can form within the pores of the metallic nickel. Therefore, the presence of a continuous, aluminum oxide precipitation zone in the Ni-Al matrix, or the metal/scale interface, impedes diffusion of chlorine and retards the corrosion rate.

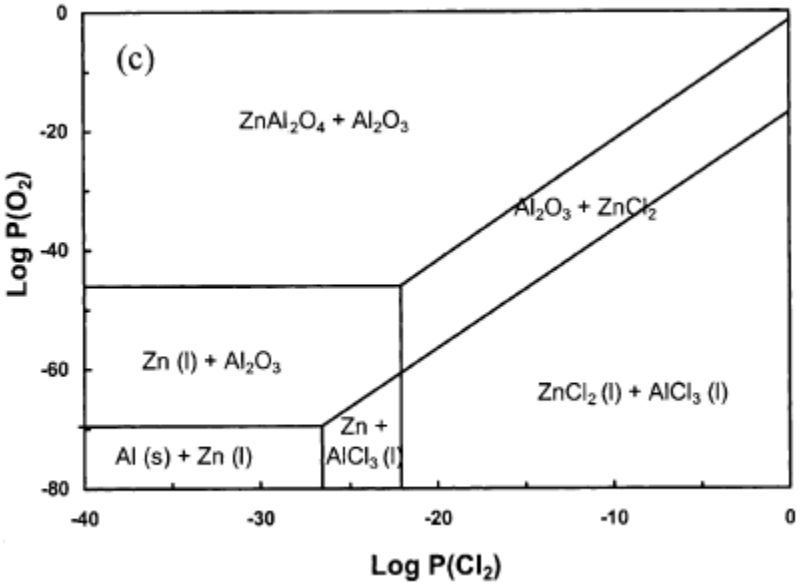

Figure 26. Phase stability diagram for Al-Zn-O_2-Cl systems at 450°C [34].

3.5.5 Development of New Alloys Based on High [Cr+Ni+Mo] Content

A number of studies were carried out to find the best combination of metals for producing the best alloy that minimizes corrosion in the boiler tubes of waste-to-energy facilities. Alloys consisting of proportionately large amounts of chromium (Cr), nickel (Ni), or molybdenum (Mo), elements with corrosion resistant properties, were evaluated to develop new types of austenitic steels. In determining the composition range of the alloy, a number of factors must to be considered: a) high-temperature structural stability, b) high temperature strength, c) hot workability and d) weldability. Tables 13 and 14 list the chemical composition of the conventional and newly developed alloys in field corrosion tests [29].

Table 13. Chemical Composition (Ni+Cr+ Mo Content)[29]

Material	Composition	Ni +Cr +Mo Content (wt %)
Conventional Tubing		
SA213-T22 (UNS K21590)	2.25% Cr-1% Mo	3.16
TP347H (UNS S34709)	18%Cr, -12%Ni-Nb	30.2
310HCbN (UNS 31042)	25%Cr-20%Ni-Nb	45
SB444 (Alloy 625)(UNS No6625)	21%Cr-9%Mo-4%Mb-62%Ni	93.9
HR11N	30%Cr-40%Ni-1%Mo-N	69.9
Hastelloy (UNS No6022)	21%Cr-13%Mo-59%Ni-W-Fe	91.9
New Tubing		
HR30M	30%Cr-28%Ni-1%Mo-N	59.5
JHN24	20%Cr-18%Mo-58%Ni-Nb	96.5
Weld Overlay Tubing		
625M	21%Cr-9%Mo-625Ni	94
C-726M	20%Cr-13%Mo-W, Co, Fe-57%Ni	89.1

Table 14. Chemical Composition of Alloys [29]

Material	C	Si	Mn	P	S	Ni	Cr	Mo	Fe	Al	W	Co	Nb	N	Ti
Conventional tubings															
SA213 -T22	0.10	0.32	0.49	0.013	0.002	–	2.21	0.95	Bal.	–	–	–	–	–	–
TP347H	0.09	0.44	1.50	0.021	0.001	12.0	18.2	–	Bal.	–	–	–	0.80	–	–
310HCbN (HR3C)	0.06	0.40	1.28	0.013	0.001	20.3	24.7	–	Bal.	–	–	–	0.44	0.23	–
SB444 (Alloy 625)	0.03	0.19	0.24	0.001	0.001	64.3	21.1	8.5	1.5	0.28	–	< 0.1	3.44	–	0.28
HR11N	0.004	0.51	0.52	0.012	0.001	39.7	28.9	1.0	Bal.	–	–	–	–	0.12	–
Hastelloy C-22[1]	0.005	0.03	0.06	0.01	< 0.01	Bal.	21.5	13.3	4.3	–	3.0	1.0	–	–	–
New tubings															
HR30M	0.016	0.51	0.53	0.011	0.001	30.4	28.1	1.0	Bal.	0.06	–	–	–	0.15	–
JHN24	0.003	< 0.01	0.01	0.002	< 0.001	Bal.	20.2	18.2	2.6	0.2	–	< 0.01	0.64	–	–
Weld overlay tubings															
625M	0.009	0.17	0.08	0.005	0.008	Bal.	21.1	8.5	3.7	–	–	1.4	–	–	–
C-276M	0.009	0.20	0.15	< 0.001	0.002	Bal.	19.7	12.7	2.8	–	1.82	2.4	–	–	–

The relation between the concentration of chromium-nickel-molybdenum in the alloys and the maximum corrosion thickness was evaluated by means of several field corrosion tests in waste-to-energy facilities in Japan. The results demonstrated that despite differing conditions of facilities, the combined effect of each alloyed element showed similar tendencies in each facility. Figure 27 shows the relation between maximum thickness loss and combined Cr, Ni and Mo concentration of superheater tubes on three waste-to-energy plants in Japan. The figure shows the results of tests conducted on different alloys in these plants at 450°C and 550°C and exposure times, i.e. 700 and 3000 hours.

The following were the results observed in these field corrosion tests:

a) At 550°C, the wastage rate (loss of thickness) tended to decrease as the content Cr-Ni-Mo increased. Cr-Ni-Mo combination seems to act effectively to both gaseous and deposit-induced corrosion.

b) At 450°C, there was little difference in corrosion resistance for the range of approximately 30%-70% in Cr-Ni-Mo content. This may due to the fact that at this temperature the amount of molten phases in the deposit was small.

c) An increase in Mo content reduces the corrosion rate, as shown in Figure 28.

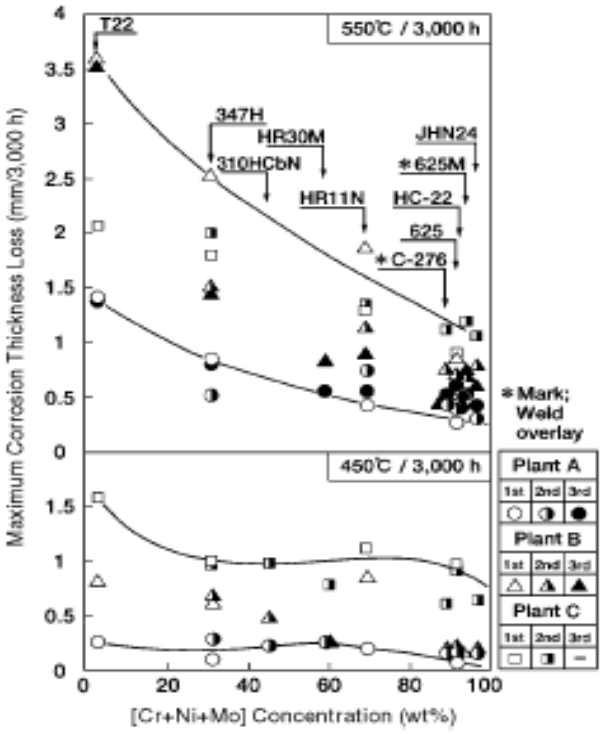

Figure 27. Relationship between maximum thickness loss and combined Cr-Ni-Mo concentration of alloys after 3000-hour test [29].

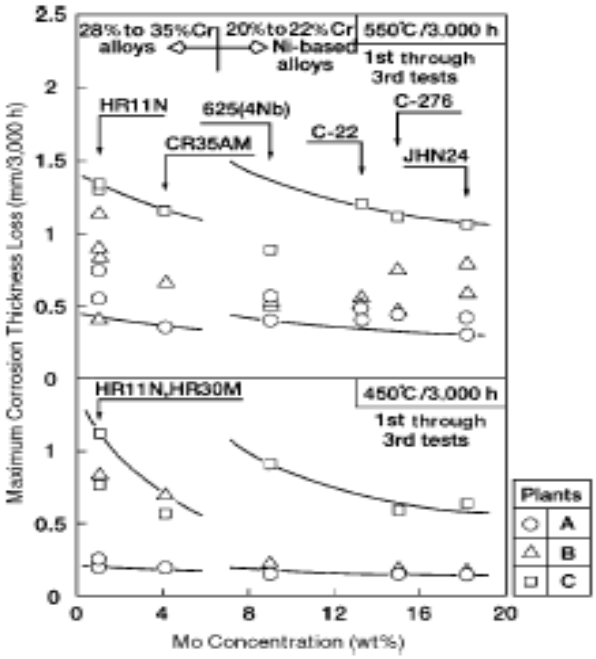

Figure 28.Relation between maximum corrosion thickness loss and Mo concentration [29].

3.6 Summary

The prevailing methods of protection from high temperature corrosion of boiler tubes in waste-to-energy facilities were presented in this chapter. Current methods of protection used are: by refractory shielding, i.e. silicon carbide tiles covering the waterwall tubes in the flame zone of the combustion chamber, and the use of nickel-based alloys, in particular, Alloy 625 (Inconel 625). Nickel-based alloys are applied as surface coating in the waterwalls; either solid tube or weld-overlay on superheater tubes. Highly nickel-alloyed steels are also used by some facilities as base metals both in waterwalls and superheater tubes. Alternatively, an alloy 625 weld-overlay is added on the base metal tubes.

The results of laboratory studies and field corrosion tests were presented in this chapter. In particular, the results of studies by Prof. Grabke, Dr. Spiegel and Dr Zahs, all from Max Plank Institute for Eisenforschung GmbH, were discussed in detail. Several field corrosion tests done in WTE facilities in Japan were also presented and discussed.

To summarize, the following suggestions were made to come up with the best method of protection for corrosion in WTE facilities depending on the corrosion environment:

1. For relatively high-chlorine containing environment in the furnace and in the passes where the primary and secondary or final superheaters were located, high nickel-based alloys may be used. Nickel-based alloys, i.e. Alloy 625 and 825, are resistant to high chlorine-containing environment but susceptible to attack in relatively high-sulfur containing environment. For the waterwall, where the metal temperatures reach only 300°C, high nickel-chromium steel as a base metal can be used. For high HCl atmospheres and high chlorine deposits, highly alloyed steel rich in nickel can be used. Similarly, in waterwalls where sulfate deposits are dominant, highly alloyed steel rich in chromium can be used. It is noted that as long as heat flux to the waterwall is such that temperatures are maintained below 450°C, high temperature active oxidation will not occur, and the protective oxide scale will be flux by molten chlorides.
2. For relatively high sulfur containing environment, in the furnace and the passes where the primary, secondary or final superheaters are located, the use of alloys with sufficient amount of chromium should be recommended. Chromium-rich alloys seem to favor better protection from high sulfur-containing gases. On the waterwall, iron-chromium alloys can be used for protection from deposits where sulfates are dominant.
3. For atmospheres were both sulfur and chlorine are relatively high, in the furnace and the passes where the superheaters are located, field corrosion tests suggest that a combination of high nickel-chromium-molybdenum alloys provide better corrosion protection. It should be noted that the presence of sulfur in the gas phase may retard corrosion for high-alloyed steels but accelerate corrosion in alloys with relatively high nickel content rather than chromium. Thus, on the waterwalls, the use of high chromium-iron based alloy as a base metal can provide protection from the sulfate deposits and retard of corrosion due to presence of sulfur in gas. The use of a nickel-rich weld overlay will also provide protection from deposits rich in chlorides.

The design problem is to find the percentage (%) share of metals that resemble the best possible combination of alloying elements. Finding the right combination can be done either by laboratory scale analyses and field corrosion tests if applicable. Also, in the opinion of the author, knowing the corrosion environment in the facility is the first step in solving the problem; thus, knowledge of the essential composition of the potential deposit, i.e. the composition of the fly ash attaching the tube, is an integral part of solving the problem. Secondly, efforts should be made to at least estimate the range of metal temperatures of both the waterwalls and superheaters during normal operation before making a choice of alloy in the tubes. Generic use of nickel-containing alloys prevailing in the present maintenance practice may be unnecessary in some environment, not to mention its relatively higher cost as compared to highly alloyed steels, i.e. iron-

chromium, iron-nickel or iron-aluminum, if applicable. Suggestions for desirable combinations of alloy compositions for a specific corrosion environment are shown in Figure 29.

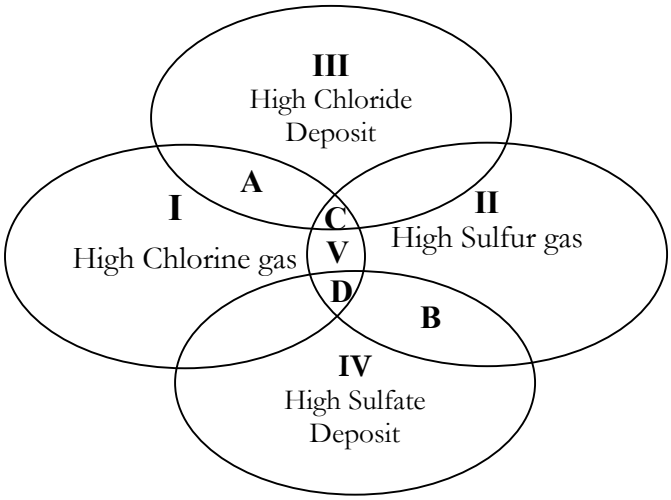

Figure 29. Proposed alloy combination based on prevailing corrosion atmosphere for water wall and superheater tubes.

For Waterwall:

Regions	Suggested alloy combinations
I (High chlorine containing gas)	Nickel-alloyed steels
A (High chlorine gas-high chloride deposit)	Nickel-alloyed base metal, nickel-based overlay
II (High sulfur containing gas)	Chromium rich alloy steels
B (High sulfur-hi sulfate deposit)	Chromium rich alloy steels
III (High chloride deposit)	Nickel-based alloys
IV (High sulfate deposit)	Chromium-based alloys
V (High chlorine-high sulfur gas)	High nickel-high chromium steels
C (High chlorine-high sulfur gas and chlorine deposit)	High nickel-chromium-molybdenum alloys
D (high-chlorine-sulfur gas and sulfate deposits)	High chromium steels with nickel-based overlay

For Superheaters:

Regions	Suggested alloy combinations
I (High chlorine containing gas)	Nickel-based alloys
A (High chlorine gas-high chloride deposit)	Nickel-based alloys
II (High sulfur containing gas)	Chromium-based alloys
B (High sulfur-hi sulfate deposit)	Chromium-based alloys
III (High chloride deposit)	Nickel-based alloys
IV (High sulfate deposit)	Chromium-based alloys
V (High chlorine-high sulfur gas)	High nickel-higher chromium alloys
C (High chlorine-high sulfur gas and chlorine deposit)	High [Ni+Cr+Mo] content alloy
D (high-chlorine-sulfur gas and sulfate deposits)	High [Ni+Cr+Mo] content alloy

3.7 Thermodynamic Calculations

Tabulations of heats of reaction formation and equilibrium constants presented in this chapter are listed. The calculations were done using HSC Chemistry software [25].

$2ZnSO_4$ (l) + 4HCl(g) = $2ZnCl_2$ (g) + $2H_2O$ (g) + $2SO_2$ (g) + O_2 (g) **(39)**

T C	H kcal	S cal/K	G kcal	K	Log(K)
0	162.6	148.3	122.1	2.00E-98	-97.7
100	159.9	139.9	107.7	8.06E-64	-63.1
200	157.5	134.2	94.0	3.66E-44	-43.4
300	155.4	130.1	80.8	1.50E-31	-30.8
400	153.4	126.9	68.0	8.44E-23	-22.1
500	151.6	124.5	55.4	2.16E-16	-15.7
600	150.0	122.4	43.1	1.65E-11	-10.8
700	148.4	120.7	30.9	1.14E-07	-6.9
800	146.8	119.2	18.9	1.39E-04	-3.9
900	145.3	117.8	7.1	4.79E-02	-1.3
1000	143.9	116.7	-4.6	6.26E+00	0.8

$2PbSO_4$ (l)+4HCl(g)= $2PbCl_2$(g)+ $2H_2O$(g) +$2SO_2$(g)+O_2 (g) (40)

T C	H kcal	S cal/K	G kcal	K	Log(K)
0	177.7	175.4	129.8	1.42E-104	-103.8
100	172.9	160.6	113.0	6.23E-67	-66.2
200	168.5	149.9	97.5	8.84E-46	-45.1
300	164.2	141.8	83.0	2.30E-32	-31.6
400	160.2	135.3	69.1	3.60E-23	-22.4
500	156.3	129.8	55.9	1.60E-16	-15.8
600	152.5	125.2	43.1	1.60E-11	-10.8
700	148.7	121.1	30.8	1.20E-07	-6.9
800	145.0	117.5	18.9	1.43E-04	-3.8
900	141.4	114.3	7.3	4.38E-02	-1.4
1000	137.8	111.4	-4.0	4.84E+00	0.7

$2AlCl_3$ (l) + $1.5O_2$ (g)=Al_2O_3 + $3Cl_3$ (g) (47a)

T C	deltaH kcal	deltaS cal/K	deltaG kcal	K	Log(K)
0	-77.2	18.4	-82.3	6.59E+65	65.8
100	-79.9	10.1	-83.6	9.91E+48	49.0
200	-82.1	4.9	-84.4	9.54E+38	39.0
300	-84.0	1.2	-84.7	1.95E+32	32.3
400	-85.8	-1.7	-84.6	3.04E+27	27.5
500	-87.5	-4.1	-84.4	7.02E+23	23.8
600	-89.2	-6.1	-83.8	9.72E+20	21.0
700	-90.8	-7.8	-83.1	4.72E+18	18.7
800	-92.3	-9.4	-82.3	5.73E+16	16.8
900	-93.9	-10.7	-81.3	1.39E+15	15.1
1000	-95.4	-12.0	-80.1	5.72E+13	13.8

$2AlCl_3$ (s) + 1.5O_2 (g)=Al_2O_3 + 3Cl_3 (g) (47b)

T C	H kcal	S cal/K	G kcal	K	Log(K)
0	-121.0	-51.5	-107.0	3.96E+85	85.6
100	-121.2	-51.9	-101.8	4.21E+59	59.6
200	-121.0	-51.6	-96.6	4.25E+44	44.6
300	-120.7	-51.0	-91.5	7.65E+34	34.9
400	-120.3	-50.4	-86.4	1.14E+28	28.1
500	-119.9	-49.8	-81.4	1.03E+23	23.0
600	-119.4	-49.2	-76.4	1.37E+19	19.1
700	-119.0	-48.7	-71.5	1.17E+16	16.1
800	-118.4	-48.2	-66.7	3.85E+13	13.6
900	-117.9	-47.7	-61.9	3.42E+11	11.5
1000	-117.3	-47.3	-57.2	6.49E+09	9.8

CHAPTER 4

Corrosion Kinetics, WTE Emissions and the Effects of HCl and SO_2 to Corrosion

4.1 Introduction

In this chapter the kinetics of high temperature corrosion are discussed. Three different kinetic models are discussed in detail to understand the growth of the oxide scale with time. This section on kinetics is aimed to provide an understanding how to control the rate-determining step in order to minimize corrosion. This chapter also examines the concentrations of HCl and SO_2 encountered in the combustion gases of WTE and coal-fired power plants as well as the respective emissions of these two types of plants. The purpose of the comparison is to see the relative differences between emissions of modern WTE technology to that of the dominant technology for electricity generation. The impact of MACT (Maximum Achievable Control Technology) to emissions from WTE is also examined.

4.2 Corrosion Kinetics

4.2.1 Basic Kinetics Principles [10]

Three basic kinetic laws have been used to characterize the oxidation rates of pure metals namely: 1) the parabolic rate law, 2) logarithmic rate law and 3) linear rate law and catastrophic oxidation.

The parabolic rate law (equation 48) assumes that the diffusion of metal cations or oxygen anions is the rate-controlling step and is derived from Fick's first law of diffusion. The concentrations of diffusing species at the oxide-metal and oxide-gas interfaces are assumed to be constant. The diffusivity of the oxide layer is also assumed to be invariant. This assumption implies that the oxide layer has to be uniform, continuous and of the single phase type. The diffusion rate constant, k_p, changes with temperature according to an Arrhenius type relationship:

$$x^2 = k_p t + x_0 \qquad (48)$$

where x = *oxide film thickness* (*or mass gain due to oxidation*, *which is proportional to oxide film thickness*)

t = *time*

k_p= *diffusion rate constant (directly proportional to diffusivity of ionic species that is the rate controlling step)*

x_o=*constant*

The logarithmic rate law (equation 49) is an empirical relationship, that has no fundamental underlying mechanism. This law is mainly applicable to thin oxide layers formed at relatively low temperatures and therefore is rarely applicable to high temperature engineering problems.

$$x = k_p \log(ct + b) \qquad (49)$$

where: k_p =rate constant, and c and b are constants

The linear rate law (equation 50) is also an empirical relationship that is applicable to the formation and build-up of a non-protective oxide layer:

$$x = k_L t \qquad (50)$$

where k_L = constant

In general, high temperature oxidation rate decreases with time (parabolic behavior), due to an increasing oxide thickness acting as a stronger diffusion barrier. However, due to the formation of highly porous, poorly adherent or cracked non-protective oxide layers, corrosion rates may remain linear. Metals with linear oxidation kinetics at a certain temperature have a tendency to undergo so-called catastrophic oxidation (also referred to as breakaway corrosion) at higher temperatures. In this case, a rapid exothermic reaction occurs on the surface, which increases the surface temperature and the reaction rate even further. Metals that may undergo extremely rapid catastrophic oxidation include molybdenum, tungsten, osmium, rhenium and vanadium, associated with volatile oxide formation. In the case of magnesium, ignition of the metal may even occur. The formation of low-melting point oxidation products (eutectics) on the surface has also been associated with catastrophic oxidation. The presence of vanadium and lead oxide contamination in gases deserves special mention, as they pose a risk to inducing extremely high oxidation rates.

4.2 Reaction Kinetics (soon to follow)

4.3 WTE Emissions and its Effects to Corrosion

From a corrosion point of view, higher concentrations of hydrogen chloride (HCl) and Sulfur Dioxide (SO_2) in the flue gas enhance corrosion. In this section, WTE concentrations reported by various WTE facilities taken from actual operating data are presented.

4.3.1 HCl and SO_2 Emissions in WTE Facilities

Hydrogen Chloride (HCl) and sulfur dioxide (SO_2) concentrations in the combustion gas of different WTE facilities are shown in Tables 15 and 16. For confidentiality reasons, the names of the facilities are not shown. For statistical analyses, mean and standard deviation from the mean of the concentrations of HCl and SO_2 are also presented in the tables. Based on the hydrogen chloride data analyzed, it was estimated that furnace HCl

concentrations in the facilities were as low as 356 parts per million (ppmV) by volume at 7%O_2, and as high as 811 ppmV, with the mean interval and standard deviation at 620±125 ppmV. It is noted that 70% of the facilities with HCl data analyzed fall within one standard deviation. It must also be noted that both the HCl and SO_2 concentrations reported are for the combustion gases before the Air Pollution Control (APC) System. In the APC, an estimated 98% of the HCl and SO_2 content of the gas are removed by means of dry or wet scrubbing and bag filters or by electrostatic precipitators.

As shown in Table 16, it was estimated that sulfur dioxide concentrations of the different facilities were as low as 24 ppmV at 7% O_2 and as high as 147 ppmV with the mean and standard deviation at 71 ± 35 ppmV SO_2. The SO_2 concentration is approximately an order of magnitude lower as compared to the concentration of HCl in the furnace, which means that the facilities analyzed were more of a chlorine-containing environment. It is also noted that 70% of the facilities where SO_2 concentrations were obtained, fall within the mean and one standard deviation.

Table 15. Actual furnace Hydrogen Chloride concentration in combustion gases of WTE facilities before the Air Pollution Control System.

Facility	**HCl (in ppmV at 7 % O_2)**	
	Mean	**SD**
1	811.5	±310.6
2	799.9	±207.1
3	753.8	±128.3
4	745.0	±114.5
5	743.7	±108.8
6	742.7	±73.3
7	713.0	±99.5
8	696.0	±50.9
9	675.0	±88.8
10	674.0	±119.0
11	653.6	±123.7
12	626.0	±59.6
13	624.1	±115.0

14	623.8	±102.1
15	617.5	±89.7
16	599.0	±34.7
17	591.1	±26.2
18	570.3	±96.9
19	540.9	±100.0
20	499.0	±28.3
21	485.0	±17.0
22	413.8	±89.1
23	402.5	±44.2
24	356.3	±40.4
Mean	620	±125

Table 16. Furnace Sulfur Dioxide concentration in combustion gases of WTE facilities before the Air Pollution Control System.

Facilities	**SO_2 (in ppmV at 7 %O_2)**	
	Mean	**SD**
1	146.2	±27.0
2	129.9	±21.5
3	125.0	±38.3
4	118.6	±23.7
5	103.5	±48.6
6	81.1	±1.2
7	73.5	±4.9
8	70.8	±30.4

9	66.7	±15.3
10	57.8	±26.5
11	57.3	±16.5
12	56.5	±13.7
13	51.5	±18.1
14	50.2	±24.0
15	49.3	±12.8
16	47.3	±10.2
17	44.0	±9.2
18	36.7	±4.5
19	30.2	±14.6
20	23.9	±13.7
Mean	71.0	±35.3

4.4 WTE Emissions in Comparison with Coal-fired Plants

As part of the 1990 Clean Air Act mandates, EPA promulgated in 1995 new air pollution control standards for large WTE facilities. These standards require facilities to implement the Maximum Available Control Technology (MACT). The 1995 MACT standards apply to facilities with large units, i.e. that combust more than 250 tons of MSW each day. This section presented the impact of MACT to WTE emissions, and for comparison purposes, the emissions were compared to emissions from coal-fired plants. Utilization of coal to produce electricity is the principal fuel in the US where approximately 90% of the one billion tons of coal produced in the US is burned to generate electricity.

Data of the emissions from waste-to-energy and coal-fired power plants were compared in two ways: 1) on the basis of thermal energy input and electrical energy output and using nationwide data 2) by actual WTE facilities data.

4.4.1 WTE vs. Coal-fired Power Plants in thermal energy input and electrical energy output

4.4.1.1 Emissions Estimates Methodology

Emission estimates from coal-fired plants and WTE facilities are presented on the basis of thermal energy input (lb/million BTU) and electrical energy output (g/kWh). Except for trace elements (i.e. cadmium, lead and mercury) where emission factors from different combustion control technologies were available, all emissions presented are nationwide estimates. Data for total emissions [40], total energy input [41], and electrical energy output [42] were used as the basis for calculating nationwide estimate of emissions for coal-fired power plants.

In estimating the emissions from WTE facilities, estimates were made on the yearly average operating time of the units, nationwide estimate of the total waste combusted, average heating value of the waste and total electrical energy output. In the calculation of emission factor, a 310 days/year operating time, heating value of 10,500 BTU/kg feed and an electrical output of 2,600 MW were used. All data are estimates obtained from approximately 170 WTE units larger or equal to 250 tons/day feed input.

4.4.1.2 Sulfur Oxides Emission

Gaseous sulfur oxides from coal combustion are primarily sulfur dioxide (SO_2), plus a much smaller quantity of sulfur trioxide (SO_3) and gaseous sulfates. These compounds form as the organic and pyritic sulfur in coal are oxidized during the combustion process. On the average, about 95% of the sulfur present in bituminous coal is emitted as gaseous SO_x whereas somewhat less of sulfur is volatilized when sub-bituminous coal is fired [42].

Emissions of sulfur dioxide from coal-fired plants were reduced from 13.8 million tons in 1990 to 9.6 million tons in 2000, which represented 65% of the total U.S. sulfur emissions. With regard to WTE sulfur dioxide emissions, they were reduced by 87% from a pre-MACT emission estimate of 31 thousand tons to a post-MACT estimate of 4 thousand tons, which represented only 0.03 % of the total U.S. sulfur dioxide emissions in the year 2000. The MACT regulation limits the emission concentration of sulfur dioxide at the source to 29 parts per million dry volume (ppmdv) at 7 % O_2. Table 2 shows the emissions of sulfur dioxide from coal-fired plants and post-MACT WTE facilities in terms of thermal energy input and electrical energy output. It shows that emissions of sulfur dioxide from WTE plants amounts to about 0.03 lb/million BTU (0.01 g/MJ) while that of coal-fired plants is several times higher, at approximately 1.0 lb/million BTU (0.45 g/MJ).

Table 17. Sulfur dioxide emission in coal-fired and WTE plants

Year	Total Emissions (in 1000 tons)		% of Total SO_2 Emissions		Emission Factor[d]			
	Coal-fired[a]	WTE	Coal-fired	WTE	lb/10^6 Btu (g/MJ)		g/kWh	
					Coal-fired	WTE	Coal-fired	WTE
1990	13,836	30.7[b]	65.95	0.15	1.87 (0.81)	nd	8.7	nd
1995	10,548	nd	62.32	na	1.33 (0.57)	nd	6.2	nd
1998	11,335	nd	65.81	na	1.3 (0.56)	nd	6.1	nd
2000	9,625	4.076[c]	64.88	0.03	1.05 (0.45)	0.031 (0.013)	4.9	0.21

Source: [a]EPA, (2003), Average Annual Emissions, All Criteria Pollutants (Table A-8)

[b]EPA, Docket A-90-45, Item VIII-B-7 (pre-MACT Emissions)

[c]EPA, Docket A-90-45, Item VIII-B3 (post-MACT Emissions)

[d]Data for energy input and energy output were taken from Energy Information Administration/Annual Energy Review 2001 (Table 2.1f and Table 8.2a) respectively

4.4.1.3 Nitrogen Oxide Emissions

Emissions of nitrogen oxides from coal-fired plants were reduced from 5.1 million tons in 1990 to 4.1 million tons in the year 2000; this represented a reduction from 22% to 19.5% of the total U.S. nitrogen oxide emissions. During the same period, emissions of large WTE facilities were reduced 17% from a pre-MACT emission estimate of 56.4 thousand tons to 46 thousand tons in the year 2000; this emission represents only 0.03 % of the total U.S. nitrogen oxide emissions. MACT regulation limits emission of nitrogen oxides at the source below a concentration from 160-250 ppmdv at 7% O2 (depending on the type of burning technology; i.e. mass burn, refuse-derived fuel or fluidized bed).

Table 18 shows a comparison of the emission factors of coal-fired and large WTE facilities complying MACT standards. It can be seen that emissions from coal-fired plants ranged from 0.69 lb/million BTU (0.3 g/MJ) in 1990 to 0.45 lb/million BTU in the year 2000. Emission from post-MACT WTE facilities is lower at 0.35 lb/million BTU (0.15 g/MJ). However, NOx emission is slightly higher in terms of electric energy produced: 2.41 g/kWh compared to 2.1 g/kWh in coal-fired plants; this is attributed to the fact that coal-fired plants have a higher thermal efficiency (30-33%) as compared to that of WTE facilities (17-20%).

Table 18. Nitrogen Oxides emission in coal-fired and WTE plants

Year	Total Emissions (in 1000 tons)		% of Total US Emissions		Emission Factor[d]			
	Coal-fired[a]	WTE	Coal-fired	WTE	lb/10^6 Btu (g/MJ)		g/kWh	
					Coal-fired	WTE	Coal-fired	WTE
1990	5,129	56.4[b]	22.1	0.24	0.69 (0.30)	nd	3.2	Nd
1995	5,072	nd	22.36	nd	0.64 (0.28)	nd	3.0	Nd
1998	4,942	nd	22.33	nd	0.57 (0.24)	nd	2.6	Nd
2000	4,124	46.5[c]	19.55	0.22	0.45 (0.19)	0.35 (0.15)	2.1	2.4

Source: [a]EPA, (2003), Average Annual Emissions, All Criteria Pollutants (Table A-4)

[b]EPA, Docket A-90-45, Item VIII-B-7 (pre-MACT Emissions)

[c]EPA, Docket A-90-45, Item VIII-B3 (post-MACT Emissions)

[d]Data for energy input and energy output were taken from Energy Information Administration/Annual Energy Review 2001 (Table 2.1f and Table 8.2a) respectively, nd: no data

4.4.1.4 Particulate Matter

Approximately 2.5% of U.S. particulate matter (PM10) emissions were emitted from coal-fired power plants in the year 2000. PM emission reached 240,000 tons in the year 1990 and has increased to approximately 570,000 tons in the year 2000. PM emissions from WTE facilities reached 7 thousand tons in 1990 and were reduced to 0.7 thousand tons in the year 2000. MACT regulation limits PM concentration at the source at 27 milligram per dry standard cubic meter (mg/dscm) at 7% O_2 for compliance. Table 19 compares the emissions from coal-fired and WTE facilities after MACT retrofit. PM emissions from coal-fired plants are in the range of 33 lb/billion BTU (14 g/GJ) to 62 lb/billion BTU (27 g/GJ) while that of post-MACT WTE facilities is significantly lower at 5 lb/billion BTU (2.3 g/GJ).

Table 19. Particulate matter emissions from coal-fired and WTE plants

Year	Total Emissions (in 1000 tons)		% of Total Emissions		Emission Factor[d]			
	Coal-fired[a]	WTE	Coal-fired	WTE	lb/10^9 Btu (g/GJ)		g/kWh	
					Coal-fired	WTE	Coal-fired	WTE
1990	241	6.93[b]	0.95	0.03	33 (14)	nd	0.15	nd
1995	222	nd	0.95	nd	28 (12)	nd	0.13	nd
1998	179	nd	0.86	nd	21 (8)	nd	0.10	nd
2000	566	0.707[c]	2.52	0.003	62 (27)	5(2.3)	0.29	0.037

Source: [a]EPA, (2003), Average Annual Emissions, All Criteria Pollutants (Table A-6: PM10)

[b]EPA, Docket A-90-45, Item VIII-B-7 (pre-MACT Emissions)

[c]EPA, Docket A-90-45, Item VIII-B3 (post-MACT Emissions)

[d]Data for energy input and energy output were taken from Energy Information Administration/Annual Energy Review 2001 (Table 2.1f and Table 8.2a) respectively

4.4.1.5 Heavy Metals

Cadmium Emissions

Table 20 shows measured cadmium emission factors for coal-fired plants, for different coals and pollution control technologies. Table 23 shows the nationwide emissions of cadmium from WTE facilities after implementation of the MACT standards. As shown, cadmium emissions from coal are in the range of <4.3 to 18 lb/trillion BTU and from post-MACT WTE facilities, 2.5 lb/trillion BTU.

Table 20. Typical cadmium emission factors for coal combustion

Coal-type	Control Status[a]	Measured Emission Factors
		lb/10^{12} BTU (g/10^{12} J)
Bituminous	ESP	18 (7.7)
Bituminous	ESP/wet scrubber	<18 (<7.7)
Bituminous	ESP-2 stage	<18 (<7.7)
Sub-bituminous	ESP	10 (4.4)
Sub-bituminous	ESP/wet scrubber	<4.3 (<1.8)
Sub-bituminous	ESP-2 stage	<4.3 (<1.8)
Anthracite	ESP	4.3 (1.8)
Anthracite	ESP/wet scrubber	<4.3 (<1.8)
Anthracite	ESP-2 stage	<4.3 (<1.8)
Lignite	ESP	19 (<8.4)
Lignite	ESP/wet scrubber	<19 (<8.4)
Lignite	ESP-2 stage	<19 (<8.4)

Source: EPA, Locating and Estimating Air Emissions from Sources of Cadmium and Cadmium Compounds, (EPA-454/R-93-040, September, 1993), Table 6-8

Note: [a]ESP: electrostatic precipitator

Lead Emissions

Emissions of lead from coal-fired power plants reached 42 tons in 1990 and increased to 49 tons in 1998, which represented about 1% and 1.4% of the total U.S. emissions, respectively [44]. Emissions of lead from large WTE plants were 52 tons in 1990 and were reduced to 4.7 tons in 2000. Lead emission factor for controlled coal-fired utility boilers is about 14 lb/trillion BTU [45], while that of WTE facilities is estimated at 36.1 lb/trillion BTU. Table 22 presents the nationwide estimate of emission factors, using actual emissions of WTE facilities complying with MACT standards.

Mercury Emissions

Total nationwide mercury emissions from coal-fired utilities, as estimated by EPA in its report to Congress in 1998 [46], reached 51.3 tons (short tons) in 1994, which represented

approximately 33 percent of the total US emissions. For WTE facilities, emissions of mercury were reduced from 45.2 tons in 1990 to 2.2 tons in 2000. MACT regulation limits concentration of mercury to 0.08 mg/dscm at 7% O_2. Measured mercury emissions from coal varied from as low as 0.2 lb/trillion BTU to as high as 30.2 lb/trillion BTU (Table 21). Using actual WTE emissions, the estimated mercury emissions from post-MACT WTE facilities are 16.7 lb/trillion BTU and 0.25 lb/GWhr (Table 23).

Table 21. Measured mercury emission factors for coal combustion

Coal-type	Control Status	Measured Emission Factors
		lb/10^{12} BTU (g/TJ)
Bituminous	Uncontrolled	8.8 (3.8)
Bituminous	MP or MC	29.9 (12.9)
Bituminous	ESP or MP/ESP	8 (3.4)
Bituminous	ESP-2 stage	0.2 (0.1)
Bituminous	WS or MC/WS	18.4 (7.9)
Bituminous	FF	4.6 (2.0)
Sub-bituminous	Uncontrolled	30.2 (13.0)
Sub-bituminous	ESP or MP/ESP	2.7 (12.1
Lignite	MC	9.6 (4.1)
Lignite	ESP	0.4 (.2)
Anthracite	Uncontrolled	5.3 (2.3)

Source:Locating and Estimating Air Emissions from Sources of Mercury and Mercury Compounds, EPA-454/R-97-012, Dec.1997, Table 6-7

Notes: MP: mechanical precipitation, MC: multicyclone, ESP: electrostatic precipitator, WS: wet scrubber

Table 22. Estimated nationwide emission factor of cadmium and mercury from WTE plants

	Emissions (tons)	Emission Factors			
		lb/10^{12} BTU	g/10^{12} J	lb/GWh	g/MWh
Cadmium	0.333[a]	2.5	1.1	38	17
Lead	4.76[a]	36.1	10		250
Mercury	2.2[a]	16.7[b]	7.2[b]	0.251[c]	0.114[c]

Source: [a]EPA, Docket A-90-45, Item VIII-B-3 (post-MACT emissions);

[b]Assumed average heating value of 10,500 BTU/kg MSW, 0.85 availability factor

[c]assumed availability factor of 0.85 (2,590 MW total power generation)

4.4.1.6 Dioxins and Furans

Emissions of CDD/CDF from coal-fired plants have increased from 50 gram TEQ in 1987 to 60 gram TEQ in 2002 [47]. With regard to WTE emissions, total CDD/CDF was reduced significantly by 99% from a 1987 emission estimate of 8,877 gram TEQ to just 15 gram TEQ in 2000 and was estimated to be at 12 gram TEQ in 2002 [47]. MACT regulation limits the emission concentration of total dioxin/furan at the source to 30 ng/dscm at 7% O_2. The data of TEQ emissions from all measured sources of dioxins as published by the U.S. EPA can be found in Table 23; it should be noted that dispersed or unknown sources of emissions and flaring of emission from landfill, oil/gas productions and refining are not included [47].

Table 23. Sources of dioxin emissions in the U.S., 1987-2002 (U.S.E.P.A.)

Category	1987[a]	% Total	1995[a]	% Total	2002[a]	% Total
Incineration						
MSW	***8877***	***77***	***1250***	***71***	***12***	***0.96***
Medical Waste	*2590*	*22*	*488*	*27*	*7*	*0.54*
Sewage sludge	*6*	*0.05*	*14*	*0.84*	*14*	*1.17*
Hazardous waste	*5*	*0.04*	*5*	*0.33*	*3*	*0.03*
Total Incineration	11478	82	1758	54	37	3
Backyard barrel burning	604	4	628	19	628	56
Metal smelting	955	6	301	9	35	3
Cement kilns	131	0.94	173	5	25	2
Land-appl'd sewage sludge	76	0.55	76	2	76	6
Pulp and paper	372	2.67	23	0.71	15	1
Coal-fired utilities	**50**	**0.36**	**60**	**1**	**60**	**5**
Industrial wood burning	26	0.19	27	0.85	27	2
Residential wood burning	89	0.64	62	1	62	5
Diesel trucks	27	0.2	35	1	35	3
Other	137	0.98	103	3	100	9
TOTAL	13949	100	3252	100	1106	100

[a]Dioxin/furan emission units of toxic equivalent quantity (TEQ), using 1989 toxicity factors; total may not add up to 100 % due to rounding

4.4.1.7 Emissions Summary

Nationwide estimates were obtained on the emissions of sulfur dioxide, nitrogen oxides and trace metals such as cadmium, lead and mercury from coal-fired and WTE facilities. Due to insufficient nationwide data from coal-fired plants, the emission of HCl in terms of thermal input and electrical energy output both for coal-fired and WTE are not compared, although HCl emission in terms of concentration is presented.

The estimates showed that, per unit of thermal energy input and also per unit of power generated, the emissions of sulfur dioxide, particulate matter and nitrogen oxides were lower in WTE facilities than for coal-fired power plants; emissions of cadmium, lead and mercury from WTE facilities were comparable to that of coal-fired plants. With regard to dioxin/furans, the emission factors of WTE are considerably higher than for coal-fired utilities. However, in total emission terms, the toxic equivalent dioxin/furan emissions of U.S. coal-fired utilities and also of WTE facilities are a small fraction of the documented total U.S. dioxin emissions: 60 grams TEQ for coal-fired utilities and 15 grams TEQ for the post-MACT WTE power.

Table 24 shows a comparison of these emissions in terms of percentage share of total emissions, emission factors and percent reduction of emission from WTE from 1990. This paper notes the impact made by MACT regulations in lowering down the emissions of WTE facilities particularly the emissions of mercury, cadmium, lead, and dioxin/furans that have been reduced by 95%, 93%, 91%, and 99% respectively, between the years of 1990 and 2000.

Table 24. Summary of emission factors of coal-fired and WTE plants

Emissions (Year 2000)	Percent (%) Share of Total Emissions		Emission Factors				Percent (%) Emissions Reduction from 1990 (Pre-MACT) to year 2000 (Post-MACT)
			In terms of thermal energy input: lb/10^6 BTU (g/10^6J)		In terms of electrical energy output: g/kWh		
	Coal-fired	WTE	Coal-fired	WTE	Coal-fired	WTE	WTE
Sulfur Dioxide	64.08	0.03	1.05 (0.45)	0.031 (0.01)	4.9	0.21	86.7
Nitrogen Oxides	19.55	0.22	0.45 (0.19)	0.35(0.15)	2.1	2.4	17.6

Particulate Matter	2.52	0.003	0.067(0.027)	0.005(0.002)	0.29	0.037	89.8
Trace Metals			lb/10^{12} BTU (g/10^{12} J)		lb/TWh(g/GWh)		
Cadmium			<4.3-18 (<1.8-7.7)	2.5 (1.1)		38 (17)	93
Lead	1.36	0.13	<14-507>	36.1 (10)		250	90.9
Mercury	33[a]		0.4-29 (0.2-12.9)	16.7 (7.2)		0.25(0.11)	95.1
Dioxin/Furans	5	1	60[b]	15[b]			99+

[a]1994 total mercury emissions; [b]in grams TEQ (grams Toxic Equivalent Quantity)

4.4.2 Concentrations of Contaminants in WTE and Coal-fired Power Plants Stack Gas

4.4.2.1 Methodology

In order to determine the amount of emissions per unit of process gas produced in the stack gas of WTE and coal-fired power plants, actual emissions from WTE facilities coal-fired plants were estimated, in terms of ppmV and milligram per dry standard cubic meters of gas. Emissions from WTE were taken from several WTE facilities complying MACT standards, a large number of samples from 1996 to 2002, as reported in the facilities emissions report. For coal-fired power plants, the following assumptions were made: a) one ton of coal requires approximately 10,000 dscm of combustion air, b) the total US energy input from coal is 20,220 trillion BTU which is equivalent to 822,962 tons of coal (data taken from Energy Information Agency Annual Energy Review, 2001), c) coal-fired emissions were taken from EPA Annual Emissions Trend (2000), and d) NO_x emissions were assumed to consist of 90% NO and 10% NO_2. For HCl and emissions of cadmium, an emission factor of 0.04lb HCl/million BTU and 18 lb Cadmium/trillion BTU of coal were used respectively.

4.4.2.2 Discussion

Table 25 shows the MACT rules for existing large Municipal Solid Waste Combustion units and Table 26 shows the actual emissions from WTE and the calculated emissions from coal-fired plants. As shown in Table 26, the concentrations of emitted HCl, SO_2 and NO_x and particulate matter (PM) were lower in WTE facilities than in coal-fired power plants. This could be attributed to the impact of stringent MACT regulations imposed to large existing and new WTE facilities. It should be noted that the concentrations of HCl in the combustion chamber of coal-fired plants were more diluted as coal-fired plants use twice as much combustion air as in WTE and with chlorine content in coal less than WTE. Thus, the lower emissions in WTE can be attributed to higher removal efficiency following MACT. For SO_2, sulfur content in MSW is less than in coal, will NO_x emissions can be

attributed to the fact that coal-fired plant were operated at much higher operating temperature than WTE and thus more production of thermal NO_x. Emissions of heavy metal were slightly higher in WTE than in coal, as heavy metal content in MSW fuel is significantly higher than in coal fuel.

Table 25. MACT rules for existing large Municipal Waste Combustion Units

Emissions	**Limits**	
Metals		
Cadmium	0.04 mg/dscm	
Lead	0.44 mg/dscm	
Mercury	0.080 mg/dscm or 85% removal	
Acid Gases		
Sulfur Dioxide	29 ppm or 75 % removal	
Hydrogen Chloride	29 ppm or 95 % removal	
Nitrogen Oxides	Option A	Option B
Mass Burn/Water Wall	205 ppm	180 ppm
RDF	250 ppm	220 ppm
Mass Burn/Rotary	250 ppm	220 ppm
Fluidized bed	180 ppm	160 ppm
Particulates	27 mg	

Source: http://www.wte.org/m_act.html

Table 26. Estimated concentrations of various contaminants of WTE and coal-fired power plants

Pollutant	WTE Emission	Coal fired Plants*
HCl	11 (in ppmV@ 7%O_2)	25 ppmV
NOx	175 (in ppmV@ 7%O_2)	342 ppmV
SO_2	8 (in ppmV@ 7%O_2)	371 ppmV
Hg (mg/dscm)	0.009	0.006
Pb (mg/dscm)	0.007	0.005
Cd (mg/dscm)	0.02	0.00002
PM (mg/dscm)	3.6	62

*Calculated

4.5 Summary

The emissions from WTE were presented, in particular, the emissions of HCl and SO_2 that are known to contribute to corrosion. Other emissions from WTE were also presented, to address the issue of emissions from power plants that use Municipal Solid Waste (MSW) as fuel. The emissions of sulfur dioxide, nitrogen oxides, hydrogen chlorides, heavy metals and dioxin and furans were presented both in terms of energy emission factors (thermal energy input and electrical energy output) and in concentrations (in parts per million per volume of gas or in milligram per dry standard cubic meter of gas). The emissions were presented to demonstrate the impact that implementation of Maximum Achievable Control Technology (MACT) regulations on WTE emissions. For comparison purposes, these emissions were compared to coal-fired power plants to show the relative differences of emissions between WTE and power plants burning coal, the main source of fuel for generating electricity in the US. It was shown that MACT indeed had a tremendous impact in lowering WTE emissions, particularly heavy metals and dioxins in WTE facilities.

References:

[1] Themelis, N.J., *Status of the Global WTE Industry*, Waste Management World, July-August 2003

[2] Integrated Waste Services Association web site, http://www.wte.org/

[3] Albina, D and Themelis NJ, *Emissions from Waste-to-Energy: A comparison with coal-fired plants,* Proceedings of the 2003 ASME International Mechanical Engineering Congress and Exposition, Washington D.C., November 2003

[4] Deriziotis, P. and Themelis NJ, *Substance and perceptions of environmental impacts of dioxin emissions*, Proceedings of the 11th North American Waste-to-Energy Conference, ASME International, Tampa FL, April 2003

[5] Adams B, Peeters K, Earaets D, Diederen H and Wijnhoven JPF, *Seghers Boiler Prism: A proven primary measure against high temperature corrosion*, 12th North American Waste-to-Energy Conference, Savannah Georgia, USA, May 2004

[6] Bart E.M. Adams, Kris K.E. Peters, Herman S.W. Diederen and Jac P.F. Winjhoven, *"Preventing Boiler Corrosion"*, Waste Management World, September-October 2004,

[7] D.O. Albina, K. Millrath and N.J. Themelis, *"Effects of Feed Composition on Boiler Corrosion in Waste to Energy Plants"*, 12th North American Waste to Energy Conference (NAWTEC 12), Georgia, USA, 2004

[8] Tchobanoglous G, Theisen H, and Vigil S, (1993), *Integrated Solid Management: Engineering Principles and Management Issues(text),* MacGraw Hill, USA

[9] P. Rademakers, W. Hesseling and J van de Wetering, *"Review on Corrosion in Waste Incinerators, and possible effects of bromine."* TNO Report, 2002

[10] P.R. Roberge, *Handbook of Corrosion Engineering*, Mc Graw Hill, 2000

[11] G.Y. Lai, *High Temperature Corrosion: Issues in Alloy Selection,* Journal of Materials, 43:11, 54-60, 1991

[12] Tillack, D.J., and Guthrie, J.E., *Wrought and Cast Heat-Resistant Stainless Steels and Nickel Alloys for the Refining and Petrochemical Industries*, NiDI Technical Series 10071, Toronto Canada, Nickel Development Institute, 1992. (As referred by the Handbook of Corrosion Engineering, Chapter 3, page 265)

[13] Jones, D.A., *Principles and Prevention of Corrosion, 2nd Edition*, Upper Saddle River, NJ Prentice Hall 1996

[14] Gaskel, *D.R., "Introduction to Metallurgical Thermodynamics*", 2nd edition. McGraw-Hill, p.287

[15] Zahs, A., Spiegel, M. and Grabke J.H, *" Chloridation and oxidation of iron, chromium, nickel and their alloys in chloridizing and oxidizing atmospheres at 400-700°C,* Corrosion Science (42), 1093-1122, 2000

[16] Nielsen, H.P., Frandsen F.J., Dam-Johansen, K., and Baxter, L.L., *"The implications of chlorine-associated corrosion on the operation of biomass-fired boilers"*, Progress in Energy and Combustion Science (26),p 283-298 , 2000

[17] Spiegel M, Grabke HJ, In: Bryers RW, editor. *"Incinerating municipal and industrial waste. Fireside problems and prospects for improvement*, New York: Hemisphere, p.758, 1991. *(As referred by Nielsen et al. [12])*

[18] Grabke, H.J, Reese E. and Spiegel M. "*The Effects of Chloride, and Sulfur Dioxide in the Oxidation of Steels Below Deposits"*, Corrosion Science (7), 1023-1043, 1995

[19] Abels JM, and Strehblow HH, '*A surface analytical approach to the high temperature chlorination behavior of Inconel 600 at 700°C",* Corrosion Science (39), pp.115-132, 1997

[20] Uusitalo, M.A., Vouoristo P.M.J. and Mantyla, T.A., *"High temperature corrosion of coatings and boiler steels below chlorine containing deposits",* Corrosion Science (46), 1311-1331, 2004

[21] Li YS, Niu Y, and Wu WT, *"Accelerated corrosion of pure Fe, Ni, Cr and several Fe-based alloys induced by $ZnCl_2$-KCl at 450°C in oxidizing environment.*" Material Science and Engineering A345, p64-71, 2003

[22] Karlsson A, Moller P and Johansen V, "*Iron and Steel Corrosion in a System of O_2, SO_2 and Alkali Chloride. The Formation of Low Melting Point Salt Mixture*", Corrosion Science (30), pp. 153-158, Pergamon Press, 1990

[23] Harb JN and Smith EE, *"Fireside Corrosion in PC-Fired Boilers"*, Prog. Energy Combustion Science, 1990, Vol.16, pp 169-190

[24] Cutler, AJB and Raask E., *External Corrosion in Coal-fired Boilers: Assessment from Laboratory Data,* Corrosion Science (41), pp 789-800, Pergamon Press (1981)

[25] Outokumpu HSC Chemistry: *"Chemical Reaction and Equilibrium Software."* Outokumpu Research Oy, Finland, ISBN 952-9507-08-9.

[26] P. Amador and G. Lai, *"Application of Unifuse Overlay Tubes in the Convection Section of Waste-to-Energy Boilers",* Proceedings of the 11th Annual North American Waste to Energy Conference, Florida, USA, 2004

[27] L.Paul, G. Clark, M Eckhardt and B. Hoberg, *"Experience with Weld Overlay and Alloy Solid Tubing Materials in Waste to Energy Plants',* Proceedings of the 12 Annual North American Waste to Energy Conference (NAWTEC 12), Georgia, USA, 2004

[28] Stephan, PM, *" Refractory Tile Installation-Mortar or No Mortar",* 12th North American Waste to Energy Conference (NAWTEC 12), May 2004, Savannah, Georgia, USA

[29] Kawahara Y, Nakamura M, Tsuboi H. and Yukawa K, "*Evaluation of New Corrosion-Resistant Superheater Tubing in High Efficiency Waste-to-Energy Plants",* Corrosion, NACE International, 1998

[30] Hanson E and Turner M, "*2nd Year Comparison of Superheater Metal Wastage Rates Utilizing Various Boiler Tube Alloys in A Waste-to-Energy Facility",* 11th North American Waste-to-Energy Conference, Florida USA, 2003

[31] Lai GY, *"Corrosion Mechanism and Alloy Performance in Waste-to-Energy Boiler Combustion Environment",* 12th North American Waste-to-Energy Conference, Georgia USA, 2004

[32] Lai GY, "*High Temperature Corrosion of Engineering Alloys*," ASM International, Materials Park, Ohio USA, 1990

[33] Spiegel M, *"Influence of gas phase composition on the hot corrosion of steels and nickel- based alloys beneath (Ca-Na-K) mixture containing $PbSO_4$ and $ZnSO_4$",* Materials and Corrosion (51), pp303-312, 2000

[34] Li YS and Spiegel M, *"Models describing the degredation of FeAl and NiAl alloys induced by $ZnCl_2$-KCl melt at 400-450°C",* Corrosion Science (46), pp 2009-2023, 2004

[35] Zahs A, Spiegel M and Grabke HJ, *"The influence of alloying elements on chlorine-induced high temperature corrosion of Fe-Cr alloys in oxidizing atmosphere",* Materials and Corrosion (50), pp 561-578, 1999

[36] Li YS, Niu Y, and Wu WT, *"Accelerated corrosion of pure Fe, Ni, Cr and several Fe-based alloys induced by $ZnCl_2$-KCl at 450°C in oxidizing environment.*" Material Science and Engineering A345, p64-71, 2003

[37] Shinata Y, Takahashi F, Hashiura, Material Science Eng. A (87), 1987

[38] Fujikawa H and Maruyama N, Material Science Engineering A120, 1989

[39] Stott FH and Shih CY, The influence of HCl on the oxidation of iron at elevated temperature, Materials and Corrosion (51), 277-286 (2000)

[40] EPA, (2003), *Average Annual Emissions, All Criteria Pollutants*, February 2003

[41] Energy Information Administration/*Annual Energy Review 2001* (Table 2.1f), http://eia.doe.gov

[42] Energy Information Administration/*Annual Energy Review 2001*(Table 8.2a), http://eia.doe.gov

[43] EPA, *Emission Factor Documentation for AP-42 Section 1.1 Bituminous and Sub-bituminous Coal Combustion,* U.S. Environmental Protection Agency, Research Triangle Park, NC, April 1993

[44] EPA, *National Air Pollutant Emissions Trends: 1900-1998* (Table 3-7)

[45] EPA, *Locating and Estimating Air Emissions from Sources of Lead and Lead Compounds,* EPA-454/R-98-006 (May 1998), Table 5-8

[46] EPA, *Study of Hazardous Air Pollutant Emissions from Electric Utility Steam Generating Unit Final Report to Congress*, (EPA-453/R-98-004a; February, 1998) Vol.1, Table 7-1

[47] Deriziotis, P., and N.J. Themelis, *Substance and perceptions of environmental impacts of dioxin emissions*, Proceedings of the 11th North American Waste-to-Energy Conference, ASME International, Tampa FL (April 2003).

Appendix A. Corrosion Questionnaire (see next page)

Waste-To-Energy Research and Technology Council

Corrosion Data Questionnaire

Corrosion is a major cost in the operation of WTE facilities and the subject of a major research effort by the WTERT Council for 2005. In addition to the analysis of published data and experimental work, this project can benefit much by the experience of the operators of WTE facilities. The objective of this questionnaire is to collect data and benefit from the accumulated experience of the operators of WTE facilities that are members of ISWA. The identity of each plant responding to this Questionnaire will be maintained confidential but the results of the analysis will be made available to all plants and companies participating in this Survey.

Please return the completed Questionnaire and other documents requested to Prof. Nickolas J. Themelis (njt1@columbia.edu) who will assign an identification number to each responding WTE and maintain the identity of each plant confidential. Any questions related to the questionnaire or additional information that you think is relevant to the study (e.g., past corrosion studies by the plant or the company) , should be sent to Prof. Themelis or e-mailed to Mr. Dionel Albina (doa2001@columbia.edu, (212)-854-0305).

Date:
Plant Name/Company:
Respondent's (name and e-mail):
Type of WTE (mass burn, RDF):
Unit # (Please select the most representative unit in your plant).
Grate Technology (Martin, Von Roll, Roller Grate, Seghers, etc.)
Unit Actual Daily Capacity: , **Unit days of operation/year**:
Total air input: scfm or lb/h
Steam Generation (lb/hr): Design: Actual:
Boiler Outlet Steam Temperature:
Boiler diagram: Please attach boiler diagram showing steam / water /flue gas layout and approximate location of secondary air nozzles

Waterwall Data:

1. Average operating days between shutdowns because of corrosion:

2. Details of Tubing:
   a) Base Metal
   b) Tube diameter , thickness and spacing

3. Refractory Lining:
   a) Type of refractory:
   b) How is the refractory applied (as castable or tile):
   c) Anchoring system/s used:
   d) Has the use of refractory improved performance?
   e) Height above the grate where "best choice" switches from refractory to alloy cladding?
   f) Height of the furnace above the grate (at feed end)

4. Alloy Cladding:
- Type:
- Thickness:
- Area of coverage above refractory lining (height, wall areas, etc)

5. Approximate percent of waterwall cladded:
- 1st pass:
- 2nd pass:
- 3rd pass:

6. What is the saturation temperature in the steam/water mix in the waterwall and the corresponding drum pressure?

7. Flue gas conditions:
a) What is the temperature (measured or estimated) at the exit of the furnace, second pass third pass
b) What is the typical operating oxygen concentration (%)? Design Actual
c) How are these temperatures measured (unshielded short thermocouple, IR measuring device, shielded aspirating pyrometer traverse, other)?

8. Maximum observed wastage rate due to corrosion, mills/year:

9. Estimated weight of new metal used for waterwall, lb/yr?

Superheater Tube Data:

1. Average number of days between shutdowns because of corrosion:
1st superheater 2nd superheater 3rd superheater

2. Details of tubing:
a) Base Metal
b) Tube diameter thickness spacing

3. Cladding:
a) Type or types of alloys used:
b) Cladding (thickness):

4. Percent of superheater tube cladded: 1st superheater , 2nd superheater , 3rd superheater

5.Superheater Conditions if known (if more than one superheater please specify:

a) What are the steam inlet temperature pressure mass flow rate (lb/h)?

b) What are the estimated flue gas conditions (temperature, velocity) at inlet of superheater? outlet of superheater

6. Maximum observed wastage rate, mills/year:

7. Estimated weight of new metal used for superheaters, lb/yr?

Furnace and Boiler Questions.

1. Please list the principal types of corrosion that you have observed in furnace and boiler (i.e. flame impingement, erosion-corrosion, molten salts corrosion, acid gas condensation (HCl and SO_x), acid gas attack (SO_x), stress induced corrosion, etc) and also at which location in your process is this type of corrosion the most problem?

2. Please describe briefly tube-cleaning method in your plant Do you think this method and the frequency of cleaning affect tube life?

3. What is the duration in days between cleaning cycles (offline and online) of fire side deposits? Offline Online

4. How often does the boiler come off line due to grate slagging or low furnace clinkers?

Combustion Air, NO_x Reduction and Cleaning Technique Questions:

1. Ratio of primary air to secondary air?

2. Is there a flue gas recirculation system? If yes, what is the estimated % recirculation?

3. Are auxiliary burners used? If yes, do you think they contribute to corrosion?

4. Are chemicals added in the furnace for emission reduction? , If yes, please state type and flow rates used? Do you think such chemicals have an effect on corrosion?

5. Typical HCl concentration (inlet of APC):

6. Typical SO_2 concentration (inlet of APC):

Overall:

1. Estimated yearly scheduled downtime (days)

2. Estimated non-scheduled downtime due to corrosion (days):

3. Estimated yearly maintenance cost for unit due to corrosion:

4 Has the facility carried out fuel characterization? If so please attach results.

5. Has the facility carried out R&D on corrosion. If the answer is Yes, please send results, comments and any conclusions to Prof. Themelis indicating whether you like the facility to be anonymous in the communication of such results to other ISWA members.

Many thanks for your contribution to this Survey. Please return questionnaire, drawing and any previous study/report on corrosion to:

Prof. Nickolas J. Themelis
WTERT, Earth and Engineering Center
Columbia University
500 West, 120th Street, #918 Mudd
New York, New York, 10027
Tel 212 854 2138 Fax 212 854 6213
(e-Mail: njt1@columbia.edu)

WTERT

Waste-To-Energy Research and Technology Council

Appendix B: Common Names and UNS Alloy Number of Alloys Used in High Temperature Application (Composition Given in Appendix C)

Common Name	UNS Alloy Number	Generic Family
6	R30016	Ni-, Ni-Fe-, Co-base alloy
25	R30605	Ni-, Ni-Fe-, Co-base alloy
188	R30188	Ni-, Ni-Fe-, Co-base alloy
214	N07214	Ni-, Ni-Fe-, Co-base alloy
230	N06230	Ni-, Ni-Fe-, Co-base alloy
263	N07041	Ni-, Ni-Fe-, Co-base alloy
304	S30400	Austenitic stainless steel
310	S31000	Austenitic stainless steel
316	S31600	Austenitic stainless steel
330	S33000	Austenitic stainless steel
333	N06333	Ni-, Ni-Fe-, Co-base alloy
410	S41000	Martinsitic stainless steel
430	S43000	Ferritic stainless Steel
446	S44600	Ferritic stainless steel
556	R30556	Ni-Fe-, Co-base alloy
600	N06600	Ni-Fe-, Co-base alloy
601	N06601	Ni-Fe-, Co-base alloy
617	N06617	Ni-Fe-, Co-base alloy
625	N06625	Ni-Fe-, Co-base alloy
718	N07718	Ni-Fe-, Co-base alloy
825	N08825	Ni-Fe-, Co-base alloy
2205	S31803	Duplex stainless steellex
1Cr-0.5Mo	K11597	Steel
2.25Cr-1Mo	K21590	Steel
253 MA	S30815	Stainless steel
5Cr-0.5Mo	K41545	Steel
6B	R30016	Ni-Fe-, Co-base alloy

800 H	N08810	Ni-, Ni-Fe-, Co-base alloy
9Cr-1Mo	S50400	Steel
ACI HK	J94224	Cast SS
Alloy 150(UMCo-50)		Ni-, Ni-Fe-, Co-base alloy
Alloy HR-120		Ni-, Ni-Fe-, Co-base alloy
Alloy HR-160		Ni-, Ni-Fe-, Co-base alloy
Carbon Steel	G10200	Steel
Copper	C11000	Copper
Incoloy DS		Ni-, Ni-Fe-, Co-base alloy
Incoloy 801		Ni-, Ni-Fe-, Co-base alloy
Incoloy 803		Ni-, Ni-Fe-, Co-base alloy
Inconel 602		Ni-, Ni-Fe-, Co-base alloy
Inconel 671		Ni-, Ni-Fe-, Co-base alloy
Multimet	R30155	Ni-Fe-, Co-base alloy
Nickel	N02270	Ni-Fe-, Co-base alloy
René 41		Ni-, Ni-Fe-, Co-base alloy
RA330	N08330	Ni-, Ni-Fe-, Co-base alloy
S	N06635	Ni-Fe-, Co-base alloy
Waspaloy		Ni-, Ni-Fe-, Co-base alloy
X	N06002	Ni-, Ni-Fe-, Co-base alloy

Source: [10] P.R. Roberge, *Handbook of Corrosion Engineering*, Mc Graw Hill, 2000

Appendix C. Chemical Compositions of Engineering Alloys

Source: [10] P.R. Roberge, *Handbook of Corrosion Engineering*, Mc Graw Hill, 2000

TableC.1 Chemical Composition of Nickel-Nickel Iron, and Cobalt-Base Alloys

Alloy	UNS	C	Cr	Ni	Co	Fe	Mo	W	Other
263	N07041	0.06	20	Rem.	20		5.8		Al 0.5, Ti 2.2
20Cb-3	N08020	0.02	20	33		Rem.	2.2		Cu 3.3, Cb 0.5
20Mo-4	N08024	0.02	23.5	37		Rem.	3.8		Cu 1.0, Cb 0.25
20Mo-6	N08026	0.02	24	36		Rem.	5.6		Cu 3.0
625 Plus	N07716	0.02	20	Rem.		5	9		Cb 3.1, Al 0.2, Ti 1.3
Alloy 150(UMCo-50)		0.06	27		Rem.	18			
Alloy 188	R30188	0.1	22	22	Rem.	3		14	La 0.04
Alloy 214		0.04	16	Rem.		3			Al 4.5, Y
Alloy 230	N06230	0.1	22	Rem.		3	2	14	La 0.02, B 0.015
Alloy 242		0.03	8	Rem.			25		
Alloy 25 (L-605)	R30605	0.1	20	10	Rem.	3		15	
Alloy 556	R30556	0.1	22	20	18	Rem.	3	2.5	Ta 0.6, La 0.02, N 0.2, Zr 0.02
Alloy 6B	R30016	1.2	30		Rem.	1.5	4.5		
Alloy HR-120		0.05	25	37		Rem.			Cb 0.7, N 0.2
Alloy HR-160		0.05	28	Rem.	29	1.5			Si 2.75
AR 213		0.17	19		Rem.			4.5	Al 3.5, Ta 6.5, Zr 0.15, Y 0.10
Astroloy		0.06	15	Rem.	17		5.3		Al 4.0, Ti 3.5, B 0.03
Chromel D			18.5	36		Rem.			Si 1.5
Cupro 107				Rem.		0.8			Cu 68.0, Mn 1.1
D-979	N09979	0.05	15	Rem.		27	4	4	Al 1.0, Ti 3.0
Discalloy	K66220	0.06	14	26		Rem.	3		Al 0.25, Ti 1.7
Fecralloy A		0.03	15.8			Rem.			Al 4.8, Y 0.3
Ferry alloy				Rem.					Cu 55.0
Hastelloy B	N10001	0.05		Rem.	2.5	5	28		V 0.03
Hastelloy B-2	N10665	0.01		Rem.		2	28		
Hastelloy C	N10002	0.08	15.5	Rem.	2.5	6	17	4	
Hastelloy C-22	N06022	0.01	22	Rem.	2.5	3	13	3	
Hastelloy C-276	N10276	0.01	15.5	Rem.	2.5	5.5	16	4	
Hastelloy C-4	N06455	0.01	16	Rem.	2	3	15.5		
Hastelloy G	N06007	0.05	22	Rem.		19.5	6.5		Cb + Ta 2.0, Cu 2.0
Hastelloy G-3	N06985	0.015	22	Rem.	5	19.5	7	1.5	Cb + Ta 0.3, Cu 2.0

TableC.1 Chemical Composition of Nickel-Nickel Iron, and Cobalt-Base Alloys *(cont)*

Alloy	UNS	C	Cr	Ni	Co	Fe	Mo	W	Other
Hastelloy G-30		0.03	29.5	Rem.	5	15	5	2.5	Cu 2.0
Hastelloy H-9M		0.03	22	Rem.	5	19	9	2	
Hastelloy N	N 10003	0.06	7	Rem.		5	16.5		
Hastelloy S	N06635	0.02	15.5	Rem.		3	14.5		La 0.05, B 0.0l5
Hastelloy W	N10004	0.12	5	Rem.	2.5	6	24		
Hastelloy X	N06002	0.1	22	Rem.	1.5	18.5	9	0.6	
IN 100	N13100	0.15	10	Rem.	15		3		Al 5.5, Ti 4.7, Zr 0.06, V 1.0, B 0.015
IN 100 Gatorize		0.07	12.4	Rem.	18.5		3.2		Al 5.0, Ti 4.3, Zr 0.06, B0.02, V 0.8
IN 102	N06102	0.06	15	Rem.		7	3	3	Cb 3.0, Al 0.4, Ti 0.6, Mg0.02, Zr 0.03
IN 587		0.05	28.5	Rem.	20				Cb 0.7, Al 1.2, Ti 2.3, Zr 0.05
IN 597		0.05	24.5	Rem.	20		1.5		Cb 1.0, Al 1.5, Ti 3.0, Zr 0.05
Incoloy 800	N08800	0.05	21	32.5		Rem.			Al 0.3, Ti 0.3
Incoloy 800H	N08810	0.08	21	32.5		Rem.			Al 0.4, Ti 0.4
Incoloy 800HT	N08811	0.08	21	32.5		Rem.			Al + Ti 1.0
Incoloy 802	N08802	0.4	21	32.5		Rem			
Incoloy 825	N08825	0.03	21.5	Rem.		30	3		Cu 2.2
Incoloy 903	N19903			38	15	Rem.			Ti 1.4, Al 0.9, Cb 3.0
Incoloy 904	N19904			32.5	14.5	Rem.			Ti 1.6
Incoloy 907	N19907			38	13	Rem.			Ti 1.5, Cb 4.7, Si 0.15
Incoloy 909	N19909			38	13	Rem.			Ti 1.5, Cb 4.7, Si 0.4
Incoloy 925	N09925	0.01	21	Rem.		28	3		Cu 1.8, Ti 2.1, Al 0.3
Incoloy DS		0.06	17	35		Rem.			Si 2.3
Inconel 600	N06600	0.08	15.5	Rem.		8			
Inconel 601	N06601	0.1	23	Rem.		14.4			Al 1.4
Inconel 617	N06617	0.07	22	Rem.	12.5	1.5	9		Al 1.2
Inconel 625	N06625	0.1	21.5	Rem.		2.5	9		Cb 3.6
Inconel 671		0.05	48	Rem.					Ti 0.35
Inconel 690	N06690	0.02	29	Rem.		9			
Inconel 706	N09706	0.03	16	Rem.		37			Ti 1.8, Al 0.2, Cb 2.9
Inconel 718	N07718	0.04	18	Rem.		18.5	3		Cb 5.1
Inconel 751	N07751	0.05	15	Rem.		7			Ti 2.5, Al 1.1, Cb 1.0
Inconel X-750	N07750	0.04	15.5	Rem.		7			Ti 2.5, Al 0.7, Cb 1.0

Alloy	UNS	C	Cr	Ni	Co	Fe	Mo	W	Other
Kanthal AF			22			Rem.			Al 5.3, Y
Kanthal Al	K92500		22			Rem.			Al 5.8
M 252	N07252	0.15	20	Rem.	10		10		Al 1.0, Ti 2.6, B 0.005
MAR-M 918		0.05	20	20	Rem.				Ta 7.5, Zr 0.10
Monel 400	N04400			Rem.		1.2			Cu 31.5, Mn 1.1
Monel 401	N04401			Rem.		0.3			Cu 55.5, Mn 1.63
Monel 450	C71500			Rem.		0.7			Cu 68.0, Mn 0.7
Monel K-500	N05500			Rem.		1			Cu 29.5, Ti 0.6, Al 2.7
Monel R-405	N04405			Rem.		1.2			Cu 31.5, Mn 1.1
MP 159			19	25.5	Rem.	9	7		Cb 0.6, Al 0.2, Ti 3.0
MP 35N	R30035		20	35	Rem.		10		
Multimet (N-155)	R30155	0.1	21	20	20	Rem.	3	2.5	Cb + Ta 1.0, N 0.15
NA 224		0.5	27	Rem.		18.5		6	
Ni 200	N02200	0.08		99.6					
Ni 201	N02201	0.02		99.6					
Ni 270	N02270	0.01		99.98					
Nichrome 80			20	Rem.					Si 1.0
Nimonic 105		0.08	15	Rem.	20		5		Al 4.7, Ti 1.3, B 0.005
Nimonic 115		0.15	15	Rem.	lS.0		4		Al 5.0, Ti 4.0
Nimonic 70			20	Rem.		25			Al 1.0, Ti 1.25, Cb 1.5
Nimonic 75		0.1	19.5	Rem					
Nimonic 80A	N07080	0.06	19.5	Rem.					Al 1.4, Ti 2.4
Nimonic 81		0.03	30	Rem.					Al 0.9, Ti 1.8
Nimonic 86	N07090		25	Rem.			10		Ce 0.03
Nimonic 90		0.07	19.5	Rem.	16.5				Al 1.5, Ti 2.5
Nimonic 901			12.5	Rem.		36	5.8		Ti 2.9
Nimonic 91			28.5	Rem.	20				Al 1.2, Ti 2.3
Nimonic AP 1			15	Rem.	17		5		Al 4.0, Ti 3.5
Nimonic PE 11		0.05	18	Rem.		34	5.2		Al 0.8, Ti 2.3
Nimonic PE 16		0.05	16.5	Rem.		34	3.3		Al 1.2, Ti 1.2
Nimonic PK 31			20	Rem.	14		4.5		Al 0.4, Ti 2.35, Cb 5.0

Alloy	UNS	C	Cr	Ni	Co	Fe	Mo	W	Other
Nimonic PK 33		0.04	18	Rem.	14		7		Al 2.1, Ti 2.4
Nimonic PK 37	N07001		19.5	Rem.	16.5				Al 1.5, Ti 2.5
Nimonic PK 50			19.5	Rem.	13.5		4.25		Al 1.4, Ti 3.0
Pyromet 31	N07031	0.04	22.5	Rem.		15	2		Al 1.4, Ti 2.3, Cu 0.9, B 0.005
Pyromet 860		0.05	13	Rem.	4	28.9	6		Al 1.0, Ti 3.0, B 0.01
Pyromet CTX-I		0.03		37.7	16	Rem.			Cb 3.0, Al 1.0, Ti 1.7
RA 330	N08330	0.05	19	35		Rem.			Si 1.2
RA 330HC		0.4	19	35		Rem.			Si 1.2
RA 333	N06333	0.05	25	Rem.	3	18	3	3	
Refractory 26		0.03	18	Rem.	20	16	3.2		Al 0.2, Ti 2.6, B 0.015
René 100		0.16	9.5	Rem.	15		3		Al5.5, Ti 4.2, Zr 0.06, B 0.015
René 41		0.09	19	Rem.	11	5	10		Al1.5, Ti 3.0, B 0.006
René 95		0.15	14	Rem.	8		3.5	3.5	Cb 3.5, Al 3.5, Ti 2.5, Zr 0.05
S-816	R30816	0.38	20	20	Rem.	4	4	4	Cb 4.0
Sanicro 28	N08028	0.01	27	31		Rem.	3.5		Cu 1.0
Udimet 400		0.06	17.5	Rem.	14		4		Cb 0.5, Al 1.5, Ti 2.5, Zr 0.06, B 0.008
Udimet 500		0.08	18	Rem.	18.5		4		Al 2.9, Ti 2.9, Zr 0.05, B 0.006
Udimet 520		0.05	19	Rem.	12		6	1	Al 2.0, Ti 3.0, B 0.005
Udimet 630		0.03	18	Rem.		18	3	3	Cb 6.5, Al 0.5, Ti 1.0
Udimet 700		0.03	15	Rem.	18.5		5.2		A1 5.3, Ti 3.5, B 0.03
Udimet 710		0.07	18	Rem.	15		3	1.5	Al 2.5, Ti 5.0
Udimet 720		0.03	17.9	Rem.	14.7		3	1.3	A1 2 5, Ti 5.0, Zr 0.03, B
Ultimet		0.06	26	9	Rem.	3	5	2	N 0.08
Unitemp AF2-1DA		0.35	12	Rem.	10		3	6	Ta 1.5, Al 4.6, Ti 3.5, Zr 0.10
Unitemp AF2-1DA6		0.04	12	Rem.	10		2.7	6.5	Ta 1.5, Al 4.0, Ti 2.8, Zr 0.1, B 0.015
V-57		0.08	14.8	27		Rem.	1.25		Al 0.25, Ti 3.0, V 0.5, B 0.01
W-545	K66545	0.08	13.5	26		Rem.	1.5		Al 0.2, Ti 2.85, B 0.05
Waspaloy		0.08	19	Rem.	14		4.3		A1 1.5, Ti 3.0, Zr 0.05, B 0.006

Table C.2. Austenitic Stainless Steels-Standard Designations for Austenitic Stainless Steels (Composition as Maximum in % Unless Indicated as Range or Minimum)

UNS	Type	C	Mn	P	S	Si	Cr	Ni	Mo	Other
S20100	201	0.15	5.5–7.5	0.060	0.030	1.00	16.00–18.00	3.50–5.50		0.25N
S20200	202	0.15	7.5–10.0	0.060	0.030	1.00	17.00–19.00	4.00–6.00		0.25N
S20500	205	0.2	14.0–15.5	0.030	0.030	0.50	16.50–18.00	1.00–1.75		0.32–0.40N
S30100	301	0.15	2.00	0.045	0.030	1.00	16.00–18.00	6.00–8.00		
S30200	302	0.15	2.00	0.045	0.030	1.00	17.00–19.00	8.00–10.00		
S30215	302B	0.15	2.00	0.045	0.030	2.00–3.00	17.00–19.00	8.00–10.00		
S30300	303	0.15	2.00	0.20	0.15 min.	1.00	17.00–19.00	8.00–10.00	0.60	
S30323	303Se	0.15	2.00	0.20	0.060	1.00	17.00–19.00	8.00–10.00		0.15Se min.
S30400	304	0.08	2.00	0.045	0.030	1.00	18.00–20.00	8.00–10.50		
S30403	304L	0.03	2.00	0.045	0.030	1.00	18.00–20.00	8.00–12.00		
S30430	18-9-LW	0.08	2.00	0.045	0.030	1.00	17.00–19.00	8.00–10.00		3.00–4.00Cu
S30451	304N	0.08	2.00	0.045	0.030	1.00	18.00–20.00	8.00–10.50		0.10–0.16N
S30500	305	0.12	2.00	0.045	0.030	1.00	17.00–19.00	10.50–13.00		
S30800	308	0.08	2.00	0.045	0 030	1.00	19.00–21.00	10.00–12.00		
S30900	309	0.20	2.00	0.045	0.030	1.00	22.00–24.00	12.00–15.00		
S30908	309S	0.08	2.00	0.045	0.030	1.00	22.00–24.00	12.00–15.00		
S31000	310	0.25	2.00	0.045	0.030	1.50	24.00–26.00	19.00–22.00		
S31008	310S	0.08	2.00	0.045	0.030	1.50	24.00–26.00	19.00–22.00		
S31400	314	0.25	2.00	0.045	0.030	.50–3.00	23.00–26.00	19.00–22.00		
S31600	316	0.08	2.00	0.045	0.030	1.00	16.00–18.00	10.00–14.00		
S31620	316F	0.08	2.00	0.20	0.10 min.	1.00	16.00–18.00	10 00–14.00	1.75–2.5	
S31603	316L	0.03	2.00	0.045	0.030	1.00	16.00–18.00	10.00–14.00	2.0–3.0	
S31651	316N	0.08	2.00	0.045	0.030	1.00	16.00–18.00	10.00–14.00	2.0–3.0	0.10–0.16N
S31700	317	0.08	2.00	0.045	0.030	1.00	18.00–20.00	11.00–15.00	3.0–4.0	

Table C3. Ferritic Stainless Steels-Nominal Chemical Composition (%) of Ferritic Stainless Steels (Maximum unless noted otherwise)

UNS	Type	C	Mn	P	S	Si	Cr	Ni	Mo	Other
S40300	403	0.15	1.00	0.040	0.030	0.50	11.50–13.00			
S41000	410	0.15	1.00	0.040	0.030	1.00	11.50–13.50			
S41400	414	0.15	1.00	0.040	0.030	1.00	11.50–13.50	1.25–2.50		
S41600	416	0.15	1.25	0.060	0.15 min.	1.00	12.00–14.00		0.60	
S41623	416Se	0.15	1.25	0.060	0.060	1.00	12.00–14.00			0.15Se min.
S42000	420	0.15 min.	1.00	0.040	0.030	1.00	12.00–14.00			
S42020	420F	0.15 min.	1.25	0.060	0.15 min.	1.00	12.00–14.00		0.60	
S42200	422	0.20–0.25	1.00	0.025	0.025	0.75	11.00–13.00	0.50–1.00	0.75–1.25	0.15–0.30V, 0.75–1.25W
S43100	431	0.20	1.00	0.040	0.030	1.00	15.00–17.00	1.25–2.50		
S44002	440A	0.60–0.75	1.00	0.040	0.030	1.00	16.00–18.00	0 75		
S44004	440B	0.75–0.95	1.00	0.040	0.030	1.00	16.30–18.00	0.75		
S44004	440C	0.95–1.20	1.00	0.040	0.030	1.00	16.30–18.00	0.75		

Table C4. Compositions of First and Second-Generation Duplex Stainless Steels

UNS	Type	Cr	Mo	Ni	Cu	C	N	Other
			First generation					
S32900	Type 329	26	1.5	4.5		0.08		
J93370	CD-4MCu	25	2	5	3	0 04		
			Second generation					
S32304	SAF 2304	23		4		0.030	0.05–0.20	
S31500	3RE60	18.5	2.7	4.9		0.030	0.05–0.1	1.7 Si
S31803	2205	22	3	5		0.030	0.08–0.20	
S31200	44LN	25	1.7	6		0.030	0.14–0.20	
S32950	7-Mo PLUS	26.5	1.5	4.8		0.03	0.15–0.35	
S32550	Ferralium 255	25	3	6	2	0.04	0.1–0.25	
S31260	DP-3	25	3	7	0.5	0.030	0.10–0.30	0.3 W
S32750	SAF 2507	25	4	7		0.030	0.24–0.32	

Table C5. Composition of Precipitation-Hardening (PH) Stainless Steels

UNS	Alloy	C	Mn	Si	Cr	Ni	Mo	P	S	Other
					Martensitic					
S13800	PH13-8Mo	0.05	0.10	0.10	12.25–13.25	7.5–8.5	2.0–2.5	0.0l	0.008	0.90–1.35 Al, 0.0l N
S15500	15-5PH	0.07	1.00	1.00	14.0–15.5	3.5–5.5		0.04	0.03	2.5–4.5 Cu, 0.15–0.45 Nb
S17400	17-4PH	0.07	1.00	1.00	15.0–17.5	3.0–5.0		0.04	0.03	3.0–5.0 Cu, 0.I5–0.45 Nb
S45000	Custom 450	0.05	1.00	1.00	14.0-16.0	5.0–7.0	0.5-1.0	0.03	0.03	1.25–1.75 Cu, 8 × %C min Nb
S45000	Custom 455	0.05	0.50	0.50	11.0–12.5	7.5–9.5	0.50	0.04	0.03	1.5–2.5 Cu, 0.8–1.4 Ti, 0.l-0.5 Nb
					Semiaustenitic					
S15700	PH15-7 Mo	0.09	1.00	1.00	14.5–16.0	6.5–7.75	2.0–3.0	0.04	0.04	0.75–1.50 Al
S17700	17-7PH	0.09	1.00	1.00	16.0–18.0	6.50–7.75		0.04	0.04	0.75–150 Al
S35000	AM-350	0.07–0.11	0.50–1.25	0.50	16.0–17.0	4.5–5.0	2.50–3.25	0.04	0.03	0.07–0.13 N
S35500	AM-355	0.l0–0.15	0.50–1.25	0.50	15.0–16.0	4.0–5.0	2.50–3.25	0.04	0.03	0.07–0.13 N
					Austenitic					
S66286	A-286	0.08	2.00	1.00	13.5–16.0	24.0–27.0	1.0-l.5	0.025	0.025	1.90–2.35 Ti, 0.35 max. Al, 0.10–0.50 V, 0.003–0.010 B
	JBK-73	0.015	0.05	0.02	14.5	29.5	1.25	0.006	0.002	2.15 Ti, 0.25 Al, 0.27 V, 0.0015 B

Table C6. Titanium- Chemical Composition of Commercial Titanium Alloys

UNS	ASTM	N	C	H	Fe	O	Al	V	Ni	Mo	Nb	Cr	Zr	Pd
R50250	1	0.03	0.08	0.015	0.2	0.18								
R50400	2	0.03	0.08	0.015	0.3	0.25								
R50550	3	0.05	0.08	0.015	0.3	0.35								
R56400	5	0.05	0.08	0.015	0.4	0.2	5.5–6.75	3.5–4.5						
R52400	7	0.03	0.08	0.015	0.3	0.25								.12–.25
R56320	9	0.03	0.08	0.015	0.25	0.15	2.5–3.5	2.0–3.0						0.1
R52250	11	0.03	0.08	0.015	0.2	0.18								.12–.25
R53400	12	0.03	0.08	0.015	0.3	0.25			.6–.9	.2–.4				
R52402	16	0.03	0.08	0.015	0.3	0.25								.04–.08
R52252	17	0.03	0.08	0.015	0.2	0.18								.04–.08
R56322	18	0.03	0.08	0.015	0.25	0.15	2.5–3.5	2.0–3.0						.04–.08
R58640	19	0.03	0 05	0.02	0.3	0.12	3.0–4.0	7.5–8.5		3.5–4.5		5.5–6.5	3.5–4.5	
R58645	20	0.03	0.05	0.02	0.3	0.12	3.0–4.0	7.5–8.5		3.5–4.5		5.5–6.5	3.5–4.5	.04–.08
R58210	21	0.03	0.05	0.015	0.4	0.17	2.5–3.5			15–16.0	2.2–3.2			
	23	0.03	0.08	0.015	0.4	0.13	5.5–6.5	3.5–4.5						